

Reversible CO₂ Capture and On-Demand Release by an Acidity-Matched Organic Photoswitch

Abdulrahman M. Alfaraidi, Bryan Kudisch, Nina Ni, Jayden Thomas, Thomas Y. George, Khashayar Rajabimoghadam, Haihui Joy Jiang, Daniel G. Nocera, Michael J. Aziz, and Richard Y. Liu*



Cite This: <https://doi.org/10.1021/jacs.3c08471>



Read Online

ACCESS |



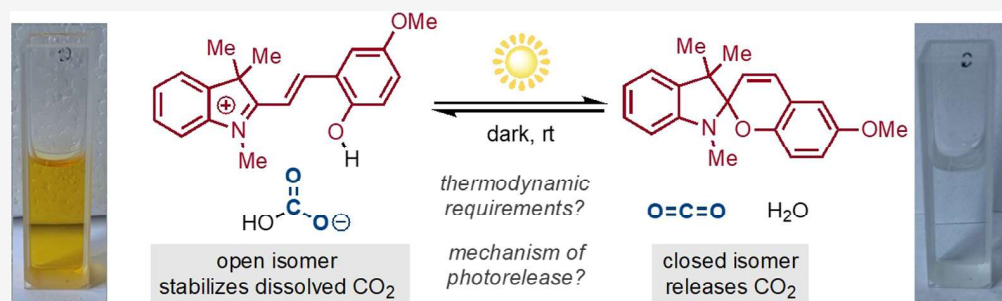
Metrics & More



Article Recommendations



Supporting Information



ABSTRACT: Separation of carbon dioxide (CO₂) from point sources or directly from the atmosphere can contribute crucially to climate change mitigation plans in the coming decades. A fundamental practical limitation for the current strategies is the considerable energy cost required to regenerate the sorbent and release the captured CO₂ for storage or utilization. A directly photochemically driven system that demonstrates efficient passive capture and on-demand CO₂ release triggered by sunlight as the sole external stimulus would provide an attractive alternative. However, little is known about the thermodynamic requirements for such a process or mechanisms for modulating the stability of CO₂-derived dissolved species by using photoinduced metastable states. Here, we show that an organic photoswitchable molecule of precisely tuned effective acidity can repeatedly capture and release a near-stoichiometric quantity of CO₂ according to dark–light cycles. The CO₂-derived species rests as a solvent-separated ion pair, and key aspects of its excited-state dynamics that regulate the photorelease efficiency are characterized by transient absorption spectroscopy. The thermodynamic and kinetic concepts established herein will serve as guiding principles for the development of viable solar-powered negative emission technologies.

INTRODUCTION

The accumulation of CO₂ in the atmosphere is a primary driver of anthropogenic climate change, and a dramatic reduction of net emissions is urgently required to avoid catastrophic future scenarios.^{1–4} Accordingly, considerable research effort has been dedicated to chemical systems for removing CO₂ from emission streams (CCS, carbon capture and storage)^{5,6} and, more recently, from the atmosphere (DAC, direct air capture).^{7,8} The most developed technologies for CO₂ capture depend on sorbents such as alkaline aqueous solutions⁹ and amines such as ethanolamine,¹⁰ which generally use energy-demanding thermal stripping to release the captured CO₂ for storage and sorbent regeneration (Figure 1A).¹¹ Complementary approaches using swings in electrical potential^{12–14} or applied pressure^{15,16} to cycle between capture and release have also been investigated. The viability of these mitigation strategies on scale will likely require that their significant energy demand be ultimately supplied by renewable electricity. As an alternative, we considered whether a chemistry can be devised that directly couples CO₂ capture and release to visible light as the only external energy input.

Such a system could be directly powered by sunlight, for example, according to the day–night cycle and distributed without requiring renewable electricity as an intermediary, along with the costs and limitations associated with its production, storage, distribution, and infrastructure maintenance.

Here, we show that photoswitchable organic molecules can effectively and repeatedly capture CO₂ from the gas phase and release it on demand upon visible-light exposure. Our study focuses on the well-known spiropyran photochromic dyes,^{17–19} which can be toggled between two forms, a closed spiropyran isomer SP and an open merocyanine isomer MC, which differ significantly in chemical properties such as color, acidity, and

Received: August 4, 2023

Revised: November 21, 2023

Accepted: November 22, 2023

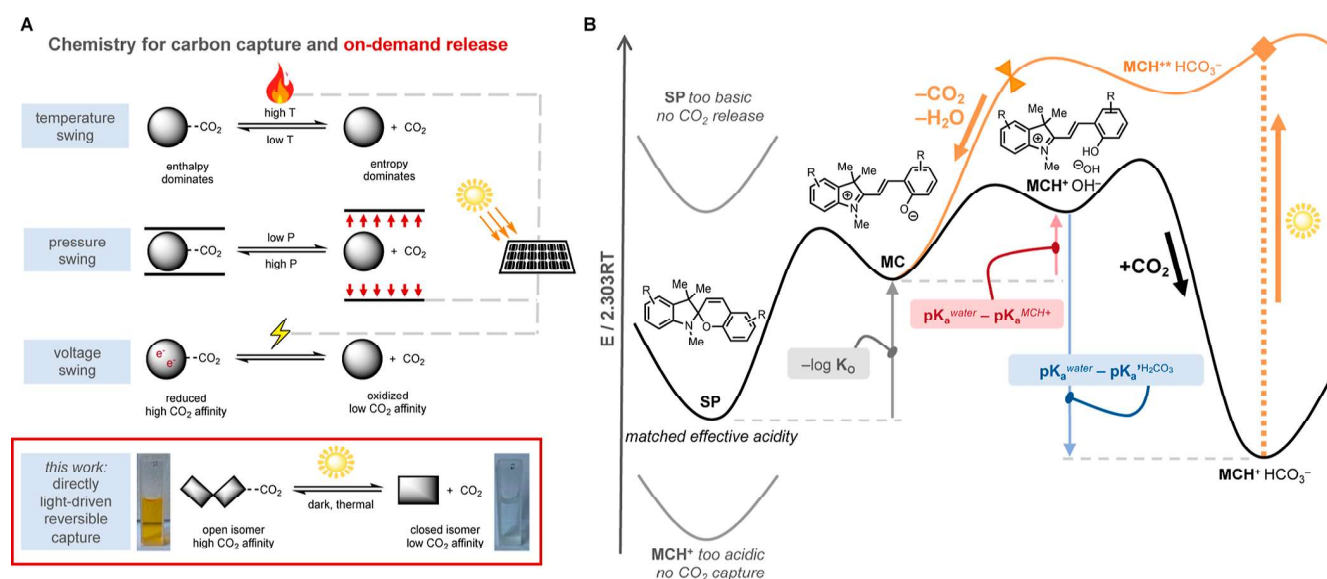


Figure 1. Carbon capture and phototriggered release. (A) Comparison of previously developed chemical processes for reversible CO₂ binding and the new approach in our work. (B) Mechanism for coupling CO₂ capture with photoisomerization of spiropyrans and the required thermodynamic balance. The orange curve shows the excited-state surface reached by MCH⁺ upon excitation with visible light. Compounds for which MCH⁺ is too acidic (SP low in energy) will never have MCH⁺ HCO₃⁻ as the most stable state and therefore will not capture CO₂ effectively. Compounds for which the SP form is too basic (SP high in energy) will not release CO₂ effectively as an impractically high intensity of light will be required to excite enough MCH⁺ to release CO₂ at a rate that competes with its recapture.

metal affinity. In particular, protonated merocyanine (MCH⁺) has been shown to engender large, light-driven pH swings^{20–22} upon irradiation by releasing its proton and cyclizing to SP, which is followed by gradual thermal reversion to its original state. By coupling this photoinduced equilibrium shift with bicarbonate protonation and carbonic acid dehydration equilibria, we envisioned a system that can sequester CO₂ in the dark but changes its resting state to release that CO₂ upon light exposure. Previous research has demonstrated photoacid-triggered formation of carbonic acid for spectroscopic characterization²³ and photoacid-accelerated CO₂ release from acidic conditions.²⁴ Very recently, an elegant strategy using an indazole photoacid to promote CO₂ release from amino acid sorbents was also reported.²⁵ However, identification of a single-component solute that can recurrently capture and release according to dark/light cycles remains a highly desirable goal. Further, a systematic framework for analyzing the thermodynamic requirements and experimental investigation of the precise mechanism of the photochemical process is needed to provide a theoretical foundation for the development of this novel approach to reversible carbon capture.

RESULTS AND DISCUSSION

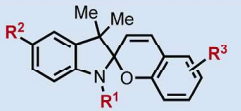
For the proposed process (Figure 1B), a detailed treatment of the thermodynamic balance shows that precise acidity tuning is critical for the realization of the efficient capture and photorelease of CO₂. In solution, a spiropyran SP interconverts with an open merocyanine isomer MC with an equilibrium constant K_O , which is typically below unity (favoring SP) in aqueous environments²⁶ (for some discussion of solvent effects, see Supporting Information). Because MC features a phenoxide moiety, it can act as a base in an aqueous solution and reversibly deprotonate water to form MCH⁺ OH⁻. The hydroxide anion can sequester dissolved CO₂ as bicarbonate. If capture is to be a spontaneous process, we require MCH⁺

HCO₃⁻ to be the lowest-energy state in the absence of an external energy input. Upon irradiation, some MCH⁺ ions will enter an excited state, the high potential energy of which accelerates reversion to SP and/or MC with the release of CO₂ and H₂O. For effective release of CO₂ to occur, irradiation must create a sufficient population of MCH⁺* HCO₃⁻ such that the net rate of CO₂ release from these excited states can compete with thermal recapture of CO₂. This is difficult to achieve if the relative free energy of SP is too high, in which case reversion will require an impractically high intensity of light. A balanced energetic landscape corresponding to optimal photoswitching of uptake and release of CO₂ occurs around (see the Supporting Information for discussion)

$$\begin{aligned} \text{p}K_{\text{aH}}'(\text{SP}) &= \text{p}K_{\text{a}}(\text{MCH}^+) - \log(1 + K_O^{-1}) \\ &\cong \text{p}K_{\text{a}}(\text{H}_2\text{CO}_3) \end{aligned}$$

The quantity on the left represents the apparent conjugate acidity of the spiropyran,²⁷ $\text{p}K_{\text{aH}}'(\text{SP})$, which accounts for both the Brønsted acidity of the phenol and the driving force for ring closure. This is an analogue of the classical Henderson–Hasselbalch equation. The optimal balance of capture and photorelease efficiency should be achieved only by molecules for which $\text{p}K_{\text{aH}}'(\text{SP})$ nears the effective $\text{p}K_{\text{a}}'$ of H₂CO₃ in its relevant conditions (6.35 in water,²⁸ although ion-pairing interactions can alter the exact target value, see below).

To validate this analysis, we synthesized spiropyrans SP1–SP8 (Figure 2), varying in substitution on nitrogen (R¹) and C5 (R²) of the indoline, as well as on the chromene fragment ortho and para to the oxygen (R³). These spiropyran structures can be easily accessed on a gram-to-kilogram scale,^{29–31} usually in a single step from commercial materials. The effective $\text{p}K_{\text{aH}}'$ values of these molecules in 1:1 DMSO/water were determined by spectrophotometric titration, using the moderate UV absorbance of SP and the strong UV-to-visible

	R ¹	R ²	R ³	λ_{MCH^+} (nm) [ϵ_{MCH^+} (M ⁻¹ cm ⁻¹)]	λ_{SP} (nm)	pK _{aH} '
SP1	Me	H	H	424 [21,750]	289	5.35
SP2	Me	H	<i>p</i> -Me	438 [19,270]	273	5.23
SP3	Me	H	<i>o</i> -OMe	401 [16,100]	291	5.51
SP4	Me	H	<i>p</i> -OMe	460 [22,080]	291	5.70
SP5	Me	H	<i>p</i> -NMe ₂	388 [16,000]	291	5.62
SP6	Me	CN	<i>p</i> -OMe	482 [7,500]	288	2.91
SP7	(CH ₂) ₃ SO ₃ ⁻	H	<i>o</i> -OMe	396 [24,333]	278	6.05
SP8	(CH ₂) ₃ SO ₃ ⁻	H	<i>p</i> -OMe	468 [19,900]	296	6.11

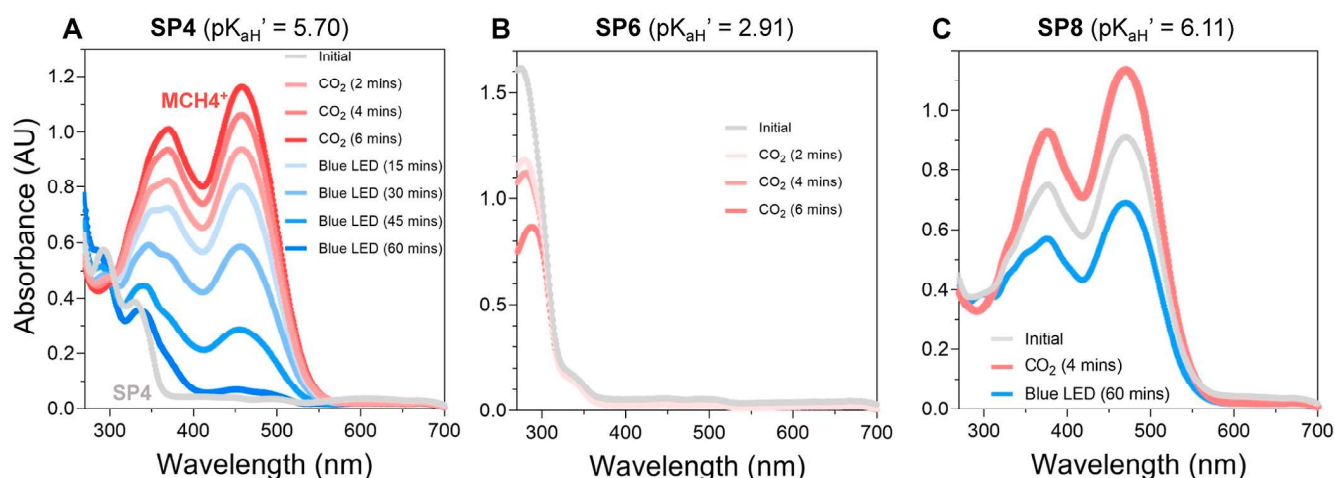


Figure 2. Spiropyran: properties and response to CO₂ and light exposure. (top) Summary of spiropyran evaluated in this work with effective acidities shown on the right. (A) An acidity-matched spiropyran **SP4** captures CO₂ rapidly to generate **MCH4⁺** and converts back to its original spiropyran form, releasing CO₂ during irradiation with 450 nm light. (B) Spiropyran **SP6** that is too acidic and therefore does not generate **MCH6⁺** in the presence of CO₂. (C) Spiropyran **SP8** that is too basic and already exists in its merocyanine form **MCH8⁺** in neutral solution. This material captures CO₂ but does not undergo efficient photorelease. This compound is synthesized in the -SO₃H form, and the presence of this acidic group can contribute to the initial protonation state.

absorbance of **MCH⁺** generated upon isomerization and protonation of **SP**. The parent spiropyran **SP1** is moderately basic (pK_{aH}' = 5.30) in its ground state, and the installation of electron-donating groups on the chromene unit results in the expected increase in basicity of the phenoxide, elevating the pK_{aH}' of **SP3** (R³ = *o*-OCH₃, pK_{aH}' = 5.51), **SP4** (R³ = *p*-OCH₃, pK_{aH}' = 5.70), and **SP5** (R³ = *p*-N(CH₃)₂, pK_{aH}' = 5.62) relative to that of **SP1**. An electron-withdrawing group on the indoline of **SP6** (R² = CN), while likely imparting minimal influence on the phenoxide basicity, greatly enhances the effective acidity (pK_{aH}' = 2.91) of the corresponding protonated merocyanine form by favoring the closed, spiropyran form (lowering K_O). The attachment of a solubilizing sulfonate chain on the indoline nitrogen was found to reduce the effective acidity, presumably due to electrostatic effects, as exemplified by **SP7** (R¹ = (CH₂)₃SO₃⁻, R³ = *o*-OCH₃, and pK_{aH}' = 6.05) and **SP8** (R¹ = (CH₂)₃SO₃⁻, R³ = *p*-OCH₃, and pK_{aH}' = 6.11).

DMSO–water solutions containing these spiropyran were evaluated for their competence in the capture of gaseous CO₂ and subsequent release under visible-light irradiation. The range of effective acidities represented by our panel of

analogues allowed us to experimentally confirm our acidity-matching hypothesis, which states that there is an optimal pK_{aH}' for switchable binding to CO₂. In accordance with these predictions, for the most acidic photochromes such as **SP6** (pK_{aH}' = 2.91), exposure to pure CO₂ (1 atm) did not result in any formation of the corresponding protonated merocyanine **MCH6⁺** (λ_{max} = 482 nm, Figure 2B). Conversely, the most basic photochromes such as **SP8** (pK_{aH}' = 6.11), when dissolved in 1:1 DMSO/water, exist significantly in their open isomer **MCH8⁺** form (λ_{max} = 468 nm) due to their ability to reversibly deprotonate water (Figure 2C). Although exposure to pure CO₂ (1 atm) resulted in only a minor increase in the observed quantity of **MCH8⁺**, a significant amount of CO₂ capture was indicated by the change in pH of the solution from 7.8 to 5.3 (Figure S32). For compounds that exist significantly in the **MCH⁺** form in solution, the extent of CO₂ capture is difficult to infer from spectrophotometry alone as the UV–vis absorbance spectrum primarily reflects the concentration of the merocyanine-derived cation and is essentially independent of the anion. As anticipated, **MCH8⁺** HCO₃⁻ is extremely stable, and irradiation by blue LEDs (λ_{max} = 450 nm) resulted in a relatively small change in the spectrum and a 0.7 pH unit

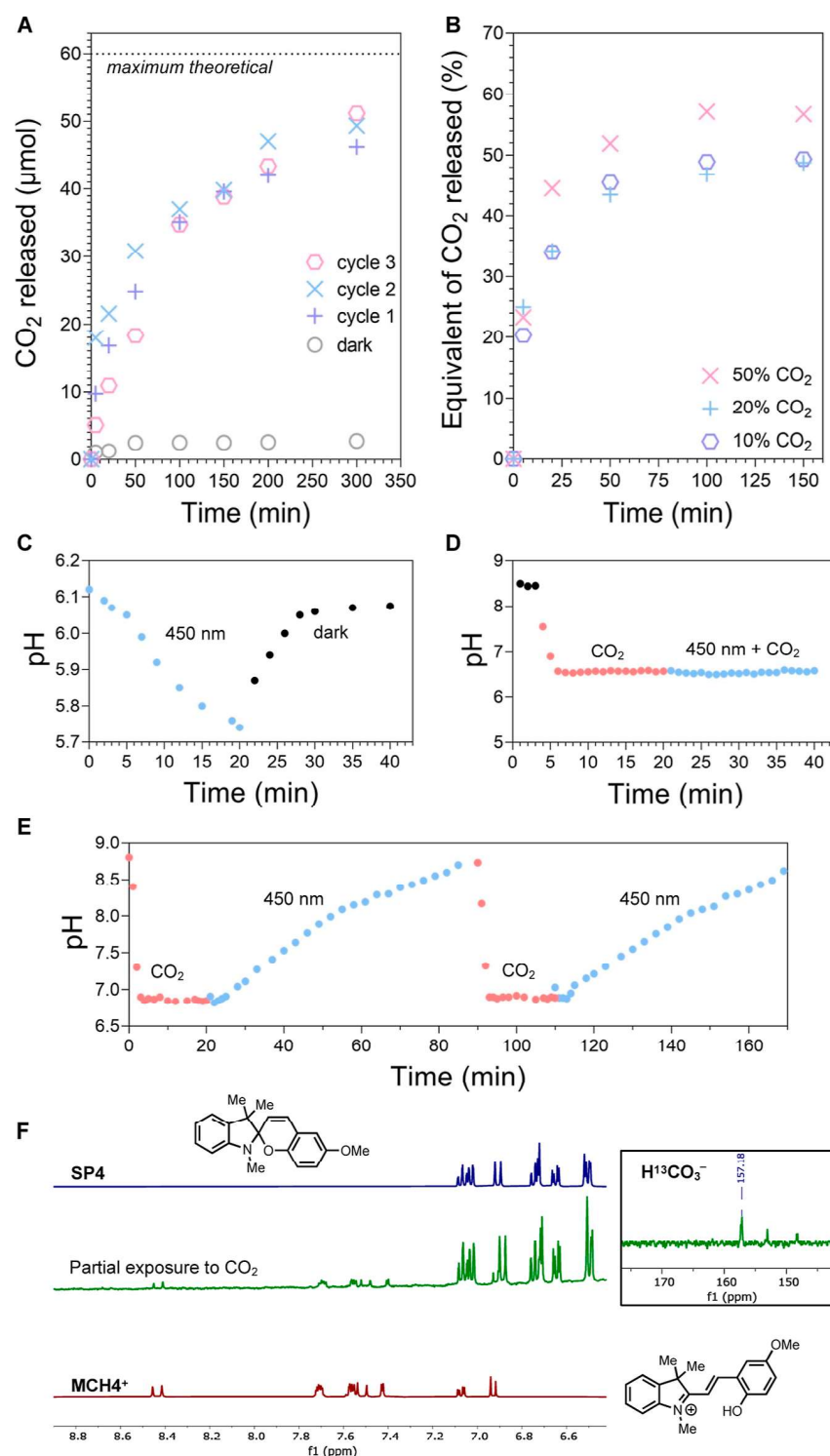


Figure 3. CO₂ passive capture and photorelease: performance and mechanism. (A) GC quantification of the released CO₂ from three consecutive cycles of exposure to CO₂ and blue-light (450 nm) irradiation, including a control replicate performed with the sample shielded by reflective foil. (B) Released CO₂ after capture from CO₂/N₂ mixtures. In situ pH tracking of a DMSO–water solution of 5 mM SP4 (C) during irradiation and in the dark with initial adjusted pH set to 6.1 to partially convert SP4 to the MCH4⁺ Cl⁻ form, (D) during irradiation of the sample while overhead pressure of CO₂ was maintained, and (E) during CO₂ capture and photochemical release. (F) NMR spectroscopic evidence for MCH4⁺ HCO₃⁻ as the resting state of the captured CO₂.

increase even after 60 min, reflecting negligible CO₂ release. These negative examples contrast dramatically with the promising results obtained using compounds of moderate acidity such as SP4 ($pK_{\text{aH}}' = 5.70$) and, to a lesser extent, SP2

($pK_{\text{a}}' = 5.23$). For example (Figure 2A), exposure of SP4 to pure CO₂ (1 atm) resulted in rapid and isosbestic conversion to MCH4⁺, which, at this stage, we hypothesized to be paired to HCO₃⁻. We proceeded to irradiate this solution with 450

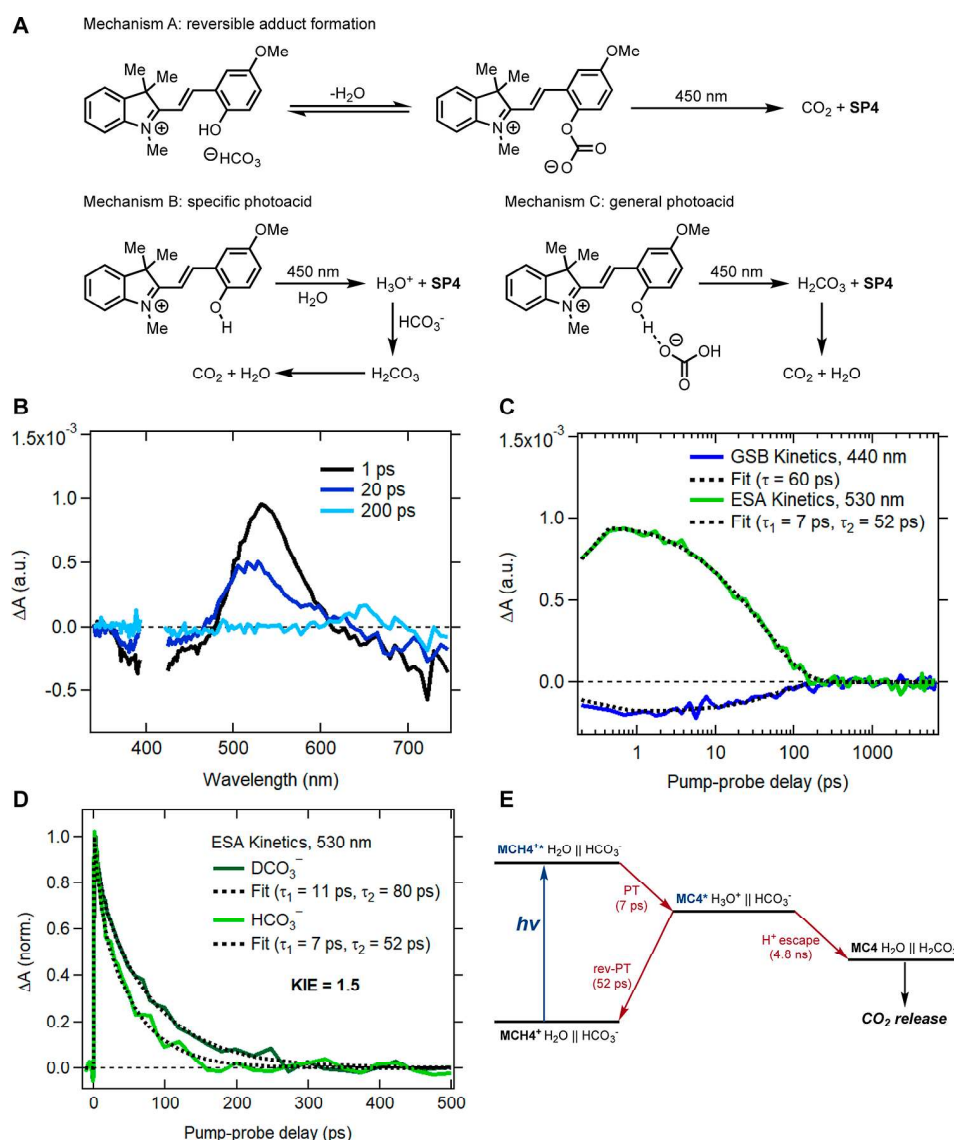


Figure 4. Mechanism of CO_2 photorelease. (A) Three mechanistic proposals considered in this study. (B) Transient absorption spectra of $\text{MCH4}^+ \text{HCO}_3^-$, with excitation at 400 nm. The laser scattering region was removed for clarity. (C) Decay kinetics of the ground-state bleach and ESA features with exponential and biexponential fits, respectively. (D) Comparative decay profiles of the ESA using $\text{MCH4}^+ \text{HCO}_3^-$ and $\text{MCD4}^+ \text{DCO}_3^-$, showing a KIE of ~ 1.5 for both processes represented in the biexponential kinetic model. (E) Proposed scheme for CO_2 release after initial electronic excitation of MCH4^+ . Ions divided by double vertical lines indicate a solvent-separated ion pair, in which the ions are not directly in contact but separated by a few enough solvent molecules that the anion still exerts a detectable influence on the reactivity of the cation.

nm blue light, upon which the disappearance of MCH4^+ occurred, accompanied by a complete recovery of the original spectrum. Similar but slower conversion in both directions was observed with **SP2** (Figure S9). This compound is also significantly less soluble than **SP4** (26 mM vs < 2 mM for **SP2**), so we elected to proceed with **SP4** for the ensuing analysis.

Successful repeated capture and light-triggered release of CO_2 by **SP4** were confirmed by quantitative gas chromatography (GC) calibrated against standard mixtures (Figure 3A). After the introduction of CO_2 into a solution of **SP4** (60 μmol in 3 mL of solvent, 4:1 DMSO/water), which elicited the appearance of an intense yellow color, the vial headspace was replaced with nitrogen, and the cuvette was exposed to 450 nm light. Aliquots of the gas in the headspace were analyzed, and the gaseous CO_2 content was observed to increase over time (half-life of ca. 60 min) to a terminal value of 46–51 μmol ,

representing on average 81% of theoretical capture capacity. The now-colorless solution was then immediately re-exposed to CO_2 , and the photorelease procedure was performed again for a total of three capture-release cycles. No difference in activity was observed, implying that the spiropyran dye shows stability under these operating conditions, including extended exposure to atmospheric oxygen, which is not tolerated by most molecular redox approaches. Temperature control during irradiation was carefully maintained using portable fans, and control experiments in which the sample was shielded from light by reflective foil displayed a negligible release of CO_2 . Spectrophotometry further confirmed that release in the dark is extremely slow even when opened to the atmosphere (11.5% decrease in $\text{MCH4}^+ \text{HCO}_3^-$ over 9 h, Figure S13). Pure gas input was not required for capture (Figure 3B): using 50%, 20%, and 10% (v/v) mixtures of CO_2 in N_2 delivered similar results, although the total quantity of CO_2 released relative to

SP4 decreased to roughly 50% in the most dilute case. Nevertheless, these experiments prove the concept of cyclic carbon capture and release using visible light as the only external energy input.

To further illustrate key mechanistic aspects of the capture and release processes, in situ pH tracking experiments were conducted (Figure 3C–E), which revealed a shift between pH-determining species resulting from the coupling of multiple equilibria. First, hydrochloric acid was added to partially convert SP4 to the $\text{MCH4}^+ \text{Cl}^-$ form. The protonated cation is a metastable-state photoacid that, upon irradiation, converts to SP4 while releasing a proton to the solvent, and accordingly, a decrease in the pH was measured. Upon removal of the light source, the pH rapidly recovered to its starting value, as SP4 thermally reverts to MC4, which is rapidly reprotonated. If instead of using a strong acid, equilibration with an atmosphere of CO_2 was used to open SP4 to its protonated merocyanine form, identical irradiation conditions resulted in no noticeable change in pH provided that the solution remained in equilibrium with an applied pressure of CO_2 . This difference is due to the buffering capacity of bicarbonate as the photoreaction of MCH4^+ now prompts net proton transfer to bicarbonate rather than the solvent and therefore cannot be perceived by pH measurement. Under a headspace of pure CO_2 , dissolved CO_2 remains in solution and can quickly reprotonate SP4 via carbonic acid. If the CO_2 -charged solution is opened to the air such that CO_2 formed from protonation and dehydration of bicarbonate can escape, photoirradiation results in a steady increase in the solution pH. The photoacidic activity of MCH4^+ results in a net basification of the solution because the released proton is not received by the solvent but participates with bicarbonate in an irreversible process ($\text{H}_2\text{CO}_{3(\text{aq})} \rightarrow \text{H}_2\text{O}_{(\text{l})} + \text{CO}_{2(\text{g})}$) that depletes carbonic acid, which has the effect of decreasing the total concentration of dissolved acidic species. Although the CO_2 outgassing process formally exchanges a higher pK_a buffer ($\text{CO}_2/\text{HCO}_3^-$) for a lower pK_a buffer ($\text{MCH4}^+/\text{SP4}$), which one might expect to lead to acidification, there is a concomitant shift in the protonation state of the buffer as carbonic acid is converted into less acidic species ($\text{H}_2\text{O}_{(\text{l})} + \text{CO}_{2(\text{g})}$). The observed rate of CO_2 evolution in the pH-tracking experiments is slightly higher than that recorded in the above GC measurements (Figure 2A), which is due to the pH-tracking being performed fully open to the atmosphere, while the GC study was performed in a sealed vial to accurately quantify gaseous CO_2 . Consistent with our model, the pH could be reverted to its starting point with the removal of the light source and equilibration under an atmosphere of CO_2 .

The assignment of dominant dissolved inorganic carbon species such as $\text{MCH4}^+ \text{HCO}_3^-$, as opposed to a direct covalent adduct such as MC4-CO_2 , could not be established on the basis of spectrophotometry alone, as TD-DFT calculations indicate that the lowest-energy excitations are similar in energy for free MCH4^+ (497 nm), $\text{MCH4}^+ \cdots \text{HCO}_3^-$ (509 nm), and MC4-CO_2 (473 nm), and all are close to the experimental λ_{max} (460 nm). However, the identity of the cation as MCH4^+ is apparent from ^1H NMR spectroscopy (Figure 3F): the protonated merocyanine could be independently prepared by protonation of SP4 with strong acid, and partial exposure of SP4 to gaseous CO_2 resulted in the evolution of identical resonances in the ^1H NMR. When this same spiropyran was exposed to ^{13}C -labeled CO_2 , a broad resonance arose in the ^{13}C NMR spectrum at a chemical shift

of 157.2 ppm, which is likely associated with ^{13}C -bicarbonate.

Having established the relevant ground-state structures involved in the light-driven capture cycle, we turned to further dissecting the mechanism of the photorelease subprocess. Three plausible pathways were considered (Figure 4A): (A) a nonphotoacid mechanism, involving reversible formation of the adduct MC4-CO_2 and subsequent photoinduced cleavage of the O-CO_2^- bond; (B) a specific photoacid mechanism, in which MCH4^+ releases its proton to water upon irradiation, and the solvent serves to transfer this proton to a separated or distant HCO_3^- to form carbonic acid; and (C) a general photoacid mechanism, in which MCH4^+ and HCO_3^- as a contact ion pair directly exchange a proton in the excited state.

A solution containing $\text{MCH4}^+ \text{HCO}_3^-$ was prepared by bubbling CO_2 into dissolved SP4, and the excited-state dynamics of this species were investigated by ultrafast transient absorption spectroscopy (Figure 4B). After excitation using a 400 nm laser pulse, significant excited-state absorption (ESA) was observed at 530 nm. We assigned this feature to MC4^* obtained upon the deprotonation of MCH4^{+*} in its excited state. The transient bleach above 600 nm is likely due to stimulated emission from MC4^* (Figure S39). The decay of ESA intensity at 530 nm fits well with a biexponential function with time constants $\tau_1 = 7$ ps and $\tau_2 = 52$ ps (Figure 4C), with relative amplitudes of 0.23 and 0.77, respectively. As examined further below, we propose these first-order decays are associated with proton-transfer (PT) and reverse-proton-transfer (rev-PT) processes from MCH4^+ to water.

A significant kinetic isotope effect (KIE) was observed in the rates of both steps by using D_2O as an alternative solvent ($\tau_1 = 7$ ps using H_2O vs $\tau_1 = 11$ ps using D_2O , $\text{KIE} = 1.6$; $\tau_2 = 52$ ps using H_2O vs $\tau_2 = 80$ ps using D_2O , $\text{KIE} = 1.5$, Figure 4D; and the relative amplitudes of the two exponentials in D_2O were 0.2 and 0.8, respectively). The magnitudes of these deuterium isotope effects are potentially consistent with proton transfer between two heteroatomic sites of widely differing acidities (mechanisms B and C). These results would be more difficult to rationalize in a nonphotoacid pathway such as mechanism A, in which no primary isotope effect should manifest. The same transient absorption experiments were also repeated with $\text{MCH4}^+ \text{Cl}^-$ and $\text{MCD4}^+ \text{Cl}^-$, and time constants ($\tau_1 = 5$ ps using HCl vs $\tau_1 = 12$ ps using DCl , $\text{KIE} = 2.4$; $\tau_2 = 46$ ps using HCl vs $\tau_2 = 73$ ps using DCl , $\text{KIE} = 1.6$) were found to be similar to those measured with bicarbonate (Figure S36), suggesting that the initial acceptor of the merocyanine-derived proton was not the anion. This observation led us to favor mechanism B, in which the immediate target is a solvent (water) molecule.

Figure 4E summarizes the proposed overall scheme for light-driven generation of carbonic acid from $\text{MCH4}^+ \text{HCO}_3^-$. After photoexcitation of MCH4^+ , rapid proton transfer ($\tau = 7$ ps) takes place from the merocyanine to a hydrogen-bonded water molecule with minimal heavy-atom motion, forming a hydrogen-bonded excited-state complex $[\text{MC4}^* \cdots \text{H}_3\text{O}^+]$. This complex can either undergo reverse proton transfer ($\tau = 52$ ps) to restore the initial MCH4^+ , or the proton can diffuse away through a von Grotthuss-type mechanism^{32–34} to find a basic bicarbonate anion. Based on a quantum yield of 1.3% for the formation of MC4 derived from nanosecond transient absorption spectroscopy, the proton escape takes place on the order of ca. 4.8 ns. Higher proton-escape quantum yields (50%) have been observed from other protonated

merocyanines that are stronger photoacids,^{35,36} as estimated based on their transient absorption spectra. These observations give us encouragement that the development of more efficient photoacids for bicarbonate protonation is possible and that the rationale for the difference between our photoacids and previous examples continues to be investigated.

Interestingly, when the sample was prepared such that the anion was chloride instead of bicarbonate, we found a minor but verifiable decrease in the quantum yield (1.1%), indicating the likely involvement of the counteranion in regulating competition between the reverse-proton-transfer and proton-escape pathways. Thus, the nature of $\text{MCH4}^+ \text{HCO}_3^-$ under these conditions is most aptly described as a solvent-separated ion pair,^{37,38} rather than as free ions. The electrostatically associated bicarbonate is not the direct recipient of the proton from MCH4^+ but does remain sufficiently proximal to influence the preorganization of the intervening solvent molecule(s) and, thereby, the frequency of carbonic acid formation. If accurate, then this scheme is informative for optimizing the rate of CO_2 photogeneration. For example, structural modifications that promote dissociation of hydronium from the $\text{MC4} \cdots \text{H}_3\text{O}^+$ complex might reduce the rate of reverse proton transfer, while strengthening the attractive interactions between MCH4^+ and HCO_3^- should accelerate the productive protonation of bicarbonate.

CONCLUSIONS

In conclusion, this work demonstrates repeated, on-demand CO_2 capture and release using photoswitchable acids. A systematic assessment of structure–activity relationships underscores the importance of effective-acidity tuning in achieving efficient cycling. Ultrafast spectroscopy and KIEs suggest a solvent-separated ion pair mechanism for photo-release, a theory that can guide the development of more efficient photoacid structures. Studies into implementing these design principles and other modifications aimed at maximizing solubility, synthetic scalability, longevity, and wavelength coverage are ongoing with the long-term intention of generalizing solar-powered carbon removal technologies.

ASSOCIATED CONTENT

Supporting Information

The Supporting Information is available free of charge at <https://pubs.acs.org/doi/10.1021/jacs.3c08471>.

Experimental methods, synthetic procedures, spectroscopic data, computational results, and additional discussion and references (PDF)

AUTHOR INFORMATION

Corresponding Author

Richard Y. Liu — Department of Chemistry and Chemical Biology, Harvard University, Cambridge, Massachusetts 02138, United States; orcid.org/0000-0003-0951-6487; Email: richardliu@chemistry.harvard.edu

Authors

Abdulrahman M. Alfaraidi — Department of Chemistry and Chemical Biology, Harvard University, Cambridge, Massachusetts 02138, United States

Bryan Kudisch — Department of Chemistry and Chemical Biology, Harvard University, Cambridge, Massachusetts 02138, United States; orcid.org/0000-0003-3352-5383

Nina Ni — Department of Chemistry and Chemical Biology, Harvard University, Cambridge, Massachusetts 02138, United States

Jayden Thomas — Department of Chemistry and Chemical Biology, Harvard University, Cambridge, Massachusetts 02138, United States

Thomas Y. George — Harvard John A. Paulson School of Engineering and Applied Sciences, Cambridge, Massachusetts 02138, United States; orcid.org/0000-0002-0159-8521

Khashayar Rajabimoghadam — Department of Chemistry and Chemical Biology, Harvard University, Cambridge, Massachusetts 02138, United States

Haihui Joy Jiang — Department of Chemistry and Chemical Biology, Harvard University, Cambridge, Massachusetts 02138, United States; orcid.org/0000-0002-7302-755X

Daniel G. Nocera — Department of Chemistry and Chemical Biology, Harvard University, Cambridge, Massachusetts 02138, United States; orcid.org/0000-0001-5055-320X

Michael J. Aziz — Harvard John A. Paulson School of Engineering and Applied Sciences, Cambridge, Massachusetts 02138, United States; orcid.org/0000-0001-9657-9456

Complete contact information is available at: <https://pubs.acs.org/doi/10.1021/jacs.3c08471>

Notes

The authors declare no competing financial interest.

ACKNOWLEDGMENTS

The authors are grateful to George M. Whitesides (Harvard) for the use of a gas chromatograph (GC) and other instrumentation and for insightful comments. We thank Eugene E. Kwan (Merck) for useful discussions during the preparation of the manuscript. A.M.A. acknowledges King Fahd University of Petroleum and Minerals and the Ministry of Education of Saudi Arabia for a doctoral scholarship. The authors acknowledge the Harvard Climate Change Solutions Fund (A.M.A., T.Y.G., and M.J.A.), the Office of Naval Research (D.G.N. under grant N00014-22-1-2470), and the Corning Fund for Faculty Development (R.Y.L.) for partial financial support of reported research for the indicated recipients.

REFERENCES

- (1) Minx, J. C.; Lamb, W. F.; Callaghan, M. W.; Fuss, S.; Hilaire, J.; Creutzig, F.; Amann, T.; Beringer, T.; de Oliveira Garcia, W.; Hartmann, J.; Khanna, T.; Lenzi, D.; Luderer, G.; Nemet, G. F.; Rogelj, J.; Smith, P.; Vicente Vicente, J. L.; Wilcox, J.; del Mar Zamora Dominguez, M. Negative Emissions Part 1: Research Landscape and Synthesis. *Environ. Res. Lett.* **2018**, *13* (6), 063001.
- (2) Masson-Delmotte, V.; Zhai, P.; Pirani, A.; Connors, S. L.; Péan, C.; Chen, Y.; Goldfarb, L.; Gomis, M. I.; Matthews, R.; Berger, S.; Huang, M.; Yelekçi, O.; Yu, R.; Zhou, B.; Lonnoy, E.; Maycock, T. K.; Waterfield, T.; Leitzell, K.; Caud, N. *Climate Change 2021: The Physical Science Basis: Contribution of Working Group I to the Sixth Assessment Report of the Intergovernmental Panel on Climate Change*; IPCC; Intergovernmental Panel on Climate Change: Cambridge University Press, Cambridge, United Kingdom and New York, NY, USA, 2021.
- (3) Edenhofer, O.; Pichs-Madruga, R.; Sokona, Y.; Minx, J. C.; Farahani, E.; Kadner, S.; Seyboth, K.; Adler, A.; Baum, I.; Brunner, S.; Eickemeier, P.; Kriemann, B.; Savolainen, J.; Schlömer, S.; von Stechow, C.; Zwickel, T. *Climate Change 2014: Mitigation of Climate Change: Working Group III Contribution to the Fifth Assessment Report of the Intergovernmental Panel on Climate Change*; IPCC; Inter-

governmental Panel on Climate Change: Cambridge University Press, Cambridge, United Kingdom and New York, NY, USA, 2014. https://www.ipcc.ch/site/assets/uploads/2018/02/ipcc_wg3_ar5_full.pdf.

(4) Giorgi, F.; Whetton, P. H.; Jones, R. G.; Christensen, J. H.; Mearns, L. O.; Hewitson, B.; vonStorch, H.; Francisco, R.; Jack, C. Emerging Patterns of Simulated Regional Climatic Changes for the 21st Century Due to Anthropogenic Forcings. *Geophys. Res. Lett.* **2001**, *28*, 3317–3320.

(5) Leung, D. Y. C.; Caramanna, G.; Maroto-Valer, M. M. An Overview of Current Status of Carbon Dioxide Capture and Storage Technologies. *Renew. Sustain. Energy Rev.* **2014**, *39*, 426–443.

(6) Gibbins, J.; Chalmers, H. Carbon Capture and Storage. *Energy Pol.* **2008**, *36* (12), 4317–4322.

(7) Hanna, R.; Abdulla, A.; Xu, Y.; Victor, D. G. Emergency Deployment of Direct Air Capture as a Response to the Climate Crisis. *Nat. Commun.* **2021**, *12* (1), 368.

(8) Sanz-Pérez, E. S.; Murdock, C. R.; Didas, S. A.; Jones, C. W. Direct Capture of CO₂ from Ambient Air. *Chem. Rev.* **2016**, *116* (19), 11840–11876.

(9) Keith, D. W.; Holmes, G.; St. Angelo, D.; Heide, K. A Process for Capturing CO₂ from the Atmosphere. *Joule* **2018**, *2* (8), 1573–1594.

(10) Rochelle, G. T. Amine Scrubbing for CO₂ Capture. *Science* **2009**, *325* (5948), 1652–1654.

(11) Mazari, S. A.; Si Ali, B.; Jan, B. M.; Saeed, I. M.; Nizamuddin, S. An Overview of Solvent Management and Emissions of Amine-Based CO₂ Capture Technology. *Int. J. Greenh. Gas Control* **2015**, *34*, 129–140.

(12) Jin, S.; Wu, M.; Gordon, R. G.; Aziz, M. J.; Kwabi, D. G. PH Swing Cycle for CO₂ Capture Electrochemically Driven through Proton-Coupled Electron Transfer. *Energy Environ. Sci.* **2020**, *13* (10), 3706–3722.

(13) Voskian, S.; Hatton, T. A. Faradaic Electro-Swing Reactive Adsorption for CO₂ Capture. *Energy Environ. Sci.* **2019**, *12* (12), 3530–3547.

(14) Sharifian, R.; Wagterveld, R. M.; Digdaya, I. A.; Xiang, C.; Vermaas, D. A. Electrochemical Carbon Dioxide Capture to Close the Carbon Cycle. *Energy Environ. Sci.* **2021**, *14* (2), 781–814.

(15) Ho, M. T.; Allinson, G. W.; Wiley, D. E. Reducing the Cost of CO₂ Capture from Flue Gases Using Pressure Swing Adsorption. *Ind. Eng. Chem. Res.* **2008**, *47*, 4883–4890.

(16) Siqueira, R. M.; Freitas, G. R.; Peixoto, H. R.; Nascimento, J. F. d.; Musse, A. P. S.; Torres, A. E. B.; Azevedo, D. C. S.; Bastos-Neto, M. Carbon Dioxide Capture by Pressure Swing Adsorption. *Energy Procedia* **2017**, *114*, 2182–2192.

(17) Kortekaas, L.; Browne, W. R. The Evolution of Spiropyran: Fundamentals and Progress of an Extraordinarily Versatile Photochrome. *Chem. Soc. Rev.* **2019**, *48* (12), 3406–3424.

(18) Klajn, R. Spiropyran-Based Dynamic Materials. *Chem. Soc. Rev.* **2014**, *43* (1), 148–184.

(19) Liao, Y. Design and Applications of Metastable-State Photoacids. *Acc. Chem. Res.* **2017**, *50* (8), 1956–1964.

(20) Wimberger, L.; Prasad, S. K. K.; Peeks, M. D.; Andréasson, J.; Schmidt, T. W.; Beves, J. E. Large, Tunable, and Reversible PH Changes by Merocyanine Photoacids. *J. Am. Chem. Soc.* **2021**, *143* (49), 20758–20768.

(21) Berton, C.; Busiello, D. M.; Zamuner, S.; Scopelliti, R.; Fadaei-Tirani, F.; Severin, K.; Pezzato, C. Light-Switchable Buffers. *Angew. Chem., Int. Ed.* **2021**, *60* (40), 21737–21740.

(22) Wimberger, L.; Andréasson, J.; Beves, J. E. Basic-to-Acidic Reversible PH Switching with a Merocyanine Photoacid. *Chem. Commun.* **2022**, *58* (37), 5610–5613.

(23) Adamczyk, K.; Prémont-Schwarz, M.; Pines, D.; Pines, E.; Nibbering, E. T. J. Real-Time Observation of Carbonic Acid Formation in Aqueous Solution. *Science* **2009**, *326* (5960), 1690–1694.

(24) Bennett, R.; Clifford, S.; Anderson, K.; Puxty, G. Carbon Capture Powered by Solar Energy. *Energy Proc.* **2017**, *114*, 1–6.

(25) Premadasa, U. I.; Bocharova, V.; Miles, A. R.; Stamberga, D.; Belony, S.; Bryantsev, V. S.; Elgattar, A.; Liao, Y.; Damron, J. T.; Kidder, M. K.; Doughty, B.; Custelcean, R.; Ma, Y.-Z. Photochemically-Driven CO₂ Release Using a Metastable-State Photoacid for Energy Efficient Direct Air Capture. *Angew. Chem., Int. Ed.* **2023**, *62* (29), No. e202304957.

(26) Berton, C.; Pezzato, C. Photoacidity of Indolinospirobenzopyrans in Water. *Eur. J. Org. Chem.* **2023**, *26* (17), No. e202300070.

(27) Berton, C.; Busiello, D. M.; Zamuner, S.; Solari, E.; Scopelliti, R.; Fadaei-Tirani, F.; Severin, K.; Pezzato, C. Thermodynamics and Kinetics of Protonated Merocyanine Photoacids in Water. *Chem. Sci.* **2020**, *11* (32), 8457–8468.

(28) Zeebe, R. E.; Wolf-Gladrow, D. CO₂ in Seawater: Equilibrium, Kinetics, Isotopes, 1st ed.; Elsevier, 2001.

(29) Barbee, M. H.; Mondal, K.; Deng, J. Z.; Bharambe, V.; Neumann, T. V.; Adams, J. J.; Boechler, N.; Dickey, M. D.; Craig, S. L. Mechanochromic Stretchable Electronics. *ACS Appl. Mater. Interfaces* **2018**, *10* (35), 29918–29924.

(30) Yang, H.; Hu, W.; Sun, C.; Ren, Y.; Qin, S.; Huang, J. Spiropyran Derivative with Color, Fluorescence and Liquid Crystal Property Triple Switching Effects as Well as Preparation Method and Application Thereof. China Patent CN 113024571 A, 2021.

(31) Wang, M.; Zhang, H.; Ji, L.; Fan, W.; Qiao, Z.; Si, Y.; Wang, Z.; Zheng, Y.; Xue, X.; Wu, X.; Liu, Y. Photochromic Optical Material. China Patent CN 107722028 A, 2018.

(32) Mohammed, O. F.; Pines, D.; Dreyer, J.; Pines, E.; Nibbering, E. T. J. Sequential Proton Transfer Through Water Bridges in Acid-Base Reactions. *Science* **2005**, *310* (5745), 83–86.

(33) Rini, M.; Magnes, B.-Z.; Pines, E.; Nibbering, E. T. J. Real-Time Observation of Bimodal Proton Transfer in Acid-Base Pairs in Water. *Science* **2003**, *301* (5631), 349–352.

(34) Mohammed, O. F.; Pines, D.; Nibbering, E. T. J.; Pines, E. Base-Induced Solvent Switches in Acid-Base Reactions. *Angew. Chem., Int. Ed.* **2007**, *46* (9), 1458–1461.

(35) Kaiser, C.; Halbritter, T.; Heckel, A.; Wachtveitl, J. Proton-Transfer Dynamics of Photoacidic Merocyanines in Aqueous Solution. *Chem.—Eur. J.* **2021**, *27* (35), 9160–9173.

(36) Aldaz, C. R.; Wiley, T. E.; Miller, N. A.; Abeyrathna, N.; Liao, Y.; Zimmerman, P. M.; Sension, R. J. Experimental and Theoretical Characterization of Ultrafast Water-Soluble Photochromic Photoacids. *J. Phys. Chem. B* **2021**, *125* (16), 4120–4131.

(37) Winstein, S.; Clippinger, E.; Fainberg, A. H.; Heck, R.; Robinson, G. C. Salt Effects and Ion Pairs in Solvolysis and Related Reactions. III.¹ Common Ion Rate Depression and Exchange of Anions during Acetolysis.^{2,3} *J. Am. Chem. Soc.* **1956**, *78* (2), 328–335.

(38) Bentley, T. W.; von R. Schleyer, P. Medium Effects on the Rates and Mechanisms of Solvolytic Reactions. *Advances in Physical Organic Chemistry*; Gold, V., Ed.; Academic Press, 1977; Vol. 14, pp 1–67..

Supporting Information for

Reversible CO₂ Capture and On-Demand Release by an Acidity-Matched Organic Photoswitch

Abdulrahman M. Alfaraidi,^a Bryan Kudisch,^a Nina Ni,^a Jayden Thomas,^a Thomas Y. George,^b
Khashayar Rajabimoghadam,^a Haihui Joy Jiang,^a Daniel G. Nocera,^a Michael J. Aziz,^b Richard Y. Liu^{a,*}

^aDepartment of Chemistry and Chemical Biology, Harvard University, Cambridge, MA 02138, USA

^bHarvard John A. Paulson School of Engineering and Applied Sciences, Cambridge, MA 02138, USA

*E-mail: richardliu@chemistry.harvard.edu

Contents

Materials and Methods.....	3
1. General Information for Materials and Analytical Methods.....	3
2. Synthesis.....	4
2.1. Synthesis of Precursors.....	4
2.2. Synthesis of Spiropyrans.....	4
3. UV-Vis Spectroscopy Studies.....	8
3.1. Determination of Apparent Conjugate Acidity ($pK_{aH'}$).....	8
3.2. UV-Vis Absorption Study of CO ₂ Response.....	13
3.3. Solvent Effects.....	16
3.4. Solubility Measurements.....	17
4. CO₂ Capture and Release	23
4.1. Experimental Setup.....	23
4.2. Gas Chromatography Analysis	27
4.3. <i>In Situ</i> pH Tracking	28
4.4. Stability of SP4	32
5. Ultrafast Transient Absorption Studies	33
5.1. Methods.....	33
5.2. Additional Data	35
6. Computational Chemistry.....	39
6.1. General Methods	39
6.2. Structures and UV-Vis Spectra of Relevant Species	39
6.3. Geometries and Energies of Minimized Structures.....	41
7. Additional Discussion of Thermodynamic Model.....	46
8. NMR Spectra of Compounds	49
SI References	65

Materials and Methods

1. General Information for Materials and Analytical Methods

Unless noted, all chemicals were obtained from reagent-grade commercial sources (MilliporeSigma, Combi-Blocks, Oakwood, Alfa Aesar, TCI, or Ambeed), stored at rt under nitrogen, and used without further purification. Iodomethane was stored at 4 °C in a refrigerator. Products of chemical reactions were purified by flash chromatography using SiliCycle SiliaFlash® F60 Irregular Silica Gel (40-63 μm , 230–400 mesh) as the stationary phase with the aid of a Biotage® Selekt Enkel Automated Flash Chromatography System. All solutions were prepared using high-purity (HPLC-grade) organic solvents and ultrapure water (18.2 $\text{M}\Omega\cdot\text{cm}$). pH measurements were performed on an Oakton pH 700 Benchtop Meter with a Mettler Toledo Micro pH Electrode LE422. Ultraviolet-visible (UV-Vis) absorption spectral data were obtained on an Agilent Cary 60 UV-Vis Spectrophotometer. The syringes used were NORM-JECT-F Luer Solo syringes equipped with BD PrecisionGlide Needles (18G x 1 1/2" TW) or Air-Tite Premium Hypodermic Needles (22G x 3" LB). ESI-HRMS (electrospray ionization) spectrometric data were recorded on a Bruker micrOTOF II mass spectrometer with ESI probe.

^1H and ^{13}C NMR spectra were recorded on a Bruker AVANCE NEO 400 or Bruker AVANCE NEO 400B instrument. ^1H and ^{13}C chemical shifts were calibrated using residual protonated solvent as an internal reference (CHCl_3 : δ 7.26 ppm and δ 77.16 ppm, respectively; DMSO: δ 2.50 ppm and δ 39.52 ppm, respectively). Broadband ^1H decoupling was used during the collection of ^{13}C . The following abbreviations are used to denote multiplicities: s = singlet, bs = broad singlet, d = doublet, t = triplet, q = quartet, p = pentet, and m = multiplet.

2. Synthesis

2.1. Synthesis of Precursors

2,3,3-Trimethyl-3*H*-indole-5-carbonitrile

Based on a literature procedure,³⁹ to an oven-dried 100 mL round-bottom flask, equipped with a magnetic stir bar, was added 3-methyl-2-butanone (1.23 mL, 0.99 g, 11.46 mmol, 2.00 equiv) using a 1 mL syringe with BD PrecisionGlide needle, followed by glacial acetic acid (18.30 mL) using a 10 mL syringe with Air-Tite needle. After stirring to ensure the mixture was fully dissolved, 4-cyanophenylhydrazine hydrochloride (1.00 g, 5.73 mmol, 1.00 equiv) was added. The round-bottom flask was attached to the bottom of a Liebig condenser and the joint was secured with a Keck clamp. The round-bottom flask was then submerged into a preheated oil bath, and the mixture was stirred at reflux overnight before it was allowed to cool to rt by removing the oil bath. The crude material that formed was then suspended in chloroform and poured into a 250 mL separatory funnel containing chloroform (50 mL) and water (50 mL). The organic phase was separated, and the aqueous phase was extracted twice more with equal quantities of chloroform. The organic phases were combined and dried over Na₂SO₄, and then filtered. The filtrate was then concentrated with the aid of a rotary evaporator and purified by flash column chromatography on silica gel, using hexane/EtOAc (80:20) as the eluent to afford the title product (0.21 g, 26%). ¹H NMR (400 MHz, DMSO-*d*₆) δ 8.21 (d, *J* = 1.7 Hz, 1H), 8.00 (dd, *J* = 8.0, 1.7 Hz, 1H), 7.83 (d, *J* = 8.0 Hz, 1H), 1.51 (s, 6H).

5-Cyano-1,2,3,3-tetramethyl-3*H*-indolium iodide

Based on a literature procedure,⁴⁰ to an oven-dried 100 mL round-bottom flask, equipped with a magnetic stir bar, was sequentially added 2,3,3-trimethyl-3*H*-indole-5-carbonitrile (270 mg, 1.47 mmol, 1.00 equiv), iodomethane (0.18 mL, 2.93 mmol, 2.00 equiv) using a 1 mL syringe with Air-Tite needle, and acetonitrile (5.13 mL) using a 1 mL syringe with Air-Tite needle. After stirring to ensure the mixture was fully dissolved, the round-bottom flask was attached to the bottom of a Liebig condenser and the joint was secured with a Keck clamp. The round-bottom flask was then submerged into a preheated oil bath, and the mixture was stirred at reflux overnight before it was allowed to cool to rt by removing the oil bath. EtOAc (25 mL) was then added to the crude mixture to precipitate the material. The solid was collected by filtration and washed with EtOAc to afford the title compound (0.149 g, 51%). ¹H NMR (400 MHz, DMSO-*d*₆) δ 7.63 – 7.50 (m, 2H), 6.82 (d, *J* = 8.2 Hz, 1H), 4.06 (d, *J* = 9.6 Hz, 3H), 3.05 (s, 3H), 1.29 (s, 6H).

2.2. Synthesis of Spiropyrans

General Procedure 1 (GP1): Synthesis of SP1–5

Based on a literature procedure,⁴¹ to an oven-dried 100 mL round-bottom flask, equipped with a magnetic stir bar, was sequentially added the indolium iodide (1.00 equiv), 2-hydroxyaryl aldehyde (1.00 equiv), an

aqueous solution of 40 wt% choline hydroxide (1.50 equiv) using a 1 mL syringe with BD PrecisionGlide needle, and isopropanol (2.5 mL/mmol) using a 10 mL syringe with Air-Tite needle. After stirring to ensure mixture was fully dissolved, the round-bottom flask was then submerged into a preheated oil bath. The mixture was stirred at 80 °C overnight, then allowed to cool to rt by removing the oil bath. The crude mixture was poured into a 250 mL separatory funnel containing ethyl acetate (50 mL) and water (50 mL). The organic phase was separated, and the aqueous phase was extracted twice more equal quantities of ethyl acetate. The organic phases were combined and concentrated with the aid of a rotary evaporator. The residue was purified by flash column chromatography on silica gel, using hexane/EtOAc as the eluent to afford the spiropyran.

Choline hydroxide

Following a literature procedure,⁴¹ to an oven-dried 500 mL round-bottom flask, equipped with a magnetic stir bar, was sequentially added choline chloride (2.79 g, 20 mmol, 1.00 equiv), potassium hydroxide (1.12 g, 20 mmol, 1.00 equiv), and methanol (200 mL). The round-bottom flask was then capped with a septum and submerged into a preheated oil bath. The mixture stirred at 60 °C for 12 h before it was allowed to cool to rt by removing the oil bath. KCl was removed by filtration, and the filtrate was concentrated with the aid of a rotary evaporator. The resulting material was diluted with distilled water to a concentration of 40 wt%.

SP1: Yellow solid, yield: 72%; ¹H NMR (400 MHz, CDCl₃) δ 7.18 (td, *J* = 7.6, 1.4 Hz, 1H), 7.11 – 7.07 (m, 2H), 7.05 (dd, *J* = 7.5, 1.6 Hz, 1H), 6.87 – 6.80 (m, 3H), 6.72 (d, *J* = 8.1 Hz, 1H), 6.53 (d, *J* = 7.8 Hz, 1H), 5.68 (d, *J* = 10.1 Hz, 1H), 2.74 (s, 3H), 1.32 (s, 3H), 1.18 (s, 3H). ¹³C NMR (101 MHz, CDCl₃) δ 154.6, 148.4, 137.0, 129.8, 129.5, 127.7, 126.8, 121.6, 120.1, 119.5, 119.2, 118.9, 115.1, 106.9, 104.3, 51.9, 29.1, 26.0, 20.3. HRMS calculated for C₁₉H₂₀NO [M + H]⁺ 278.1500 amu; found 278.1490 amu.

SP2: Light pink solid, yield: 75%; ¹H NMR (400 MHz, DMSO-*d*₆) δ 6.99 – 6.93 (m, 2H), 6.84 (s, 1H), 6.82 (d, *J* = 7.9 Hz, 1H), 6.76 (dd, *J* = 8.6, 2.7 Hz, 1H), 6.63 (td, *J* = 7.4, 1.1 Hz, 1H), 6.43 (d, *J* = 5.0 Hz, 1H), 6.41 (d, *J* = 4.4 Hz, 1H), 5.60 (d, *J* = 10.1 Hz, 1H), 3.19 (s, 3H), 2.06 (s, 3H), 1.07 (s, 3H), 0.95 (s, 3H). ¹³C NMR (101 MHz, CDCl₃) δ 152.5, 148.4, 137.0, 130.3, 129.5, 129.2, 127.7, 127.1, 121.6, 119.5, 119.1, 118.6, 114.8, 106.9, 104.1, 51.8, 29.9, 29.1, 26.00, 20.3. HRMS calculated for C₂₀H₂₂NO [M + H]⁺ 292.1657 amu; found 292.1655 amu.

SP3: Light pink solid, yield: 66%; ¹H NMR (400 MHz, CDCl₃) δ 7.15 (td, *J* = 7.6, 1.4 Hz, 1H), 7.06 (dd, *J* = 7.2, 1.4 Hz, 1H), 6.86 – 6.80 (m, 2H), 6.76 (d, *J* = 5.1 Hz, 2H), 6.69 (dd, *J* = 5.1, 4.1 Hz, 1H), 6.50 (d, *J* = 7.8 Hz, 1H), 5.67 (d, *J* = 10.1 Hz, 1H), 3.67 (s, 3H), 2.75 (s, 3H), 1.31 (s, 3H), 1.17 (s, 3H). ¹³C NMR

(101 MHz, CDCl₃) δ 148.3, 147.2, 144.1, 136.9, 129.3, 127.6, 121.6, 112.0, 119.8, 119.7, 119.4, 119.0, 114.3, 106.8, 104.4, 56.7, 51.8, 29.0, 25.9, 20.5. **HRMS** calculated for C₂₀H₂₂NO₂ [M + H]⁺ 308.1606 amu; found 308.1609 amu.

SP4: Light orange solid, yield: 70%; **¹H NMR** (400 MHz, CDCl₃) δ 7.17 (td, J = 7.6, 1.3 Hz, 1H), 7.07 (dd, J = 7.3, 0.8 Hz, 1H), 6.86–6.79 (m, 2H), 6.69–6.63 (m, 2H), 6.61 (d, J = 2.6 Hz, 1H), 6.52 (d, J = 7.8 Hz, 1H), 5.70 (d, J = 10.3 Hz, 1H), 3.76 (s, 3H), 2.73 (s, 3H), 1.31 (s, 3H), 1.16 (s, 3H). **¹³C NMR** (101 MHz, CDCl₃) δ 153.2, 148.7, 148.4, 137.0, 129.4, 127.7, 121.6, 120.4, 119.2, 119.1, 115.6, 115.4, 111.6, 106.9, 104.0, 55.9, 51.8, 29.1, 26.0, 20.4. **HRMS** calculated for C₂₀H₂₂NO₂ [M + H]⁺ 308.1606 amu; found 308.1602 amu.

SP5: Pink solid, yield: 63%; **¹H NMR** (400 MHz, CDCl₃) δ 7.16 (td, J = 7.6, 1.3 Hz, 1H), 7.06 (dd, J = 7.3, 1.4 Hz, 1H), 6.82 (td, J = 7.4, 1.1 Hz, 1H), 6.81 (d, J = 10.5 Hz, 1H), 6.66–6.58 (m, 2H), 6.55–6.48 (m, 2H), 5.68 (d, J = 10.1 Hz, 1H), 2.85 (s, 6H), 2.72 (s, 3H), 1.31 (s, 3H), 1.16 (s, 3H). **¹³C NMR** (101 MHz, CDCl₃) δ 148.5, 147.2, 145.2, 137.1, 129.9, 127.6, 121.6, 120.1, 119.04, 119.02, 115.8, 115.4, 112.2, 106.8, 103.8, 51.6, 42.1, 29.1, 26.0, 20.4. **HRMS** calculated for C₂₁H₂₅N₂O [M + H]⁺ 321.1922 amu; found 321.1922 amu.

1',3'-Dihydro-6-methoxy-1',3',3'-trimethylspiro[2H-1-benzopyran-2,2'-[2H]indole]-5'-carbonitrile (SP6)

To an oven-dried 100 mL round-bottom flask, equipped with a magnetic stir bar, was added 5-cyano-1,2,3,3-tetramethyl-3H-indolium iodide (200 mg, 0.664 mmol, 1.00 equiv) followed by *n*-propanol (3.32 mL) using a 1 mL syringe with Air-Tite needle. After stirring to ensure the mixture was fully dissolved, 2-hydroxy-5-methoxybenzaldehyde (0.09 mL, 0.73 mmol, 1.10 equiv) and piperidine (0.08 mL, 0.80 mmol, 1.20 equiv) were both added into the flask using a 1 mL syringe with BD Precision Glide needle. The round-bottom flask was attached to the bottom of a Liebig condenser and joint was secured with a Keck clamp. The round-bottom flask was then submerged into a preheated oil bath, and the mixture was stirred at reflux for 19 h before it was allowed to cool to rt by removing the oil bath. The crude mixture was concentrated with the aid of a rotary evaporator and purified by flash column chromatography on silica gel, using hexane/EtOAc (90:10) as the eluent to afford the title compound as an orange solid (72 mg, 33%). **¹H NMR** (400 MHz, CDCl₃) δ 7.48 (dd, J = 8.1, 1.8 Hz, 1H), 7.26 (d, J = 1.6 Hz, 1H), 6.86 (d, J = 9.9 Hz, 1H), 6.69 (d, J = 2.9 Hz, 1H), 6.65–6.62 (m, 2H), 6.49 (d, J = 8.1 Hz, 1H), 5.67 (d, J = 10.1 Hz, 1H), 3.76 (s, 3H), 2.78 (s, 3H), 1.30 (s, 3H), 1.16 (s, 3H). **¹³C NMR** (101 MHz, CDCl₃) δ 153.6, 151.6, 148.0, 137.9,

133.7, 130.2, 125.3, 119.0, 118.8, 115.7, 115.7, 111.8, 106.6, 103.7, 101.0, 66.0, 55.9, 51.4, 28.8, 25.8, 20.1. **HRMS** calculated for $C_{21}H_{21}N_2O_2$ $[M + H]^+$ 333.1558 amu; found 333.1541 amu.

General Procedure 2 (GP2): Synthesis of SP7 and SP8

Based on a literature procedure,⁴² to an oven-dried 100 mL round-bottom flask, equipped with a magnetic stir bar, was sequentially added 2,3,3-trimethyl-3*H*-indole (1.00 equiv), 1,3-propanesultone (1.71 equiv), and acetonitrile (3.45 mL/mmol). After stirring to ensure the mixture was fully dissolved, the round-bottom flask was attached to the bottom of a Liebig condenser and joint was secured with a Keck clamp. The round-bottom flask was then submerged into a preheated oil bath, and the solution was stirred at reflux for 16 h before it was allowed to cool to rt by removing the oil bath. Ethyl acetate was added dropwise while stirring continued, resulting in precipitation. The solid was collected by filtration and washed with ethyl acetate and recrystallized from hot acetonitrile to afford 1-sulfopropyl-2,3,3-trimethyl-3*H*-indolium. In an oven-dried 100 mL round-bottom flask, the corresponding salicylaldehyde (2.00 equiv) was added to a solution of 1-sulfopropyl-2,3,3-trimethyl-3*H*-indolium (1.00 equiv) dissolved in EtOH (ca. 20 mL/g). The solution was degassed by bubbling N_2 , then heated at 90 °C for 24 h by submersion into a preheated oil bath. Upon cooling to rt by removal of the oil bath, the resulting precipitate was filtered, washed with EtOH, and recrystallized from hot MeOH. The resulting crystals were collected and washed with MeOH and dried in vacuum to afford the desired spiropyran.

SP7: Orange solid, yield: 64%; **¹H NMR** (400 MHz, DMSO-*d*₆) δ 10.31 (s, 1H), 8.65 (d, *J* = 16.4 Hz, 1H), 8.02 (dd, *J* = 6.9, 2.2 Hz, 1H), 7.90 (dd, *J* = 8.3, 1.4 Hz, 1H), 7.88 – 7.86 (m, 1H), 7.86 – 7.80 (m, 1H), 7.67 – 7.56 (m, 2H), 7.22 (dd, *J* = 8.1, 1.4 Hz, 1H), 6.95 (t, *J* = 8.1 Hz, 1H), 4.81 (t, *J* = 7.9 Hz, 2H), 3.88 (s, 3H), 2.65 (t, *J* = 6.4 Hz, 2H), 2.25 – 2.10 (m, 2H), 1.77 (s, 6H). **¹³C NMR** (101 MHz, DMSO-*d*₆) δ 181.7, 148.5, 148.3, 148.1, 143.5, 140.9, 129.16 [2C], 123.0, 121.6, 120.2, 119.7, 116.6, 115.1, 111.64, 56.2, 51.9, 47.3, 45.5, 26.5, 24.6. **HRMS** calculated for $C_{22}H_{26}NO_5S$ $[M + H]^+$ 416.1487 amu; found 416.1500 amu.

SP8: Red solid, yield: 67%; **¹H NMR** (400 MHz, DMSO-*d*₆) δ 10.60 (s, 1H), 8.60 (d, *J* = 16.4 Hz, 1H), 7.99 (dd, *J* = 7.1, 2.2 Hz, 1H), 7.95 (d, *J* = 16.4 Hz, 1H), 7.87 – 7.84 (m, 1H), 7.83 (d, *J* = 3.0 Hz, 1H), 7.65 – 7.58 (m, 2H), 7.10 (dd, *J* = 8.9, 3.0 Hz, 1H), 6.96 (d, *J* = 9.0 Hz, 1H), 4.85 (t, *J* = 7.9 Hz, 2H), 3.87 (s, 3H), 2.64 (t, *J* = 6.2 Hz, 2H), 2.25 – 2.15 (m, 2H), 1.77 (s, 6H). **¹³C NMR** (101 MHz, DMSO-*d*₆) δ 181.6, 153.8, 152.9, 148.3, 143.5, 140.9, 129.1, 129.0, 124.8, 123.0, 121.3, 117.8, 114.9, 111.3, 110.4, 56.3, 51.8, 47.0, 45.3, 26.5, 24.6. **HRMS** calculated for $C_{22}H_{26}NO_5S$ $[M + H]^+$ 416.1487 amu; found 416.1503 amu.

3. UV-Vis Spectroscopy Studies

3.1. Determination of Apparent Conjugate Acidity (pK_{aH}')

120 μ M stock solutions of **SP** were prepared in the organic solvent of interest. These stock solutions were diluted with MilliQ water, and the pH was adjusted accordingly with dilute HCl or KOH to a range of target pH values and a precise final concentration of 60 μ M. The final pH values of these samples were measured after letting the samples equilibrate in the dark for 10 mins. UV-Vis spectra were acquired, and the pK_{aH}' was determined according to the spectrophotometric method described in the literature,⁴³ in which the equilibrium absorbance values (A_{eq}) of at the maximum absorption wavelength of **MCH**⁺ were plotted against pH and fitted to a sigmoidal curve. These curves were fitted using GraphPad Prism according to:

$$A_{eq} = A_{OH} + \frac{A_H - A_{OH}}{1 + 10^{((pH - pK_{aH}') * C)}} \quad (\text{Eq.S1})$$

in which:

A_{OH} : absorbance at high pH

A_H : absorbance at low pH

pK_{aH}' : inflection mid-point

C : Hill slope

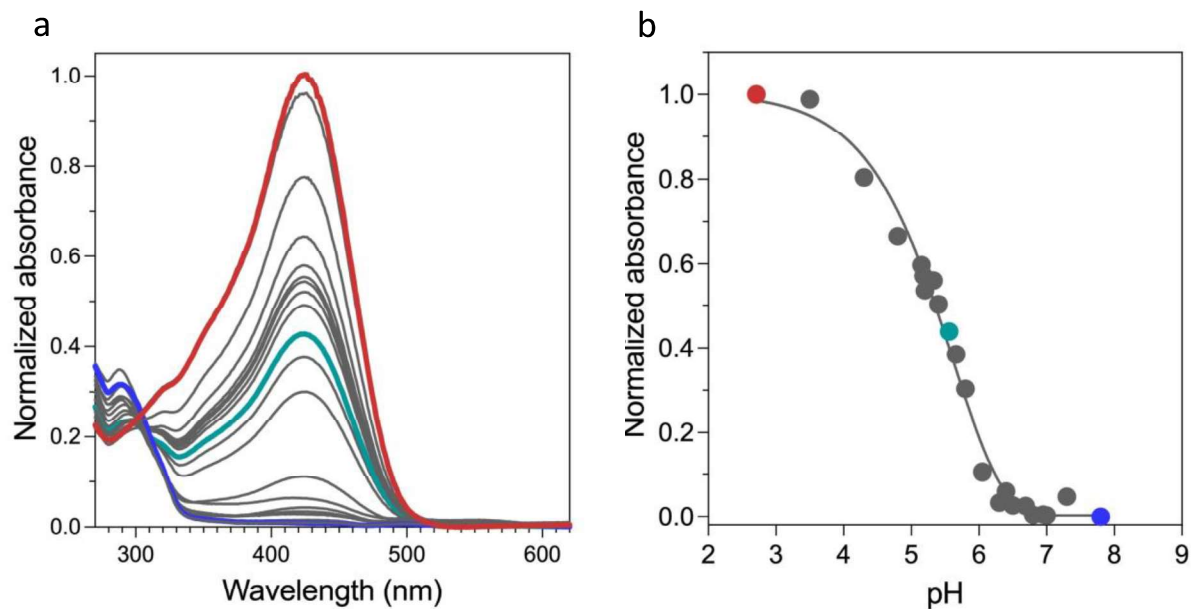


Figure S1. UV-Vis titration of 60 μM **SP1** in 1:1 DMSO/water. a) Normalized absorbance spectra at different pH values in the dark. b) Absorbance of **MCH1⁺** ($\lambda = 424$ nm) as a function of pH and its corresponding sigmoidal fit to Eq. S1 shown as a solid curve. The Hill slope C is -0.91.

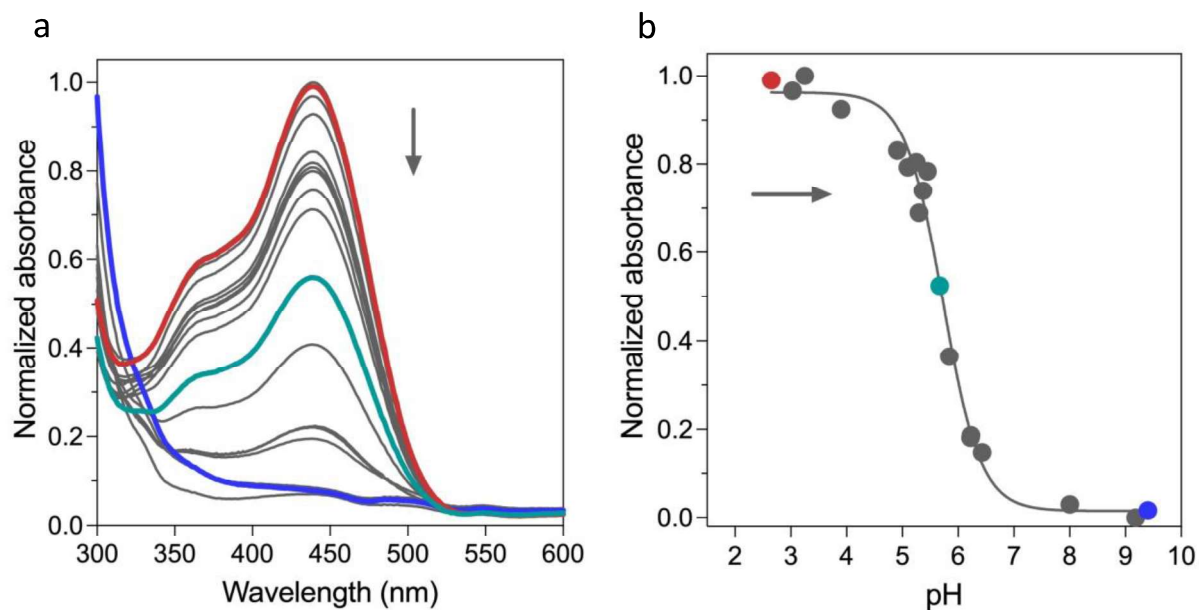


Figure S2. UV-Vis titration of 60 μM **SP2** in 1:1 DMSO/water. a) Normalized absorbance spectra at different pH values in the dark. b) Absorbance of **MCH2⁺** ($\lambda = 438$ nm) as a function of pH and its corresponding sigmoidal fit to Eq. S1 shown as a solid curve. The Hill slope C is -1.25.

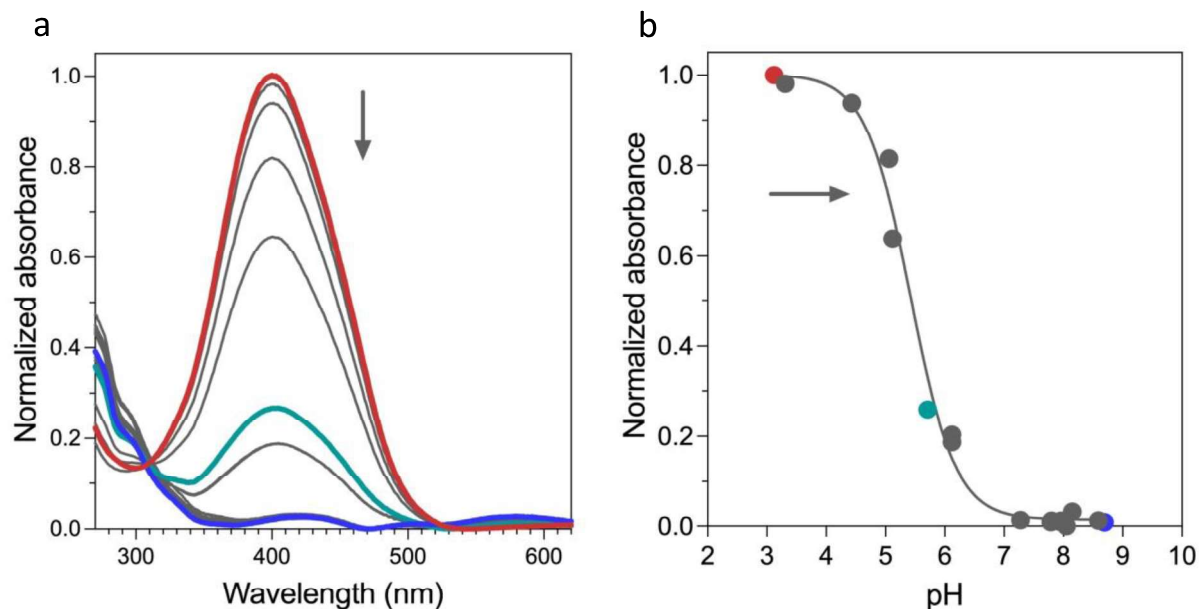


Figure S3. UV-Vis titration of 60 μM SP3 in 1:1 DMSO/water. a) Normalized absorbance spectra at different pH values in the dark. b) Absorbance of MCH3^+ ($\lambda = 401$ nm) as a function of pH and its corresponding sigmoidal fit to Eq. S1 shown as a solid curve. The Hill slope C is -1.14.

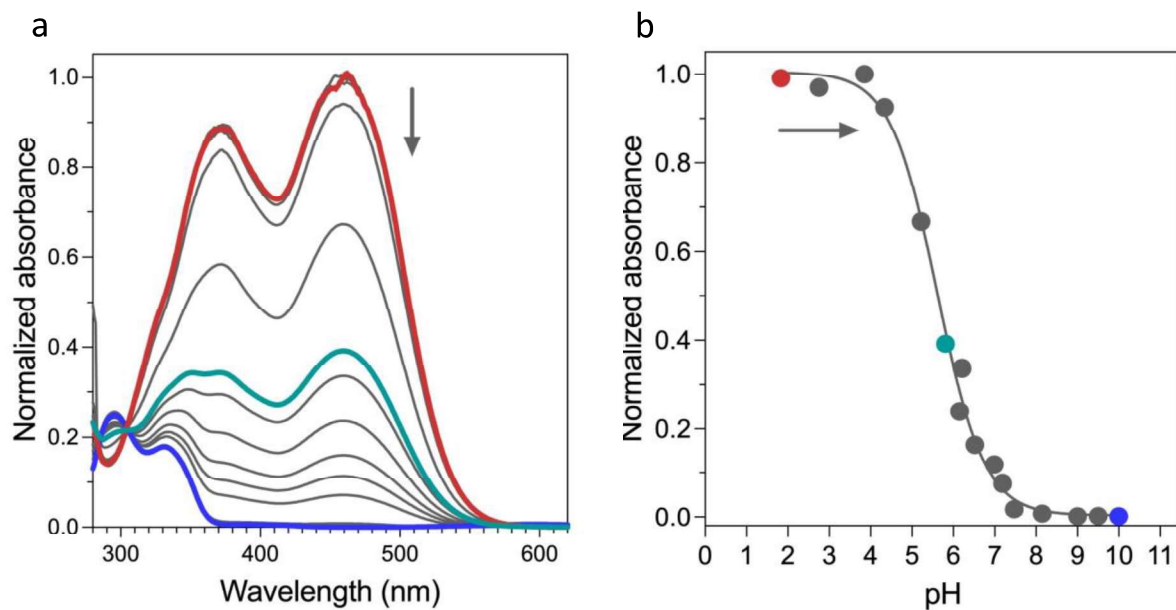


Figure S4. UV-Vis titration of 60 μM SP4 in 1:1 DMSO/water. a) Normalized absorbance spectra at different pH values in the dark. b) Absorbance of MCH4^+ ($\lambda = 460$ nm) as a function of pH and its corresponding sigmoidal fit to Eq. S1 shown as a solid curve. The Hill slope C is -1.04.

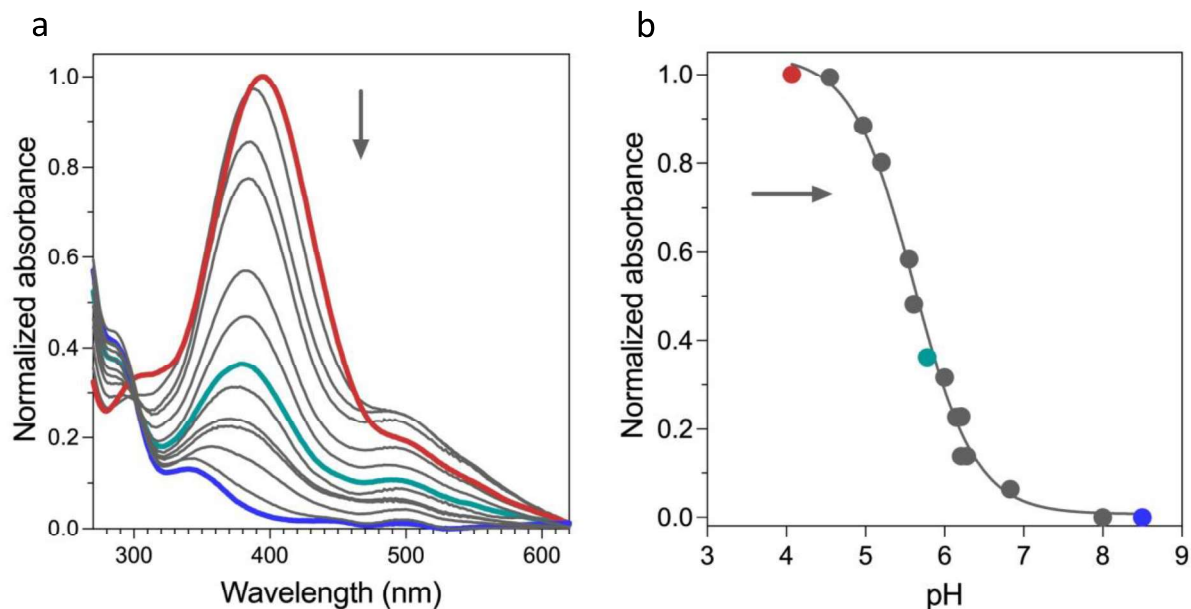


Figure S5. UV-Vis titration of 60 μM SP5 in 1:1 DMSO/water. a) Normalized absorbance spectra at different pH values in the dark. b) Absorbance of MCH5^+ ($\lambda = 388$ nm) as a function of pH and its corresponding sigmoidal fit to Eq. S1 shown as a solid curve. The Hill slope C is -1.12.

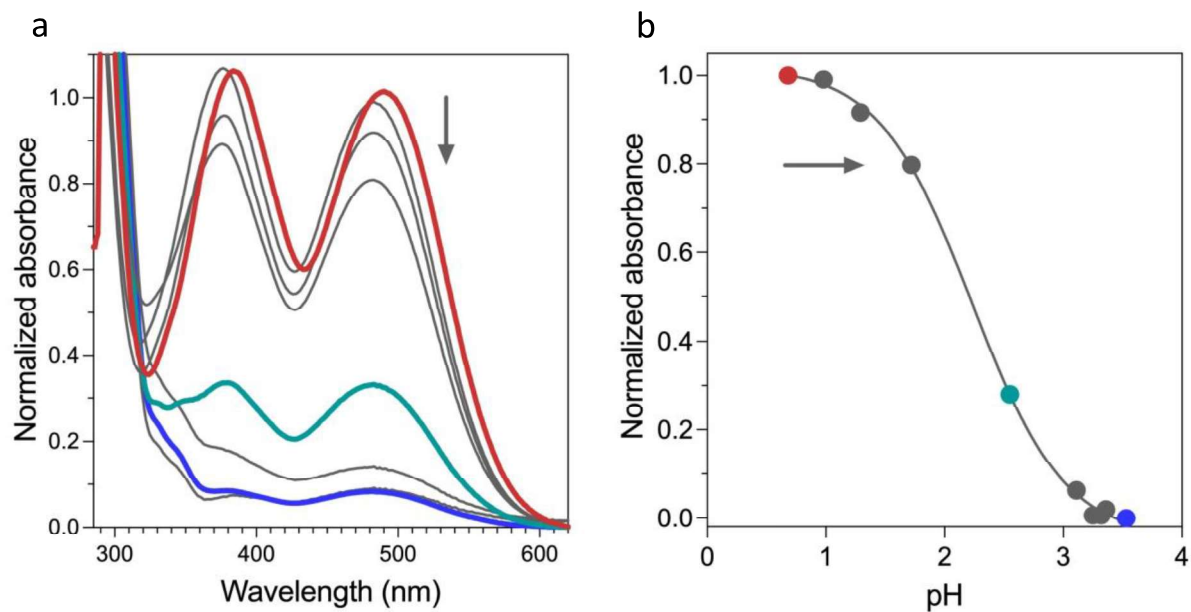


Figure S6. UV-Vis titrations of 60 μM SP6 in 1:1 DMSO/water. a) Normalized absorbance spectra at different pH values in the dark. b) Absorbance of MCH6^+ ($\lambda = 482$ nm) as a function of pH and its corresponding sigmoidal fit to Eq. S1 shown as a solid curve. The Hill slope C is -1.21.

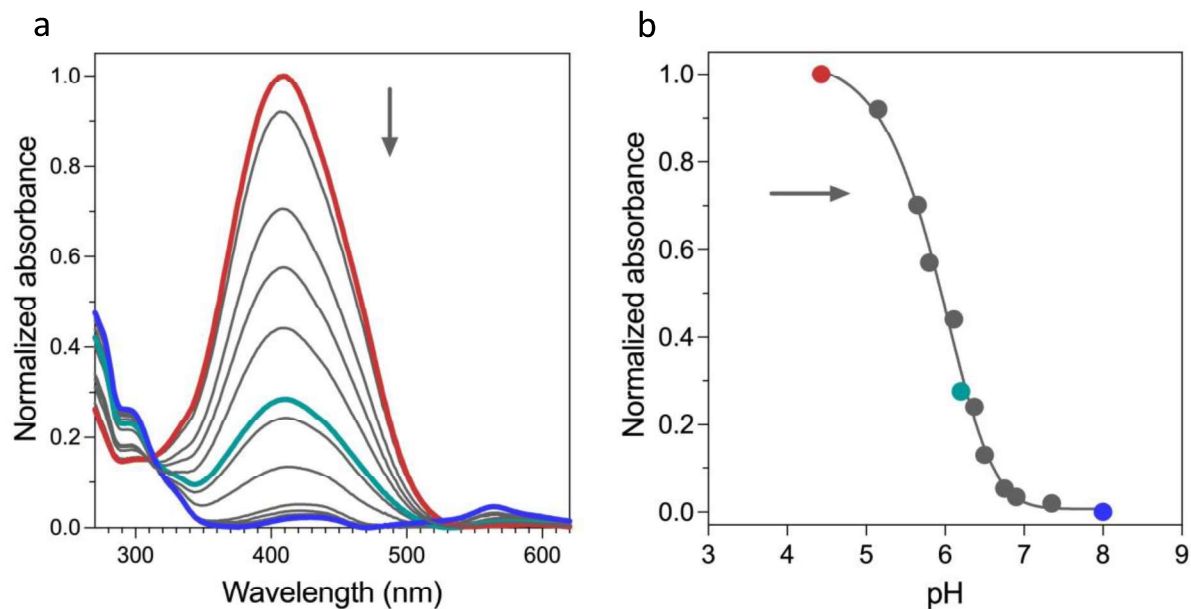


Figure S7. UV-Vis titration of 60 μM **SP7** in 1:1 DMSO/water. a) Normalized absorbance spectra at different pH values in the dark. b) Absorbance of **MCH7⁺** ($\lambda = 396$ nm) as a function of pH and its corresponding sigmoidal fit to Eq. S1 shown as a solid curve. The Hill slope C is -1.26.

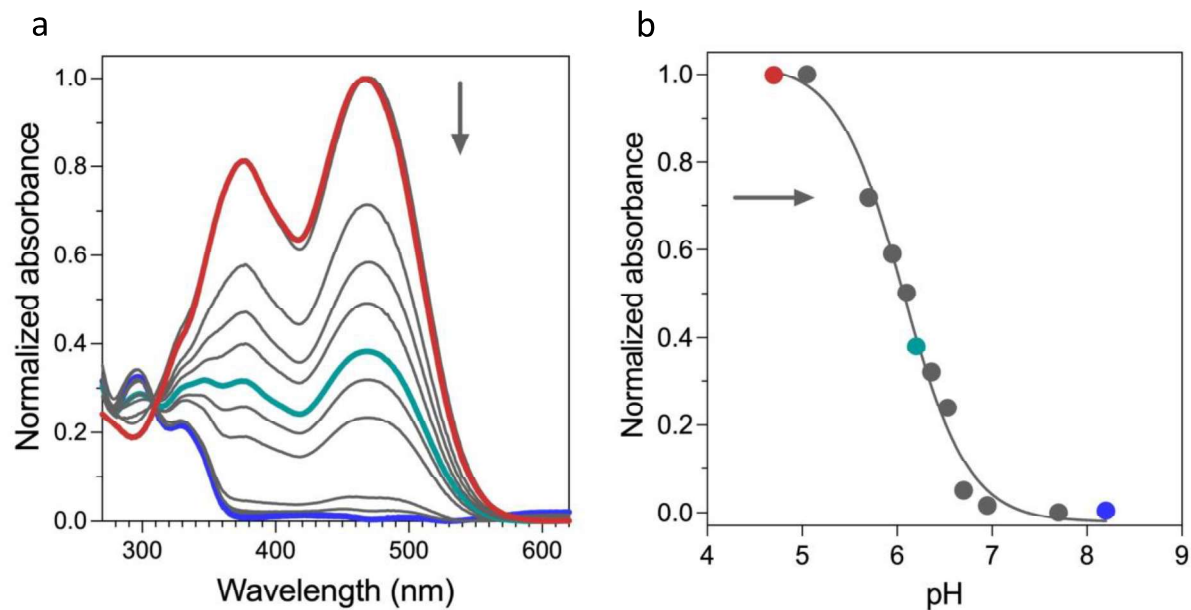


Figure S8. UV-Vis titration of 60 μM **SP8** in 1:1 DMSO/water. a) Normalized absorbance spectra at different pH values in the dark. b) Absorbance of **MCH8⁺** ($\lambda = 468$ nm) as a function of pH and its corresponding sigmoidal fit to Eq. S1 shown as a solid curve. The Hill slope C is -1.27.

3.2. UV-Vis Absorption Study of CO₂ Response

120 μ M stock solutions of **SP** were prepared in the organic solvent of interest. These stock solutions were diluted with MilliQ water to a final concentration of 60 μ M and loaded into a 1 cm path-length cuvette. The UV-Vis absorption spectrum of this initial state was acquired. Then, CO₂ or a CO₂-containing gas mixture was bubbled through the solution for a controlled duration of time in the dark. The UV-Vis absorption spectrum was recorded at time points. With the CO₂ source removed, the sample was then irradiated with a 450 nm blue LED, and the UV-Vis absorption spectrum was recorded after different durations. During irradiation, the sample was cooled by air with a portable fan to ensure minimal heat contribution to release. In some cases, the original spectrum was not exactly reproduced after the cycle of experiments above, but some slight photobleaching was observed. We have not been able to observe significant amounts of byproducts by TLC nor was any precipitate visible in the vial.

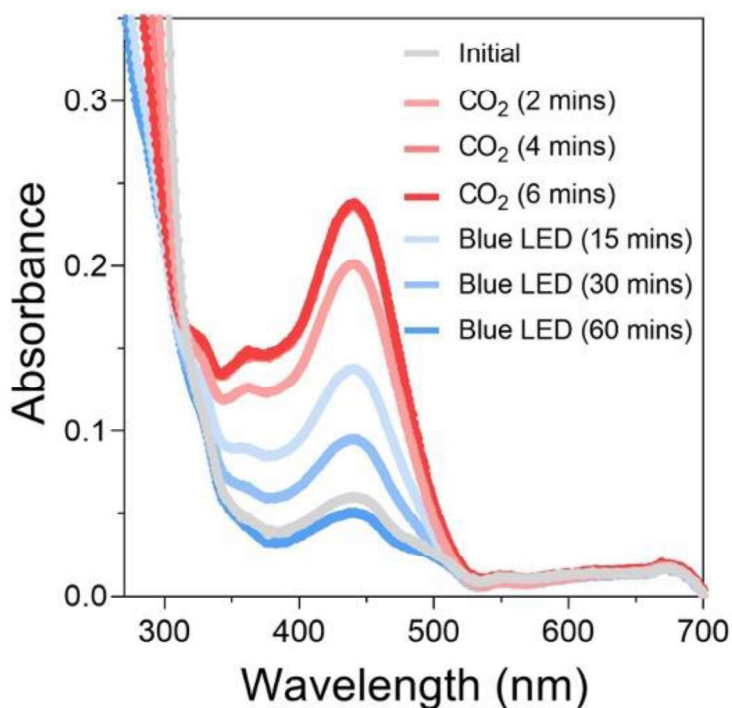


Figure S9. CO₂ response followed by 450 nm blue LED irradiation of 60 μ M **SP2** in 1:1 DMSO/water.

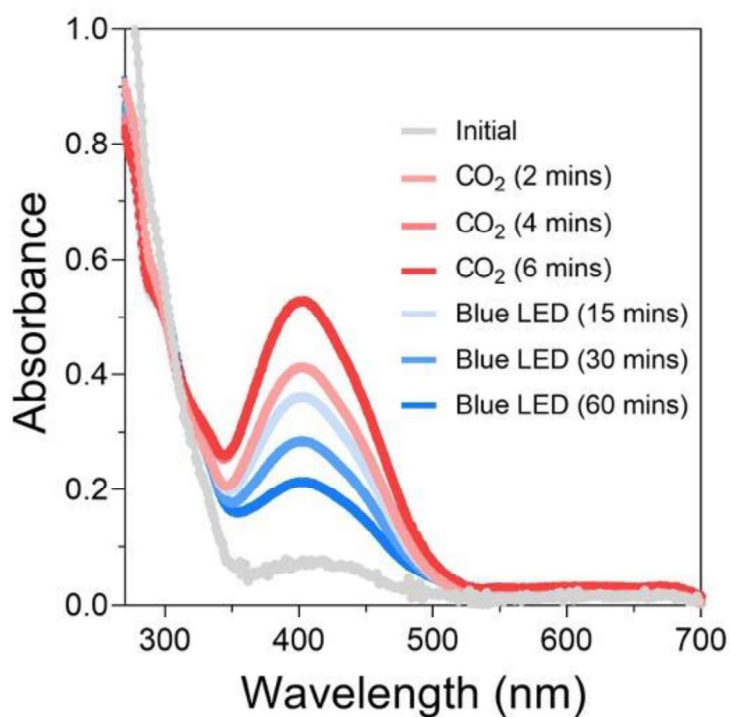


Figure S10. CO₂ response followed by 450 nm blue LED irradiation of 60 μM **SP3** in 1:1 DMSO/water.

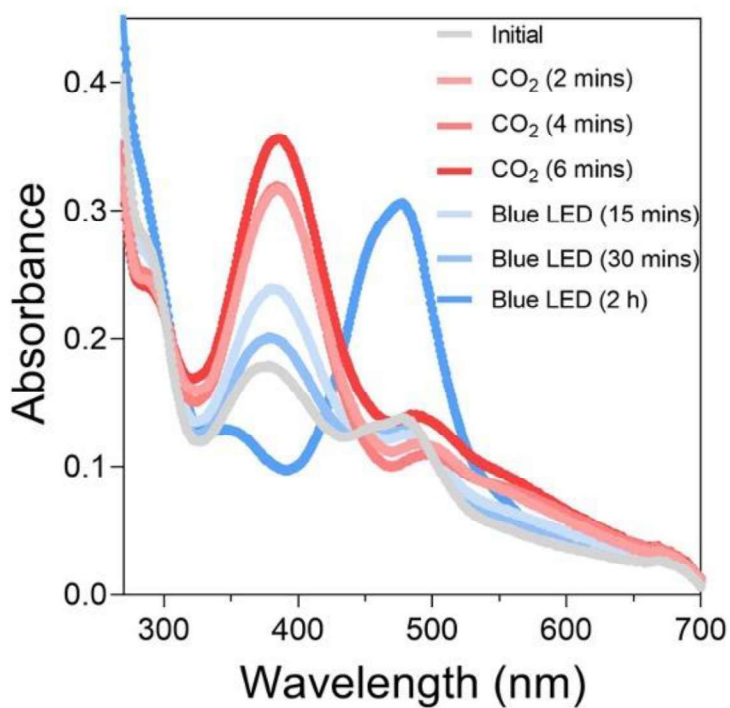


Figure S11. CO₂ response followed by 450 nm blue LED irradiation of 60 μM **SP5** in 1:1 DMSO/water. Longer irradiation led to irreversible decomposition.

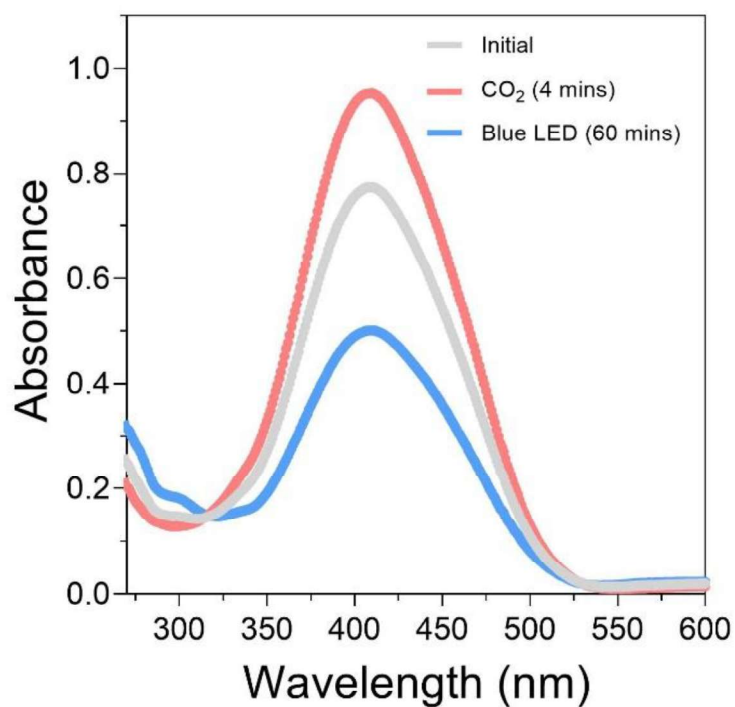


Figure S12. CO₂ response followed by 450 nm blue LED irradiation of 60 μ M **SP7** in 1:1 DMSO/water.

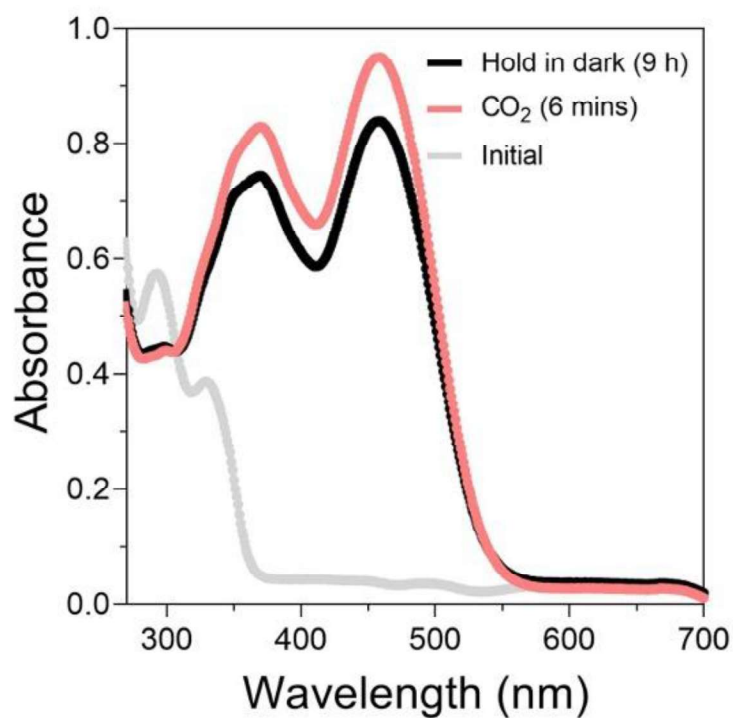


Figure S13. CO₂ retention in solution in the dark over 9 h (60 μ M **SP4** in 1:1 DMSO/water). Thermal release in the dark is very slow.

3.3. Solvent Effects

Medium effects exert a substantial influence over the initial equilibrium of spiropyran and the identity of the ground state. Other factors such as kinetics, solubility, and response to CO_2 were sensitive to the identity and proportion of the organic solvent. We chose DMSO–water as the solvent system for most of our study because of the fast, reversible interconversion between the **SP** and **MCH**⁺. Further, by adjusting the solvent composition, we could increase the solubility of **SP4** up to 27 mM without much effect on the apparent conjugate acidity nor the kinetics of release (see the transient absorption studies). Very recently, others have also found that DMSO-water mixtures can enable robust stability of light-induced proton release and isomerization.⁴⁴

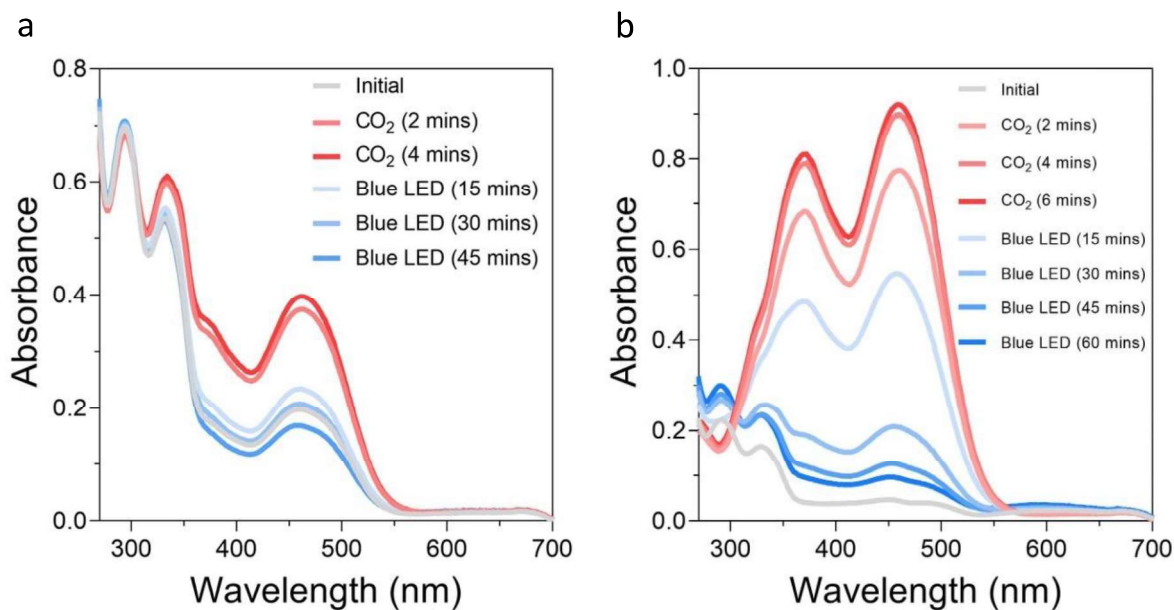


Figure S14. CO_2 response followed by 450 nm blue LED irradiation of 100 μM **SP4** in a) 1:1 DMF:H₂O and b) 1:1 MeOH:H₂O.

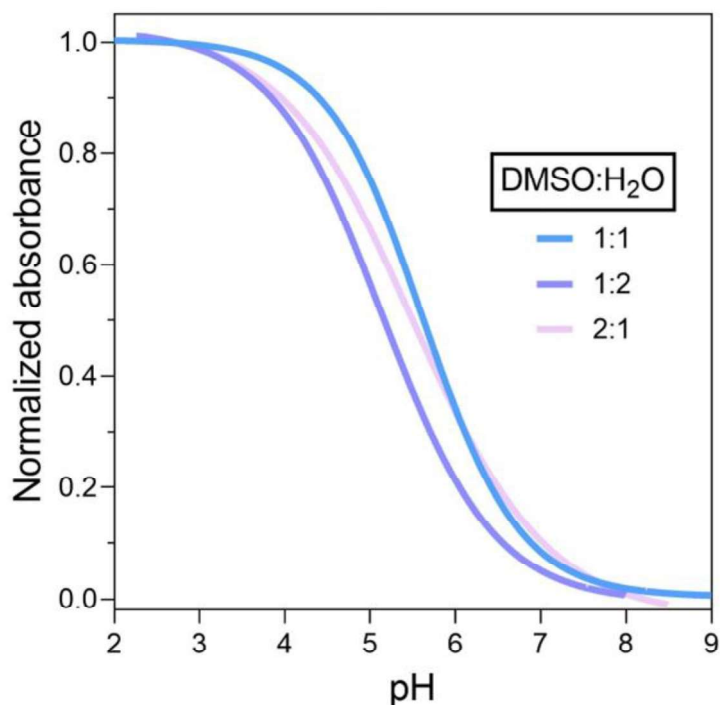


Figure S15. Sigmoidal fits of **SP4** equilibrium absorbance as function of pH at different DMSO/water volumetric ratios.

3.4. Solubility Measurements

UV-Vis absorbance spectra are taken to determine the solubility of **SP** in different DMSO/water volumetric ratios. Calibration curves were created using samples of standardized concentration, by fitting the maximum absorbance as a linear function of concentration. These measurements were made within a 1 cm path-length cuvette. Next, in the solvent system of interest, an oversaturated solution of **SP** was prepared and sonicated for 1 h to ensure full dissolution. This sample was filtered with a 0.2 μm syringe filter (VWR), diluted, and used for UV-Vis absorbance analysis to determine the concentration.

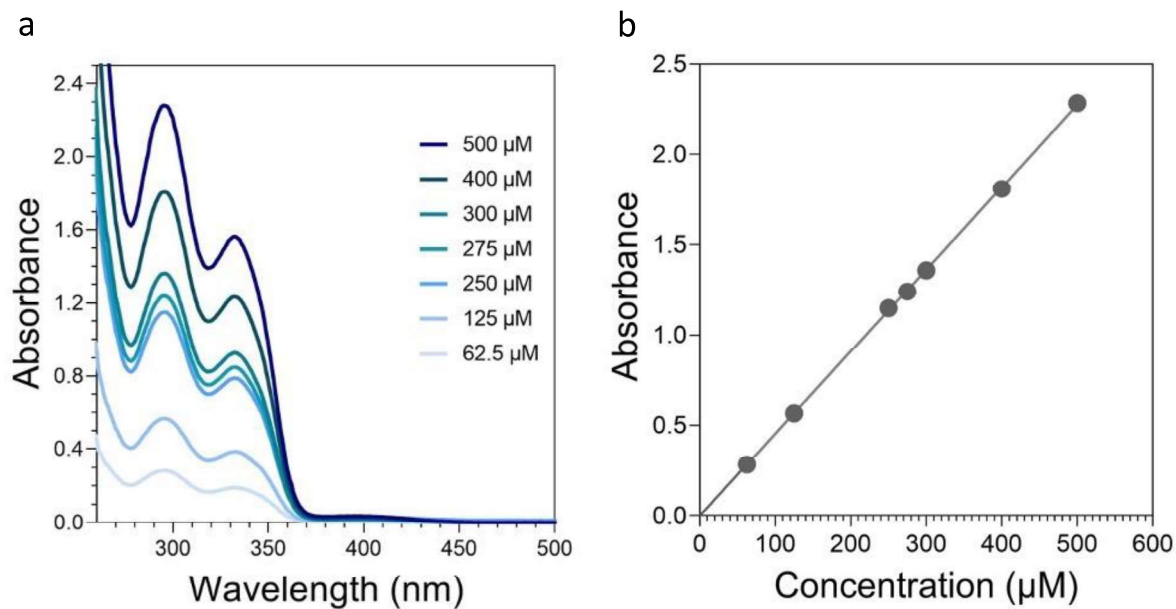


Figure S16. a) UV-Vis absorbance spectra and b) associated calibration curve at 291 nm for **SP4** in 4:1 DMSO/water.

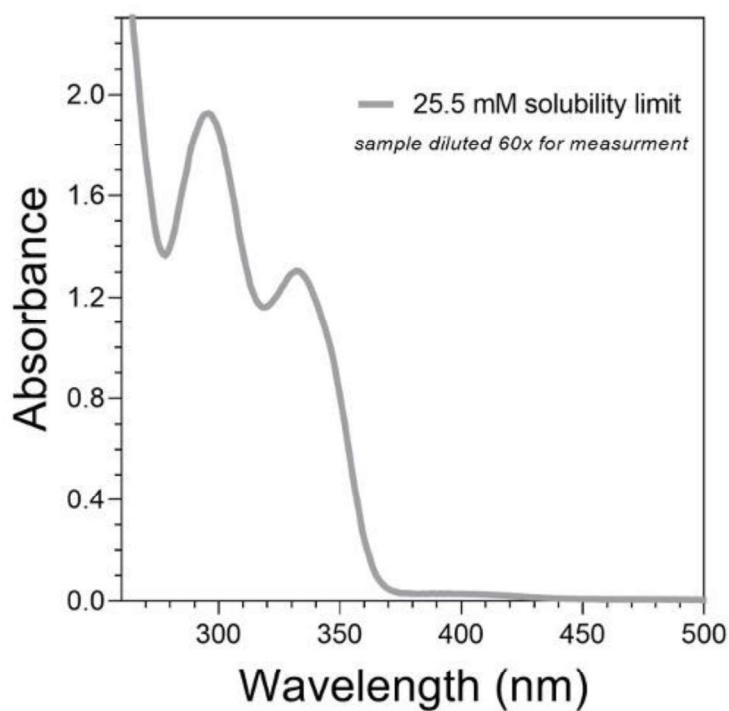


Figure S17. UV-Vis absorbance spectra taken to determine the solubility of **SP4** in 4:1 DMSO/water.

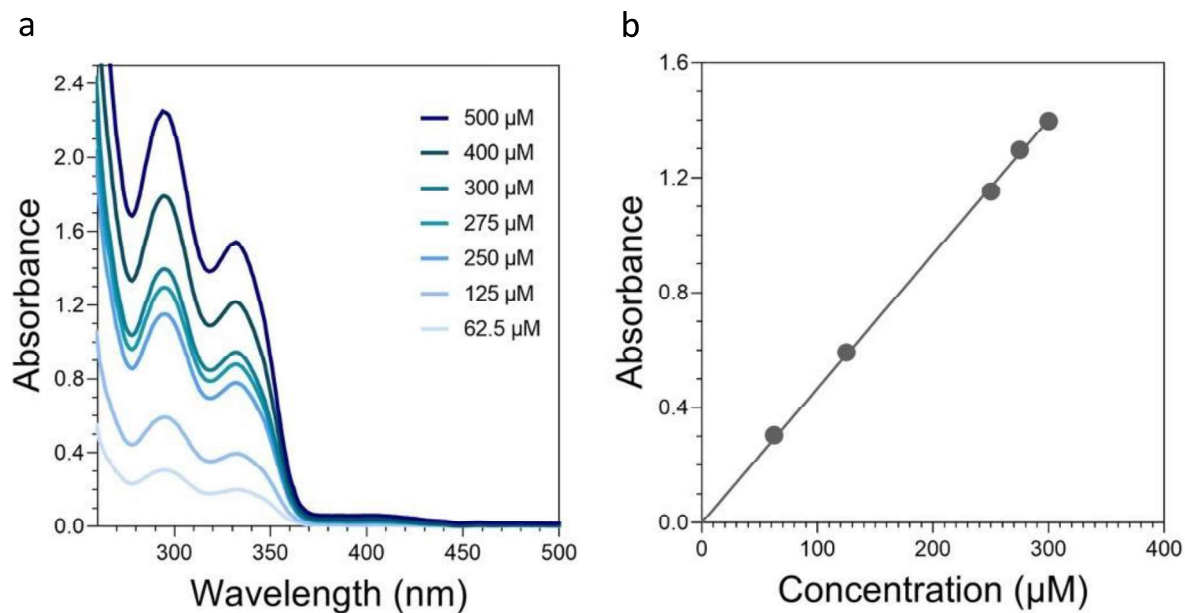


Figure S18. a) UV-Vis absorbance spectra and b) resulting calibration curve at 291 nm for **SP4** in 3:1 DMSO/water.

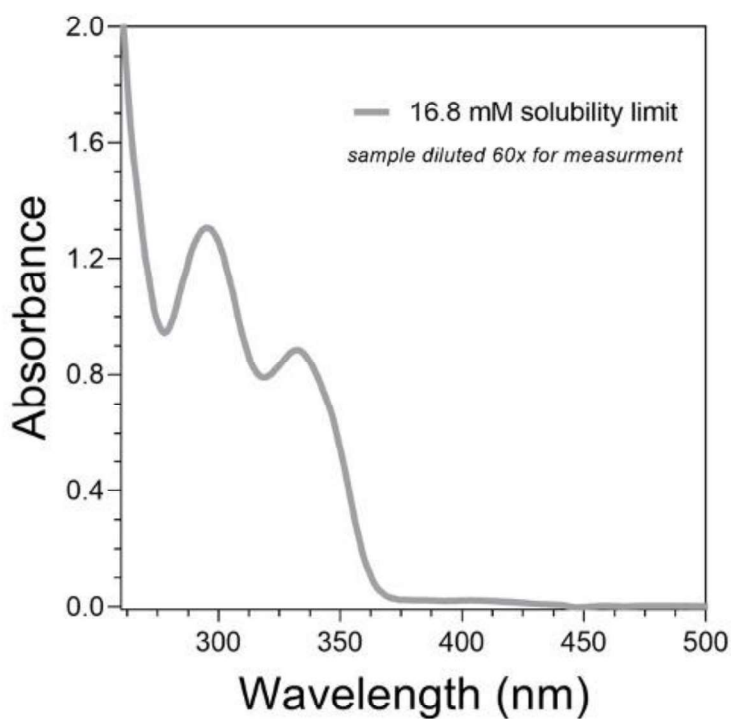


Figure S19. UV-Vis absorbance spectra taken to determine the solubility of **SP4** in 3:1 DMSO/water.

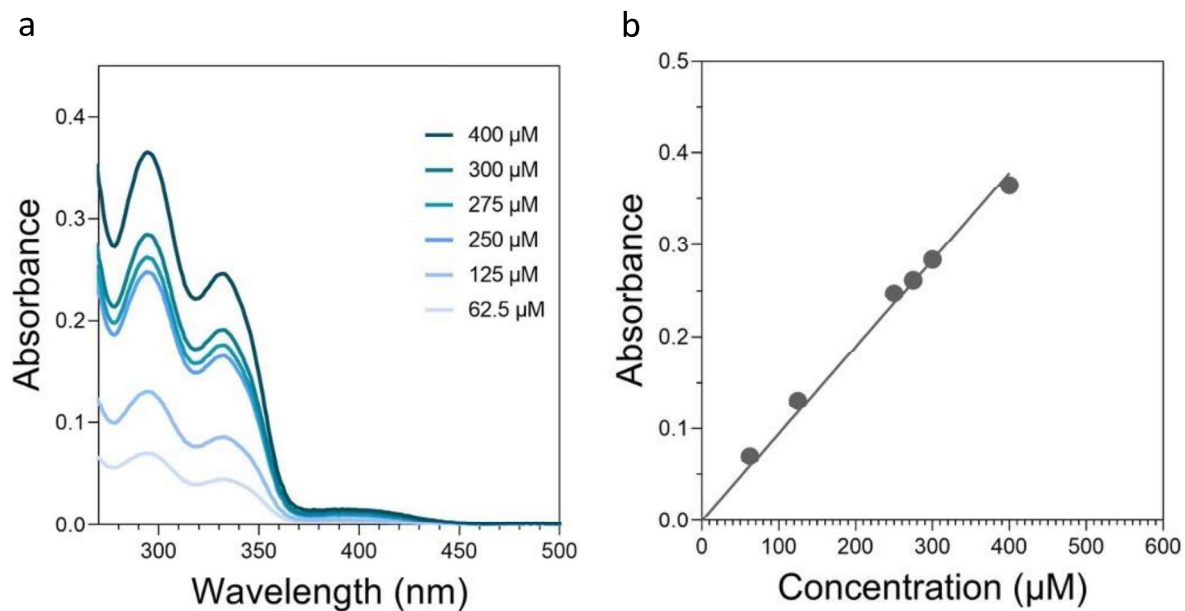


Figure S20. a) UV-Vis absorbance spectra and b) resulting calibration curve at 291 nm for **SP4** in 2:1 DMSO/water.

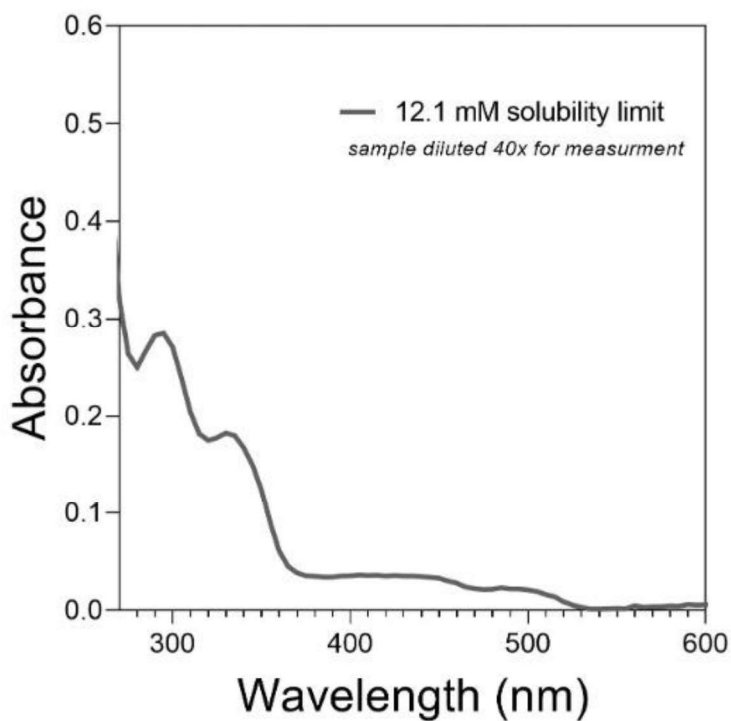


Figure S21. UV-Vis absorbance spectra taken to determine the solubility of **SP4** in 2:1 DMSO/water.

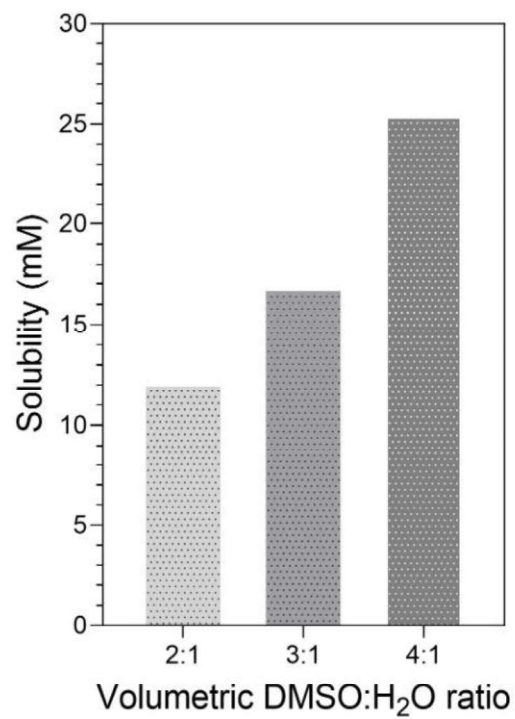


Figure S22. Summary of solubility of **SP4** at different volumetric DMSO/water ratios.

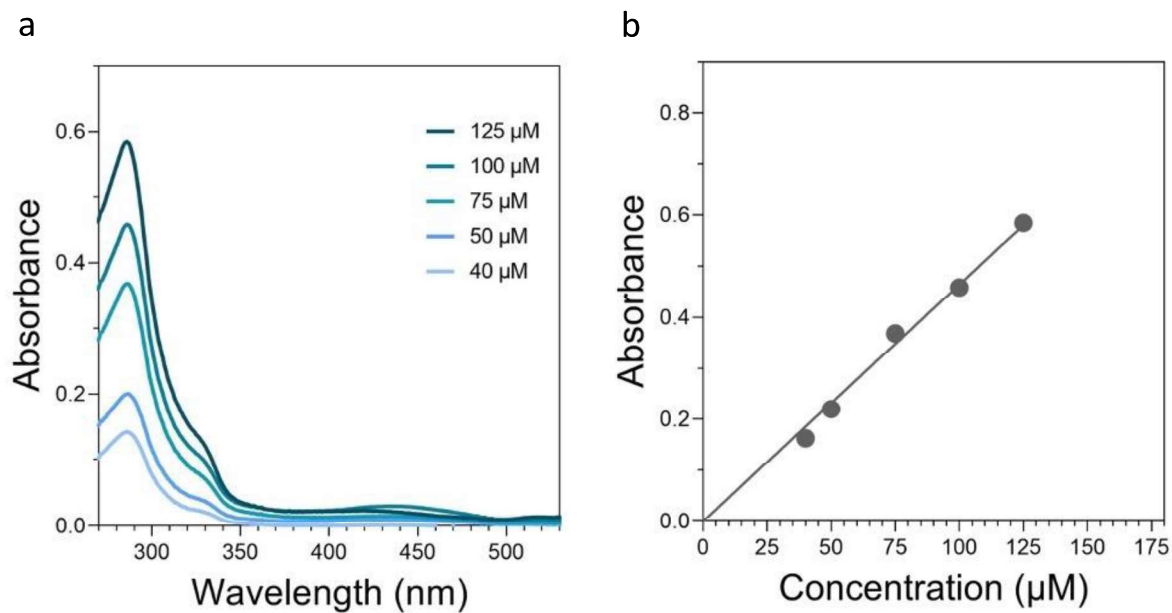


Figure S23. a) UV-Vis absorbance spectra and b) resulting calibration curve at 285 nm for **SP2** in 4:1 DMSO/water.

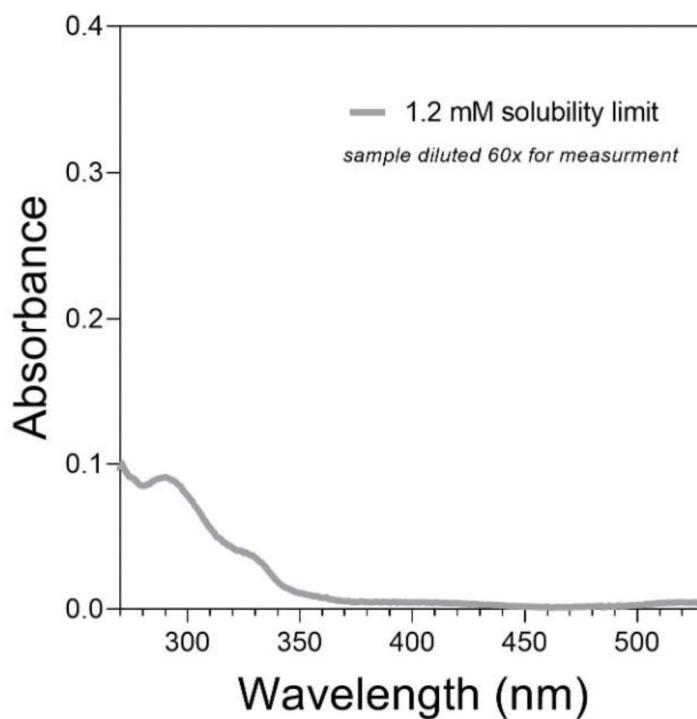


Figure S24. UV-Vis absorbance spectra taken to determine the solubility of **SP2** in 4:1 DMSO/water.

4. CO₂ Capture and Release

4.1. Experimental Setup

Assembly of LED Chamber: LED strips (16.4 ft total, 18 bulbs per ft, 3.5 W per ft, 450 nm) were installed along the inside of a 1.2 L crystallizing dish and powered by a 60 W power supply. The exterior of the crystallizing dish was covered with aluminum foil. During irradiation, a Honeywell Turboforce Fan Ht-900 (11 inches) was pointed at the LED chamber to ensure operation at rt.

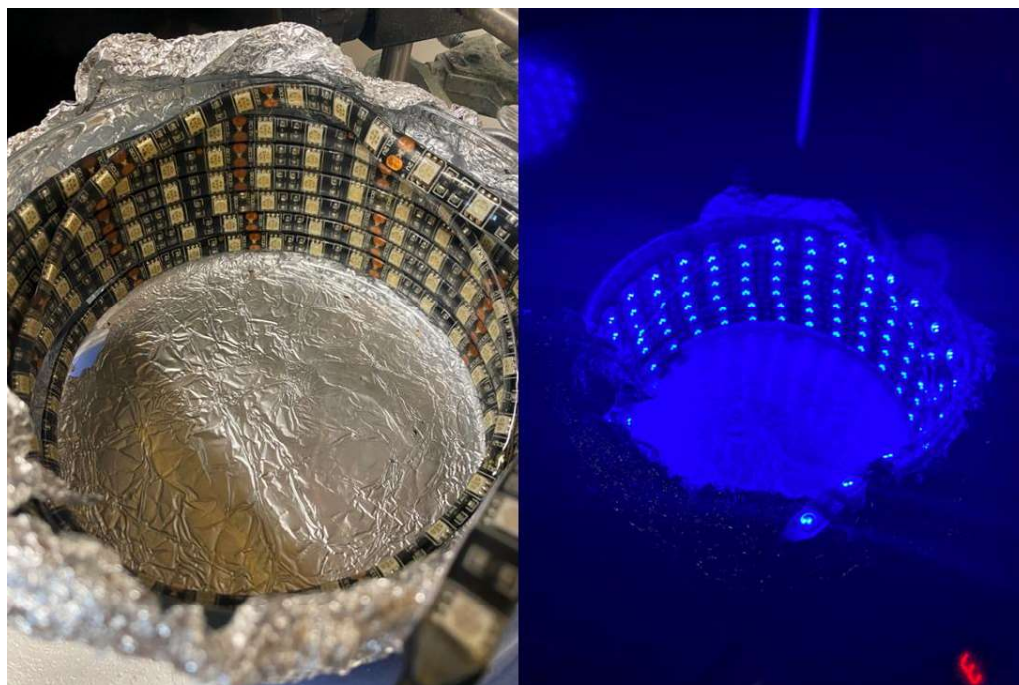


Figure S25. LED chamber setup used for CO₂ photorelease.

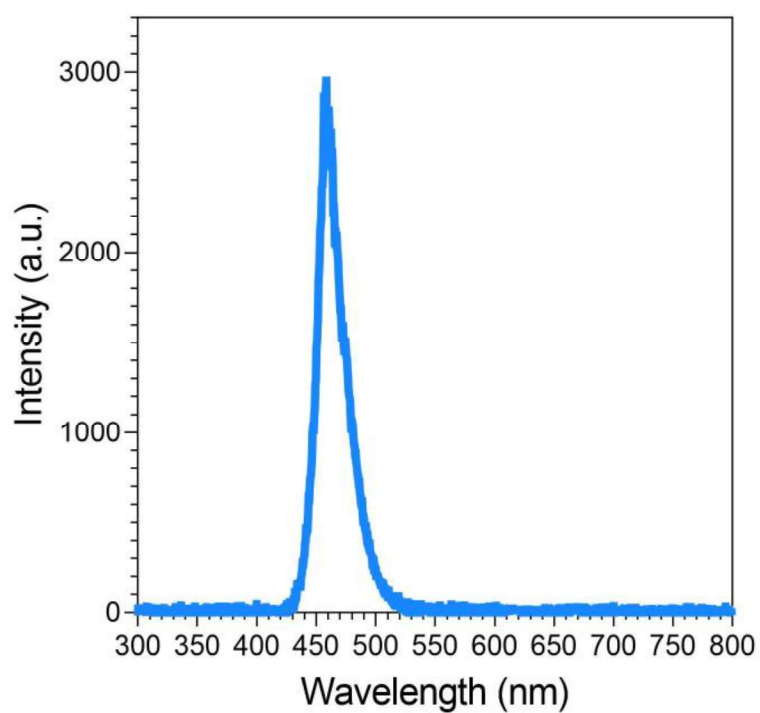


Figure S26. Emission spectrum of blue LED light source for irradiation experiments

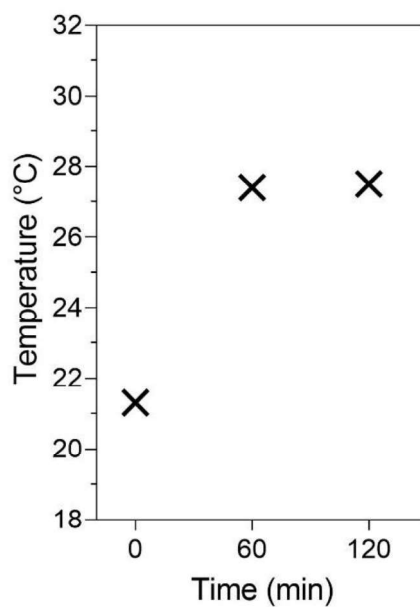


Figure S27. *In situ* temperature tracking of a DMSO/water solution of 10 mM **SP4** during blue LED irradiation.

CO₂ capture and release:

Pure CO₂ (Fig. 3A): In a 20 mL scintillation vial equipped with a small stir bar, **SP4** (18.4 mg) was dissolved in DMSO (1.0 mL) by sonication, followed by addition of H₂O (0.6 mL) and additional DMSO (1.4 mL, final concentration 20 mM). The sample was sonicated for 1 h in the dark, during which the vial was covered with foil and sealed tightly with a rubber septum. The sample was subjected to 100% CO₂ (bubbled through the solution) *via* a 10 cm length of FEP tubing with 1/16" ID through the septum with a needle for venting over a period of 3 h. The overhead space was flushed quickly with nitrogen through a syringe to remove excess CO₂, and the capped sample was left in the dark for 1 h before 450 nm blue LED irradiation and GC analysis of the overhead space (see below).

Diluted CO₂ (Fig. 3B): In a 20 mL scintillation vial equipped with a small stir bar, **SP4** (9.2 mg) was dissolved in DMSO (1.2 mL) by sonication, followed by addition of H₂O (0.8 mL) and additional DMSO (1.0 mL, final concentration 10 mM). The sample was sonicated for 1 h in the dark, during which the vial was covered with foil and sealed tightly with a rubber septum. The sample was subjected to different CO₂/N₂ partial pressure inlets (bubbled through the solution) *via* a 10 cm length of FEP tubing with 1/16" ID through the septum with a needle for venting over a period of 3 h. The inlet stream was controlled by Sierra Smart Trak 50 Mass Flow Controllers. The overhead space was flushed quickly with nitrogen through a syringe to remove excess CO₂, and the capped sample was left in the dark for 1 h before 450 nm blue LED irradiation and GC analysis of the overhead space (see below).

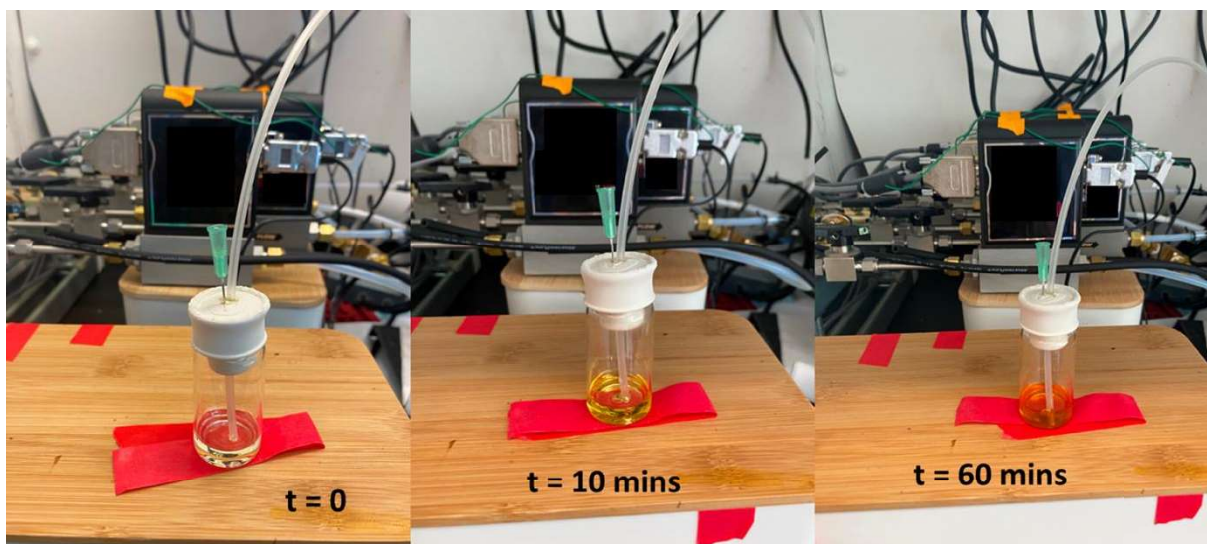


Figure S28. Spiropyran (SP4) solution in DMSO/water mixture before and during CO₂ exposure.

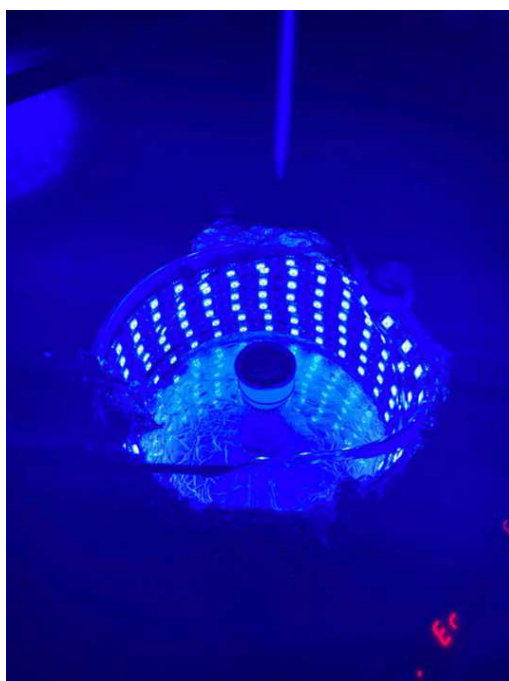


Figure S29. Photograph of the SP4 solution during irradiation with blue LED after exposure to CO₂.

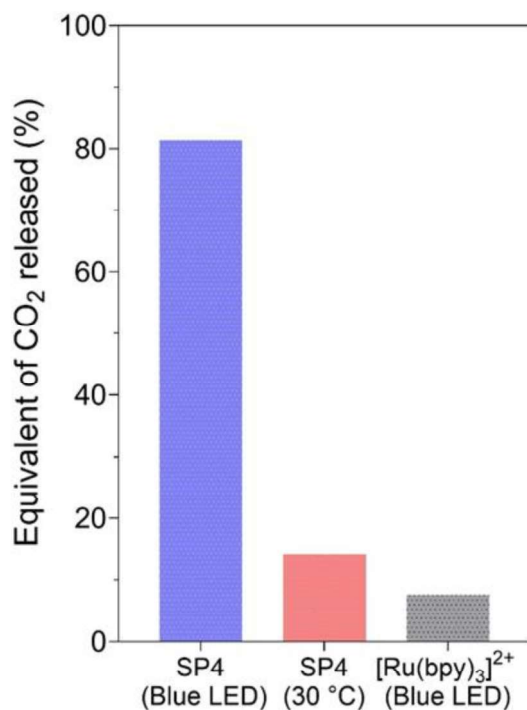


Figure S30. Comparison of CO₂ release measurement in DMSO/water solution of 10 mM **SP4** using light (blue), at 30 °C (red), and CO₂ release measurement in DMSO/water solution of 10 mM [Ru(bpy)₃]²⁺ using light.

Control experiments: We measured the irradiance of the blue LED set-up at the center of the chamber and found it to be 104.5 W/m². The exposed surface area of the reactor vial is 0.0015 m², so the net irradiation is on the order of 160 mW. Our light source is diffuse and not focused in any way. We tracked the temperature of the sample using both digital infrared thermometer and glass contact thermometers before and during irradiation of the solution under fan blowing (Honeywell Turboforce Fan HT-900). The steady-state temperature reached after roughly 2 h is 28 °C, and this value is never exceeded as shown in SI Figure 5-3. We performed a CO₂ capture/release measurement at 30 °C in the dark to estimate an upper bound on the heat effect. We saw that only 15% was released. Interestingly, when we replaced SP4 with the suggested [Ru(bpy)₃]Cl₂, with absorbance at 450 nm matched, only 5% release was observed. These results confirm that the major contribution to the release is a photochemical process rather than thermal.

4.2. Gas Chromatography Analysis

Headspace gas chromatography (GC) experiments were performed using an Agilent 7890A GC equipped with a ShinCarbon ST packed column (Restek) and a thermal conductivity detector (TCD) with helium carrier gas. To measure the amount of gas formed during blue LED irradiation experiments, we used a gastight syringe (Hamilton Company) to inject 50 µL through GC of the sample headspace. The concentration of CO₂ was determined by integrating the area under the associated peak in the chromatogram

and standardizing against a calibration curve. The calibration curve for CO₂ was established by injecting known quantities of calibration gas (Fig. S31). The integrated intensity of the calibration peaks was then used to determine the concentration of the CO₂ in the headspace of each measurement by assuming a linear relationship between the injected concentration of gas and the detector response.

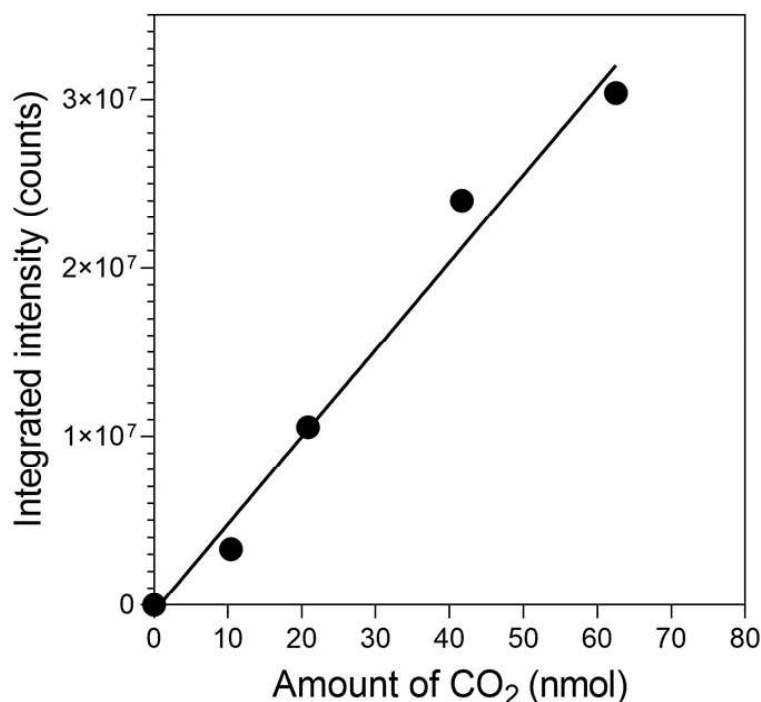


Figure S31. Calibration curve for GC. Plot of integrated intensity vs. amount of injected CO₂. The plot was fit to a linear function with a y-intercept set to zero, and the slope was used to determine the concentration of injected gas for test samples after 450 nm blue LED irradiation.

4.3. *In Situ* pH Tracking

***In situ* pH tracking for SP4:** In a 20 mL scintillation vial, **SP4** (7.7 mg) was dissolved in DMSO (3.75 mL) and H₂O (1.25 mL) to produce a final concentration of 5 mM. The solution was degassed by sonication for 1 h.

Tracking without buffer (Fig. 3C): The pH of a freshly prepared sample was adjusted to 6.1 with small added quantities of dilute aqueous HCl to partially convert **SP4** to the **MCH4⁺Cl⁻** form. With a meter tracking pH, the sample under stirring was irradiated with the 450 nm blue LED for 20 mins before it was allowed to re-equilibrate in the dark.

Tracking with bicarbonate buffer (Fig. 3D): With a meter tracking pH throughout, a freshly prepared sample under stirring was allowed to sit in the dark for 3 min before being subjected to a CO₂ atmosphere applied by balloon. After 17 min, the LED chamber was turned on to irradiate the sample with 450 nm blue LED light while overhead pressure of CO₂ was maintained.

Tracking with capture and release (Fig. 3E): With a meter tracking pH throughout, a freshly prepared sample under stirring was allowed to sit in the dark for 3 min before being subjected to a CO₂ atmosphere applied by balloon. After 20 min, the CO₂ source was removed, and the LED chamber was turned on to irradiate the sample with 450 nm blue LED light for 70 min.

***In situ* pH tracking for SP8** (Fig. S32): In a 20 mL scintillation vial, **SP8** (10.4 mg) was dissolved in DMSO (3.75 mL) and H₂O (1.25 mL) to produce final concentration of 5 mM. The solution was degassed by sonication for 1 h. With a meter tracking pH continuously, the sample under stirring was allowed to sit in the dark for 5 min before being subjected a CO₂ atmosphere applied by balloon. After 13 min passed, the CO₂ source was removed, and the LED chamber was turned on to irradiate the sample with 450 nm blue LED light.

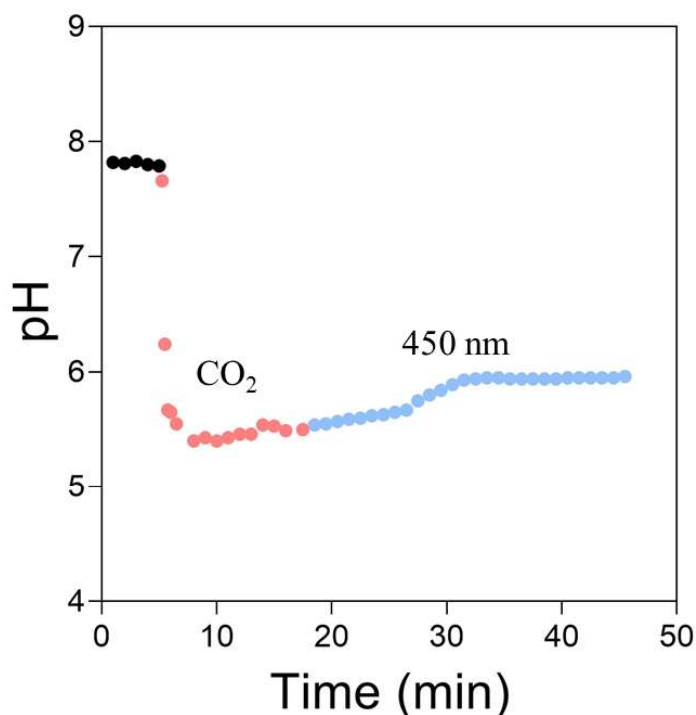


Figure S32. *In situ* pH tracking of a DMSO/water solution of 5 mM **SP8** under different conditions. The minimal change in pH upon irradiation suggests that an insignificant quantity of CO₂ was released.

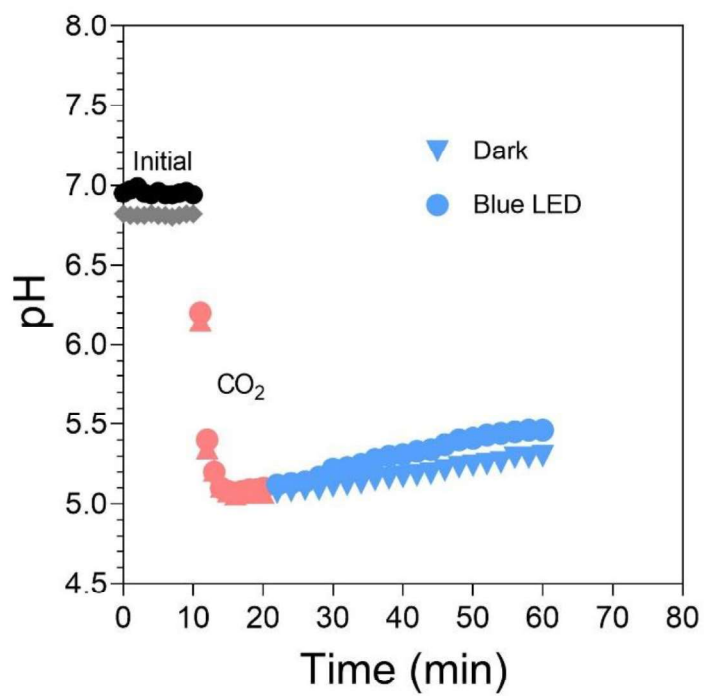


Figure S33. Control experiment comparing capture (1 atm CO₂) and release of CO₂ (to N₂ headspace) in pure DMSO–water solution.

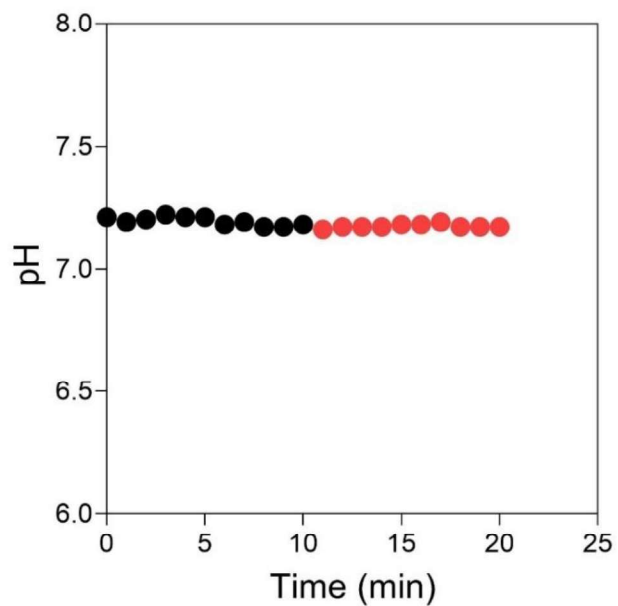


Figure S34. Illumination of the pH probe with a 450 nm LED did not affect its reading. The black points indicate the pH reading in the dark of a blank DMSO/water mixture and red points indicate the pH reading under LED irradiation. We concluded from this experiment that potential photoactivity of the device is not a confounding factor in our measurements.

4.4. Stability of SP4

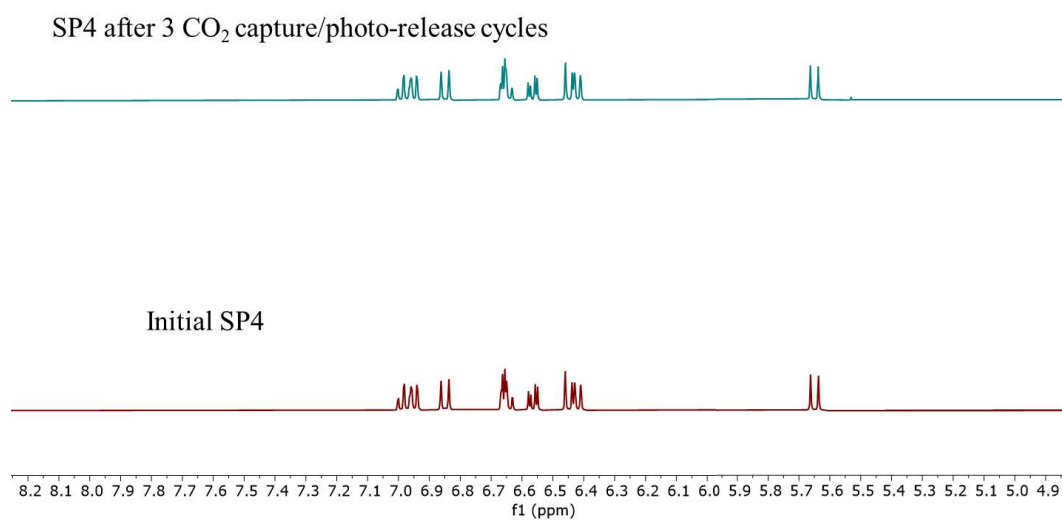


Figure S35. ¹H NMR spectrum of the DMSO–water solution of **SP4** before and after 3 CO₂ capture/photorelease cycles.

5. Ultrafast Transient Absorption Studies

5.1. Methods

Spectroscopy: The data were acquired using a single-shot probe-referenced broadband transient absorption (TA) setup, the design of which was reported previously.⁴⁵ Briefly, a Ti:Sapphire regenerative amplifier (Coherent Libra-HE) provides 3 W fundamental pulses (800 nm, 50 fs) at a frequency of 1 kHz. The 400 nm pump pulses were generated by seeding an OPerA SOLO (Coherent) with 2 W of the fundamental output of the amplifier. Another fraction (~ 1 mW) of the fundamental was aligned onto a 1.7 m computer-controlled, motorized translation stage (Aerotech ATS62150, U100 controller) equipped with a hollow retro-reflector, which furnished the pump–probe delay times used in the TA experiments. After the translation stage, the beam was focused with a 100 mm focal length lens onto a 2 mm calcium fluoride (CaF_2) crystal to generate a chirped white light continuum. To avoid thermal damage, the crystal was continuously translated back-and-forth perpendicular to the input beam. The resulting white light pulses were reflectively collimated and aligned onto a 15 mm translation stage (Physik Instrumente, M-111.DG, Mercury DC controller). A notch filter removed the residual 800 nm fundamental from the white light continuum and was subsequently sent onto a broadband reflective neutral density filter to generate probe (reflected) and reference (transmitted) pulses of approximately equal intensity. Subsequently, pump and probe pulses were focused into the sample using a lens ($f = 500$ mm) and concave mirror ($f = 500$ mm), respectively. Each sample was diluted such that its optical absorption at its absorption maxima within the probe window was below 1 OD in a 2 mm path length quartz cuvette. The samples were continuously stirred during the measurement using a thin stir bar, and no degradation of the samples was observed by UV-Vis spectroscopy measured before and after the experiment. After passing through the sample, the transmitted probe beam was recollimated prior to being sent into a fused silica prism (OptoSigma, DPSQ-20-10H) spectrograph ($f = 250$ mm) equipped with two 16-bit, 512 pixel charge-coupled devices (Hamamatsu S7030-0906). The reference beam was sent to a separate, identical spectrograph and detector pair for balanced detection. Data acquisition was enabled by a custom-built interface board from Entwicklungsbüro Stresing. Differential normalized transmittance signals were collected on a shot-to-shot basis with the pump chopped at 500 Hz. One transient absorption trace consisted of 200 probe shots resulting in 100 differential spectra which were averaged at each timepoint. Data presented in this study was obtained by recording 15 transient absorption traces and averaging the results. Time constants were calculated by fitting the kinetic data in both Surface Explorer (Ultrafast Systems) and IgorPro (Wavemetrics) with the appropriate single or double exponential fit functions that minimize the fit residuals for each best fit.

Actinometry: The laser spectroscopic setup was described in detail previously, and we made only minor changes to functionally equivalent hardware.⁴⁶ A Quanta-Ray Nd:YAG laser (SpectraPhysics) which emits 355 nm laser pulses with a repetition rate of 10 Hz and a pulse width of ~ 8 ns, which were directed into a optical parametric oscillator (MOPO-PO, SpectraPhysics) to generate 470 nm with excitation pulses that were 1 mJ/pulse. Continuous white light, generated by a xenon-arc lamp (PTI, Model A1010), was used as the probe for the transient absorption (TA) measurements. To measure the time dependent transient absorption signal, the excitation laser beam and the probe beam were focused onto the sample contained in a 1 cm path length cuvette. The transmitted probe beam was recollimated by a pair of lenses ($f = 20$ cm), passed through a monochromator (iHR 320, Horiba) to select the probe wavelength to monitor, and then detected with a photomultiplier tube (PMT R928, Hamamatsu). The signal of the PMT was recorded on a 1 GHz oscilloscope (Wavesurfer 4104 HD, Teledyne-Lecroy). Custom software was used for controlling the apparatus and data processing.

The actinometry experiments themselves were adapted from previous transient absorption actinometry studies.⁴⁷ Ru(bpy)₃Cl₂ was dissolved in MilliQ water such that its absorbance was below 1 OD for all wavelengths within the probe spectral region. Test samples were made to match the absorbance of the Ru(bpy)₃²⁺ solution at 470 nm in an identical 1 cm quartz cuvette (Spectrocell). Because of the rapid and efficient relaxation of Ru(bpy)₃²⁺ from its initially excited ¹MLCT state to a slowly decaying ($\tau_1 = 380$ ns) ³MLCT state in atmosphere-equilibrated solution, the initially measured TA signal can be approximated to be equal to the concentration of photogenerated species in the probed sample volume by dividing the signal 40 ns after the instrument response function by the $\Delta\epsilon$ of the ³MLCT state of Ru(bpy)₃²⁺ at 455 nm (*ca.* 11,300 M⁻¹ cm⁻¹). We immediately switch the sample for the **MCH**⁺ sample of interest and measure its TA signal at 455 nm. The TA values from 40 ns to 1.7 μ s were averaged and divided by 22,080 M⁻¹ cm⁻¹ to provide the concentration of depleted **MCH**⁺ resulting from photoexcitation in the probed volume, and this quantity is further divided by the concentration of photogenerated species from the Ru(bpy)₃²⁺ reference experiment to furnish the actinometric quantum yield on this timescale. The *ca.* 22,080 M⁻¹ cm⁻¹ value was derived from the extinction coefficient of **MCH** and assumes minimal absorption from MC- and SP forms of the species. From this quantum yield, we could calculate the rate of proton escape using $k_{\text{escape}} = 1/\tau_{\text{escape}} = \Phi/\tau_{\text{rev-PT}}$.

Sample Preparation: For the measurements shown in Fig. 4B and Fig. 4C, a solution of **SP4** (0.5 mM) in 1:1 DMSO/water was employed. CO₂ was bubbled into the solution to produce **MCH4**⁺ HCO₃⁻. For experiments on **MCH4**⁺ Cl⁻, dilute aqueous HCl (0.5 M) was used instead of CO₂ to generate the protonated

merocyanine state. For the deuterium isotope effects, analogous samples were prepared using D₂O and DMSO-*d*₆ as solvents.

5.2. Additional Data

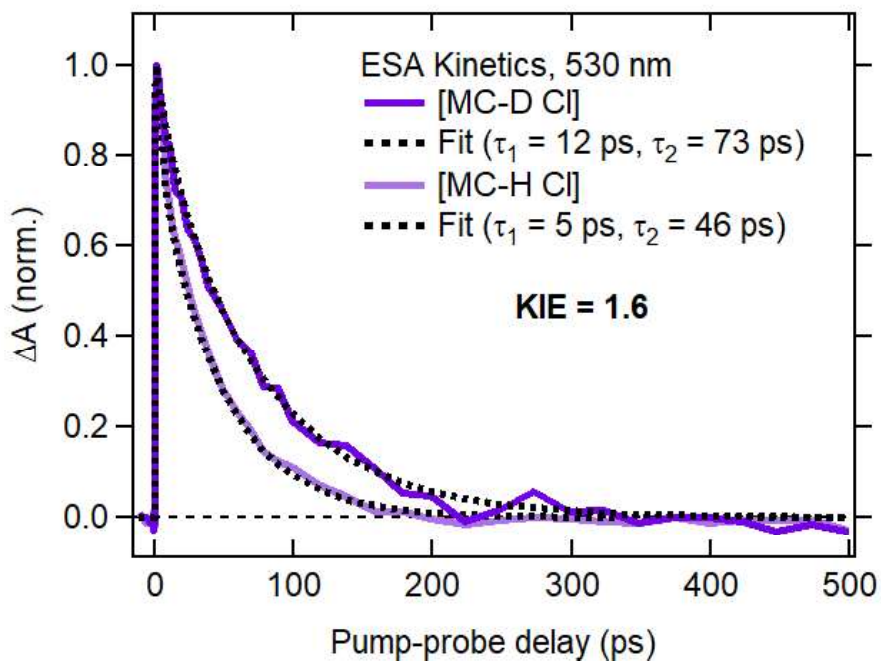


Figure S36. Decay profiles of the excited state absorption for **MCH4⁺ Cl⁻** and **MCD4⁺ Cl⁻** showing absolute time constants similar to those of the bicarbonate analogues. The relative amplitudes for the two exponentials used to fit the data were 0.19 and 0.81 (for HCl); 0.12 and 0.88 (for DCl). The indicated KIE calculated was based on the slower step (step 2). The KIE for the first step from the ratio of the τ_1 values is approximately 2.2.

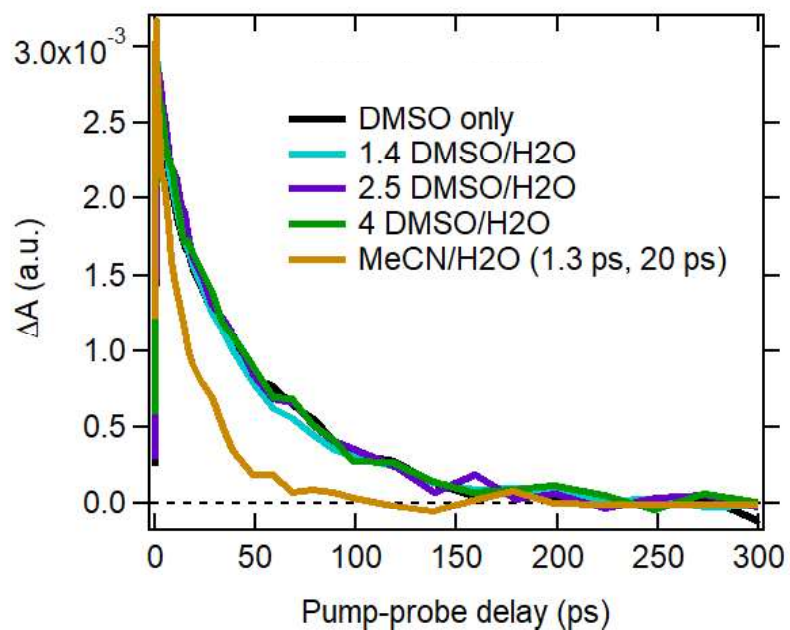


Figure S37. Decay profiles of the excited state absorption for **MCH₄⁺ Cl⁻** in different solvent mixtures. The proportion of water does not significantly affect the decay profile in DMSO, but the identity of the organic solvent has a considerable influence.

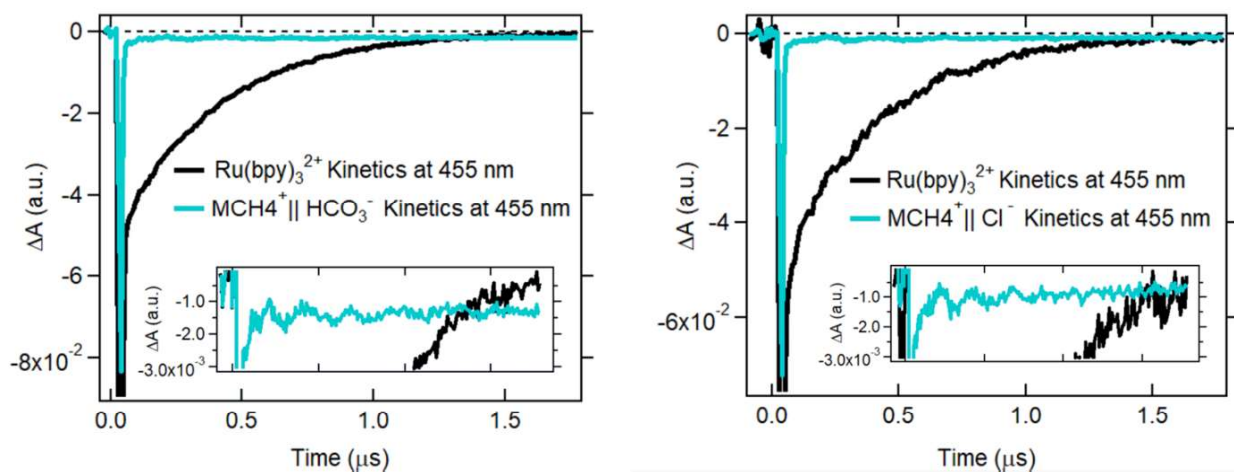


Figure S38. Actinometry experiments used to determine the quantum yield for proton escape leading to CO_2 release.

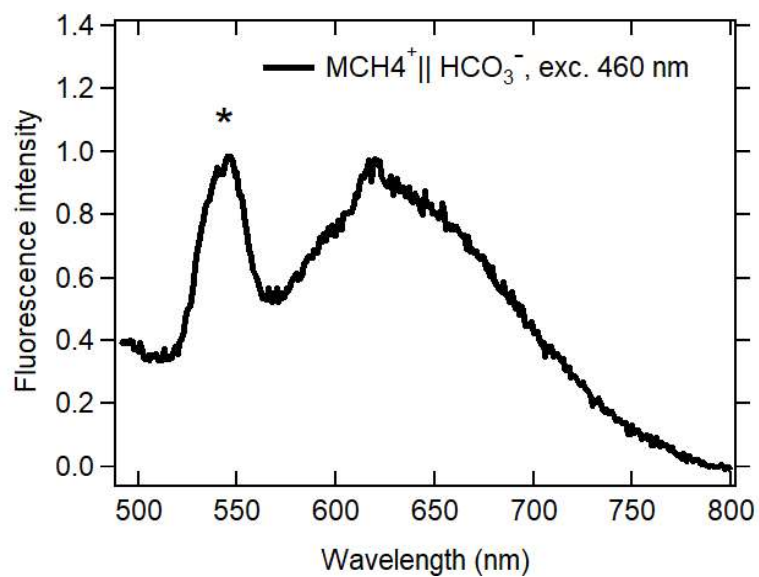


Figure S39. Fluorescence spectrum for $\text{MCH4}^+ || \text{HCO}_3^-$ in DMSO/H₂O upon photoexcitation at 460 nm. The peak at 545 nm is attributed to a solvent Raman band.

6. Computational Chemistry

6.1. General Methods

All calculations were performed with Gaussian 16, Revision A.03.⁴⁸ The geometry optimization of all ground-state structures was carried out using the B3LYP functional^{49,50} with a basis set of 6-311G(d) on all atoms. Frequency calculations were performed to confirm the nature of the stationary points and to evaluate its zero-point vibration energy (ZPVE) and thermal corrections at 298 K. The lowest energy isomers for each structure considered were located by systematic search. In these studies, the SMD⁵¹ solvation model (water) was used in geometry optimizations to reflect the experimental conditions. Time-dependent DFT (TD-DFT) was used to predict the UV-Vis spectra of species, using B3LYP/6-311G(d) with SMD solvation model. Previous benchmark studies have shown this level of theory to be reasonably accurate for related spiropyran–merocyanine systems.⁵²

Computed structures are illustrated using CYLView (<https://www.cylview.org/>).

6.2. Structures and UV-Vis Spectra of Relevant Species

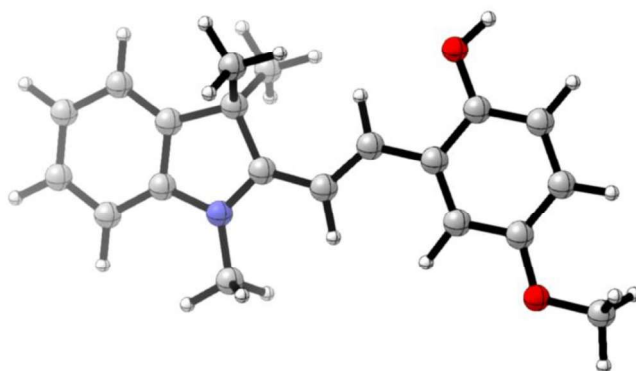


Figure S40. DFT energy-minimized structure of **MCH4⁺** in its all-*trans* configuration.

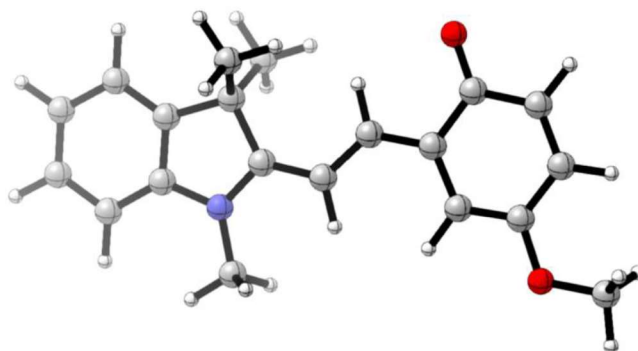


Figure S41. DFT energy-minimized structure of **MC4** in its all-*trans* configuration.

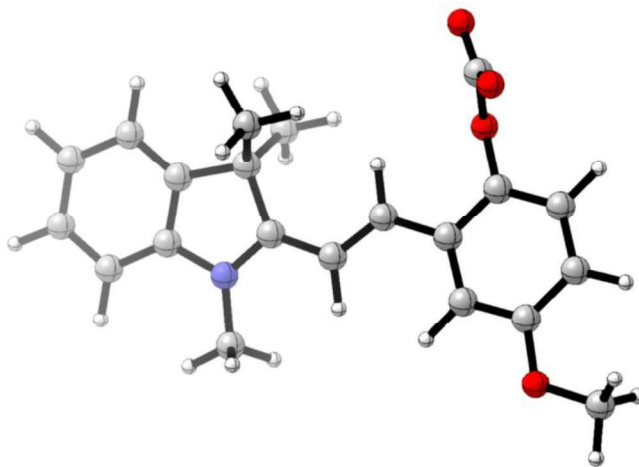


Figure S42. DFT energy-minimized structure of MC4-CO₂ in its all-*trans* configuration.

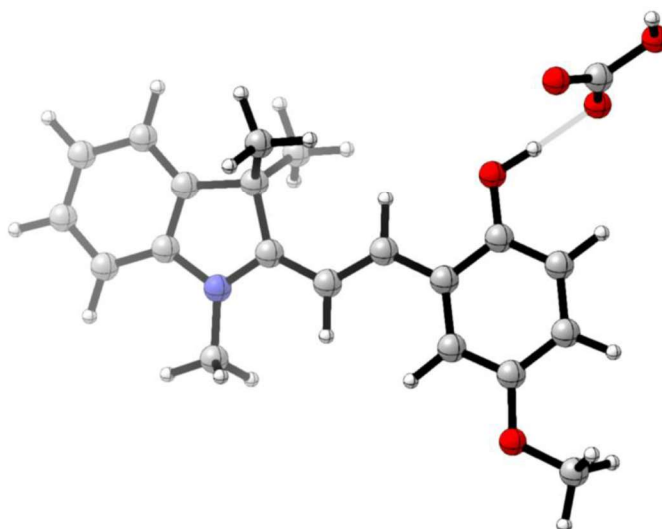


Figure S43. DFT energy-minimized structure of MCH₄⁺...HCO₃⁻ in its all-*trans* configuration.

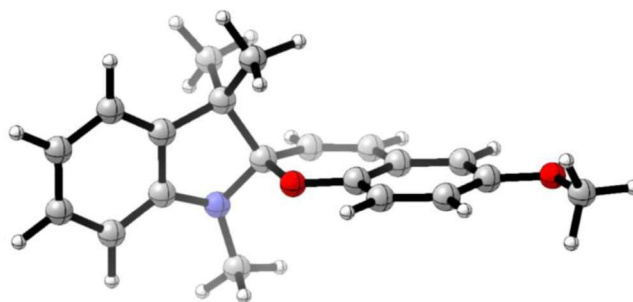


Figure S44. DFT energy-minimized structure of SP4.

Table S1. TD-DFT predicted lowest-energy optical transitions of relevant species.

Species	λ_{\max} (nm)
MCH4⁺	489
MC4	562
MC4-CO₂	465
MCH4⁺...HCO₃⁻	509
SP4	331

6.3. Geometries and Energies of Minimized Structures**MCH4⁺**

Charge: 1

Multiplicity: 1

Electronic Energy (B3LYP/6-311G(d)/PCM(water)): -980.635639074

Geometry:

```

C      4.62102100 -1.80204000 0.07877500
C      3.50377500 -0.97691700 0.03163800
C      3.59471400 0.41128000 -0.03691700
C      4.83982200 1.02076900 -0.06252900
C      5.98040800 0.21306100 -0.01710800
C      5.86930100 -1.17800000 0.05313200
H      4.54658000 -2.88041700 0.13377500
H      4.93120400 2.10002200 -0.11620900
H      6.96296800 0.67132500 -0.03576500
H      6.76492500 -1.78799000 0.08814400
C      2.20154600 1.00574400 -0.06912900
C      1.97588300 1.90608900 1.16859500
H      2.10073000 1.34210800 2.09514400
H      2.71117500 2.71300200 1.15637300
H      0.98208800 2.35465400 1.16667000
C      1.98201500 1.79248300 -1.38209900
H      0.99247900 2.24820200 -1.42145400
H      2.72346100 2.59166900 -1.44186800
H      2.10245900 1.14686500 -2.25432600
C      -0.07248300 -0.39084200 0.01631500
H      -0.45644800 -1.39962500 0.09926400
C      -0.94837000 0.65223900 -0.03461700
H      -0.53265800 1.64600500 -0.12592000
C      -2.39095600 0.56368100 0.00444500
C      -3.18458300 1.73982900 0.07767800
C      -3.05828300 -0.67941600 -0.04174000
C      -4.57552200 1.63740000 0.07894200
C      -4.44010800 -0.77110000 -0.03411200
H      -2.49165100 -1.60032200 -0.09783800
C      -5.20721000 0.40415600 0.02173200
H      -5.16026900 2.54849800 0.13105000
H      -6.28864200 0.36742500 0.02522400
O      -2.68620900 3.01295200 0.14301700
H      -1.72984200 3.02967900 0.26685300
O      -4.96733600 -2.03658200 -0.08880800
C      -6.39162700 -2.17631200 -0.06521200
H      -6.85197400 -1.69453700 -0.93195100
H      -6.58094700 -3.24718400 -0.10413400
H      -6.81486000 -1.76525200 0.85513800
C      1.34333300 -0.25989000 -0.00936500
N      2.12884700 -1.33407700 0.04268100
C      1.65548500 -2.72069100 0.11721300

```

H	1.10254200	-2.87524600	1.04324900
H	1.01572400	-2.94061900	-0.73594900
H	2.50842800	-3.38982200	0.09825100

MC4

Charge: 0

Multiplicity: 1

Electronic Energy (B3LYP/6-311G(d)/PCM(water)): -980.173450824

Geometry:

C	4.64082300	-1.76982200	-0.00002700
C	3.50263100	-0.97047800	-0.00003700
C	3.57293600	0.42287800	-0.00012800
C	4.80634400	1.05483000	-0.00022300
C	5.96661200	0.27121300	-0.00022400
C	5.87918300	-1.12191300	-0.00012400
H	4.58835000	-2.85141600	0.00003900
H	4.87552000	2.13758000	-0.00026000
H	6.93972300	0.74991600	-0.00030100
H	6.78532100	-1.71801600	-0.00012800
C	2.16853700	0.99903400	-0.00003400
C	1.93717600	1.84264300	1.27356600
H	2.07350600	1.24112100	2.17503500
H	2.65877000	2.66243200	1.29828100
H	0.93608500	2.27445700	1.29567000
C	1.93699800	1.84282000	-1.27345800
H	0.93589000	2.27459500	-1.29538000
H	2.65856100	2.66263500	-1.29812700
H	2.07325100	1.24144000	-2.17503300
C	-0.06830500	-0.42470400	0.00000300
H	-0.45034700	-1.43893900	-0.00010300
C	-0.97803100	0.62570100	0.00009500
H	-0.59972700	1.64002400	0.00008200
C	-2.38423500	0.54827700	0.00009700
C	-3.12372600	1.81588200	0.00016200
C	-3.09748600	-0.68659700	0.00004200
C	-4.56207700	1.69816100	-0.00013900
C	-4.46740900	-0.72914200	0.00001100
H	-2.55761200	-1.62746900	0.00003600
C	-5.20639400	0.48932400	-0.00016500
H	-5.13292000	2.62140200	-0.00032700
H	-6.28975100	0.46967400	-0.00038800
O	-2.55944500	2.95153600	0.00035300
O	-5.05989600	-1.97845300	0.00011600
C	-6.48660000	-2.05577400	-0.00033500
H	-6.91380800	-1.59283700	-0.89451500
H	-6.72233600	-3.11870000	-0.00039400
H	-6.91438800	-1.59285700	0.89358000
C	1.32103200	-0.28171800	0.00002000
N	2.14377900	-1.35584200	-0.00002800
C	1.68806000	-2.74271600	0.00041900
H	1.08999400	-2.94541600	0.88990800
H	1.08987900	-2.94597300	-0.88887600
H	2.54791000	-3.40482600	0.00052100

MC4-CO₂

Charge: 0

Multiplicity: 1

Electronic Energy (B3LYP/6-311G(d)/PCM(water)): -1168.81180480

Geometry:

C	-5.11598200	-1.75188000	0.08243200
C	-3.91330200	-1.05965000	0.01305900
C	-3.84025600	0.33075500	0.03327700
C	-5.00326300	1.08083100	0.11769400
C	-6.22806600	0.40921600	0.18411600
C	-6.28055900	-0.98702300	0.16801000
H	-5.16576400	-2.83315200	0.07611600
H	-4.96764900	2.16461900	0.13382700
H	-7.14837400	0.97870700	0.25130200
H	-7.23938400	-1.48986700	0.22493700
C	-2.38927000	0.75922000	-0.04397100
C	-2.14021000	1.57272100	-1.33721600
H	-2.38112600	0.98718000	-2.22671500
H	-2.78111700	2.45654100	-1.32395900
H	-1.10509600	1.90775000	-1.40845900
C	-1.99684100	1.57613800	1.20833100
H	-0.97097500	1.93920200	1.14478900
H	-2.65663200	2.44245400	1.28558800
H	-2.10198500	0.98255500	2.11871400
C	-0.29460300	-0.89336200	-0.13107300
H	-0.02263100	-1.94147200	-0.12863000
C	0.68555700	0.04932900	-0.17252400
H	0.41435600	1.09449500	-0.19928300
C	2.11352600	-0.19054200	-0.19584500
C	2.97392800	0.90925100	-0.43343300
C	2.68400100	-1.45598300	0.02664000
C	4.35132200	0.72488400	-0.42991300
C	4.06302700	-1.63112200	0.03079600
H	2.06040600	-2.32110400	0.21863800
C	4.90328600	-0.53173500	-0.19969100
H	4.99797000	1.57328600	-0.62014200
H	5.97956600	-0.64305300	-0.20354800
O	2.42431800	2.13305200	-0.74341200
O	4.50713000	-2.90528300	0.26867100
C	5.91981100	-3.13418200	0.31114500
H	6.39163900	-2.54749100	1.10371000
H	6.03738100	-4.19449600	0.52562600
H	6.38743600	-2.90315400	-0.64959600
C	-1.68662100	-0.60003200	-0.08873800
N	-2.59233300	-1.57497600	-0.07521800
C	-2.29375400	-3.00982900	-0.13619800
H	-1.61782600	-3.21216900	-0.96443500
H	-1.84176600	-3.33806300	0.79985100
H	-3.21646000	-3.55595700	-0.30024000
C	2.47899900	3.21129700	0.24338400
O	3.11052100	2.98956000	1.26077600
O	1.85177800	4.18369600	-0.14019300

MCH₄⁺ HCO₃⁻

Charge: 0

Multiplicity: 1

Electronic Energy (B3LYP/6-311G(d)/PCM(water)): -1245.28627030

Geometry:

C	5.89854700	0.79084400	0.19966200
C	4.57138900	0.39256200	0.09399000
C	4.19510400	-0.94384000	-0.01894200

C	5.16337000	-1.93603400	-0.03059300
C	6.50675600	-1.56138600	0.07361700
C	6.86563500	-0.21608000	0.18724400
H	6.18856200	1.82978700	0.28958400
H	4.88843800	-2.98151100	-0.11789700
H	7.27838500	-2.32333000	0.06674500
H	7.91197700	0.05648000	0.26804300
C	2.68572600	-1.03552400	-0.11129400
C	2.26932200	-1.66913600	-1.45884500
H	2.64366600	-1.08432000	-2.30158700
H	2.69284500	-2.67336500	-1.52338200
H	1.18630200	-1.75288900	-1.54918500
C	2.12480800	-1.83835500	1.08563800
H	1.03928700	-1.92830600	1.04095500
H	2.54852100	-2.84442100	1.06612500
H	2.39515200	-1.37096500	2.03481000
C	1.00891300	1.03742700	-0.04703000
H	0.97892600	2.11461700	0.05887600
C	-0.16581600	0.35221400	-0.18146700
H	-0.14089600	-0.72095900	-0.30670900
C	-1.49120300	0.91504700	-0.17962700
C	-2.59862800	0.04061900	-0.37499900
C	-1.74063300	2.28921500	0.01741900
C	-3.89515900	0.57017600	-0.36338400
C	-3.02798800	2.79849600	0.02424200
H	-0.92085700	2.98004800	0.17373100
C	-4.11360200	1.92658200	-0.16662200
H	-4.73689400	-0.09510600	-0.51454000
H	-5.13129000	2.29507900	-0.16440700
O	-2.36393300	-1.27221200	-0.57282100
H	-3.21891500	-1.80477700	-0.65241600
O	-3.14900800	4.15337700	0.22495200
C	-4.46154700	4.72129900	0.21835800
H	-5.07751500	4.30820200	1.02187100
H	-4.32031700	5.78773200	0.38356600
H	-4.95708300	4.56511400	-0.74381300
C	2.29666800	0.44320700	-0.03109100
N	3.39721200	1.19069900	0.07962900
C	3.40998700	2.65314000	0.18485200
H	2.91867200	3.09237600	-0.68240700
H	2.89702900	2.96532000	1.09435000
H	4.43627300	3.00168500	0.22028500
C	-4.86270800	-3.24866900	0.26921500
O	-4.32882000	-3.15760900	1.38528300
O	-6.00850800	-4.03344700	0.15189200
H	-6.19569100	-4.39797600	1.02744700
O	-4.51456900	-2.72063700	-0.82549400

SP4

Charge: 0

Multiplicity: 1

Electronic Energy (B3LYP/6-311G(d)/PCM(water)): -980.171800784

Geometry:

C	-3.82258300	-1.08658700	-1.29156300
C	-2.84828500	-0.28500500	-0.69957800
C	-2.80833100	-0.10136400	0.69073300
C	-3.74901900	-0.70957700	1.50391600
C	-4.74099400	-1.51562200	0.92272600
C	-4.77096200	-1.69523000	-0.45880800
H	-3.85116700	-1.24381700	-2.36381500
H	-3.72073900	-0.57130300	2.58056900

H	-5.48085300	-2.00103800	1.55035000
H	-5.53562200	-2.32465600	-0.90320200
C	-1.66788300	0.84419200	1.02827700
C	-2.23406600	2.26427100	1.24438000
H	-2.79282000	2.62388400	0.37785100
H	-2.91453300	2.25217500	2.09913000
H	-1.43750500	2.98077300	1.46144200
C	-0.85810700	0.43841700	2.26311400
H	0.01315300	1.08757100	2.38892300
H	-1.47592200	0.54290400	3.15871800
H	-0.51432400	-0.59445700	2.21051100
C	-0.04109500	1.99831100	-0.65016600
H	-0.63115000	2.87033400	-0.90369200
C	1.29485600	2.05703500	-0.62987600
H	1.80763100	2.98522600	-0.86341900
C	2.09574100	0.88515100	-0.31469600
C	1.41876000	-0.33019900	-0.12171100
C	3.48850300	0.91040100	-0.22620600
C	2.13335400	-1.49131400	0.14336700
C	4.20981900	-0.25337500	0.04931000
H	4.02391300	1.84239000	-0.37609400
C	3.52795200	-1.45952600	0.23167000
H	1.59960600	-2.42506000	0.28296400
H	4.05950100	-2.37740400	0.44626900
O	0.05424600	-0.42223400	-0.22021100
O	5.57774400	-0.11241300	0.11817100
C	6.35736300	-1.27893500	0.38890400
H	6.22612200	-2.03481900	-0.39065400
H	7.39352500	-0.94569900	0.39788800
H	6.10591200	-1.70842500	1.36283300
N	-1.82453100	0.44289900	-1.31994400
C	-1.38745200	0.08347000	-2.66223200
H	-0.58180800	0.74954800	-2.97042700
H	-1.03192000	-0.95163200	-2.72639600
H	-2.21169200	0.20992300	-3.36583800
C	-0.81982000	0.76056100	-0.31122600

7. Additional Discussion of Thermodynamic Model

Consider the equilibrium for the deprotonation of \mathbf{MCH}^+ :



Here, K_O is the equilibrium constant for opening of \mathbf{SP} . The equilibrium concentrations of these species are related by:

$$\frac{[H^+][MC]}{[MCH^+]} = K_a$$

$$\frac{[MC]}{[SP]} = K_O$$

We can define an apparent acidity by taking into account that the deprotonated form can either be in the \mathbf{MC} or \mathbf{SP} form:

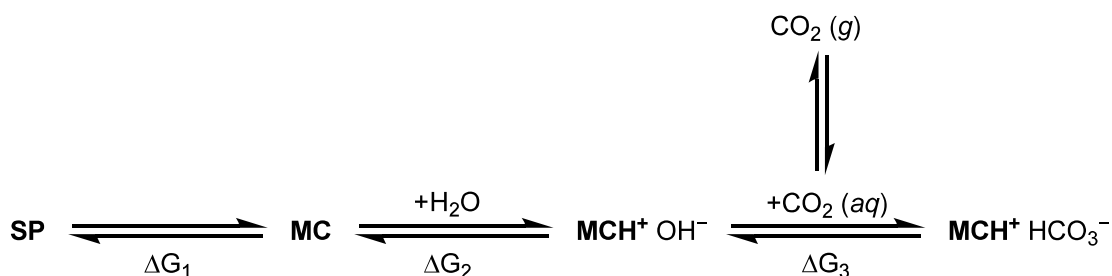
$$\frac{[H^+][\text{deprotonated species}]}{[MCH^+]} = \frac{[H^+]([MC] + [SP])}{[MCH^+]} = K_a(1 + K_O^{-1}) \equiv K_a'$$

When $[MC] + [SP] = [MCH^+]$, this simply reduces to:

$$[H^+] = K_a'$$

Thus, $\text{p}K_a'$ can be measured by spectrophotometric titration and is equivalent to the pH at which half of the organic species is in the \mathbf{MCH}^+ form and the other half is distributed between \mathbf{MC} and \mathbf{SP} .

In the carbon capture system of interest, there are four relevant equilibria:



In order for the most populous state to efficiently invert upon optical excitation of \mathbf{MCH}^+ , the original thermodynamic balance must barely favor $\mathbf{MCH}^+ \text{ HCO}_3^-$ over $\mathbf{SP/MC}$ (whichever is lower in energy) only very slightly. If this is satisfied, then a practical level of energy input can drive the system back to $\mathbf{SP/MC}$.

Case I: \mathbf{SP} is more stable than \mathbf{MC}

In most cases we consider, $K_O < 1$ and \mathbf{SP} is the major form of the CO_2 -free species. The energy balance condition can then be rewritten as:

$$\Delta G_1 + \Delta G_2 + \Delta G_3 \approx 0$$

If this sum is too negative, the system will never revert to **SP**, even with high-intensity illumination, and therefore photorelease is not possible. If instead the sum is too positive, capture of CO₂ will not occur in the first place. We can further analyze the three contributing energy terms:

$$\Delta G_1 = -RT \ln K_O$$

$$\Delta G_2 = -RT \ln(K_{a(water)} - K_{a(MCH+)})$$

$$\Delta G_3 = -RT \ln(K_{a(H_2CO_3)} - K_{a(water)})$$

Substituting these expressions into the energy balance condition, we obtain:

$$\ln K_O - \ln K_{a(MCH+)} + \ln K_{a(H_2CO_3)} \approx 0$$

$$pK_{a(MCH+)} + \log K_O \approx pK_{a(H_2CO_3)}$$

$$pK_a' \approx pK_{a(H_2CO_3)}$$

In the last step, we have taken advantage of the fact that $K_O \ll 1$ and thus $1 + K_O^{-1} \approx K_O^{-1}$.

Case II: MC is more stable than SP

In this situation, we need only consider the ΔG_2 and ΔG_3 contributions and need their sum to be just barely negative.

$$\Delta G_2 + \Delta G_3 \approx 0$$

This condition can be again dissected in terms of the equilibrium constants:

$$\Delta G_2 = -RT \ln(K_{a(water)} - K_{a(MCH+)})$$

$$\Delta G_3 = -RT \ln(K_{a(H_2CO_3)} - K_{a(water)})$$

$$pK_{a(MCH+)} \approx pK_{a(H_2CO_3)}$$

Now, since $K_O \gg 1$, we have that $1 + K_O^{-1} \approx 1$, and therefore the effective pK_a of the merocyanine is precise the normal pK_a with no contribution from the ring closing, which is unfavorable. Thus, again, we have:

$$pK_{a(MCH+)} \approx pK_{a(MCH+)} (1 + K_O^{-1}) = pK_a' \approx pK_{a(H_2CO_3)}$$

As exemplified by the two cases analyzed above, regardless of the position of the **SP/MC** equilibrium, the effective conjugate acidity is the key quantity that should be matched to the pK_a of carbonic acid. Note that if the nature of $\text{MCH}^+ \text{HCO}_3^-$ is not a separated ion pair, but there is an attractive interaction between the ions, there is an additional negative contribution to ΔG_3 , and the ideal pK_a' is slightly less to counteract this contribution. This can be one potential explanation for the experimentally matched pK_a' being around 5.8 to 6.0. The existence of some ion pairing with bicarbonate is consistent with the solvent-separated intimate ion pair model derived from transient absorption experiments.

8. NMR Spectra of Compounds

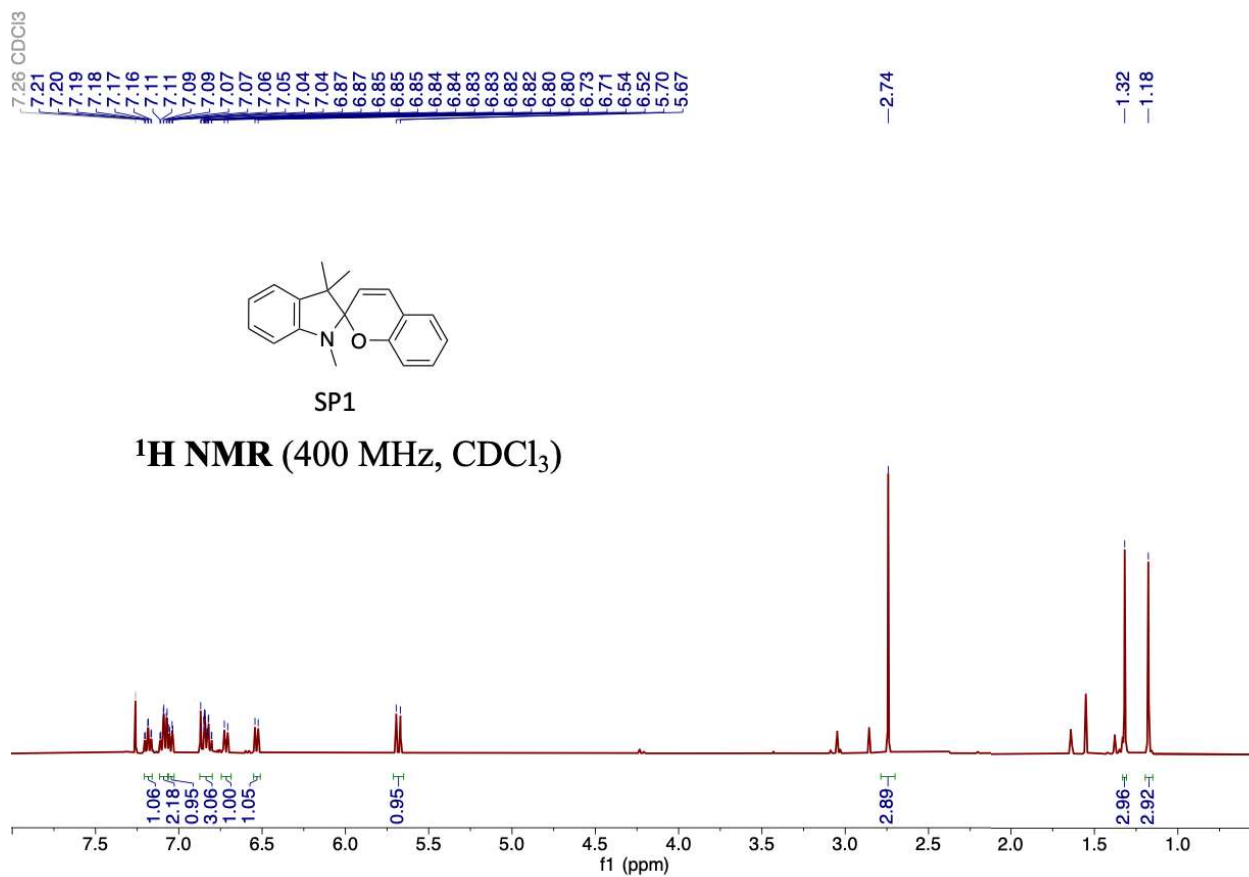


Figure S45. ¹H NMR spectrum of SP1.

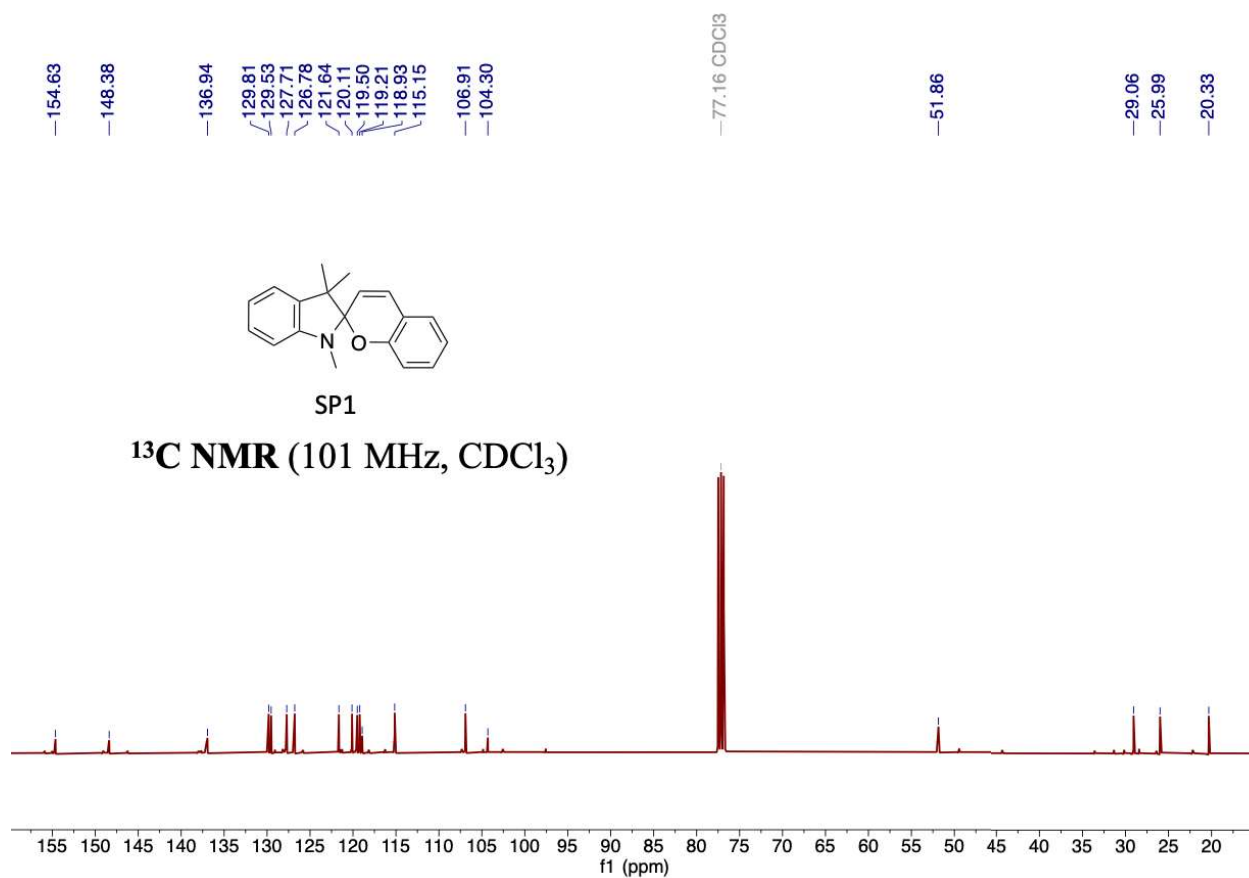


Figure S46. ^{13}C NMR spectrum of SP1.

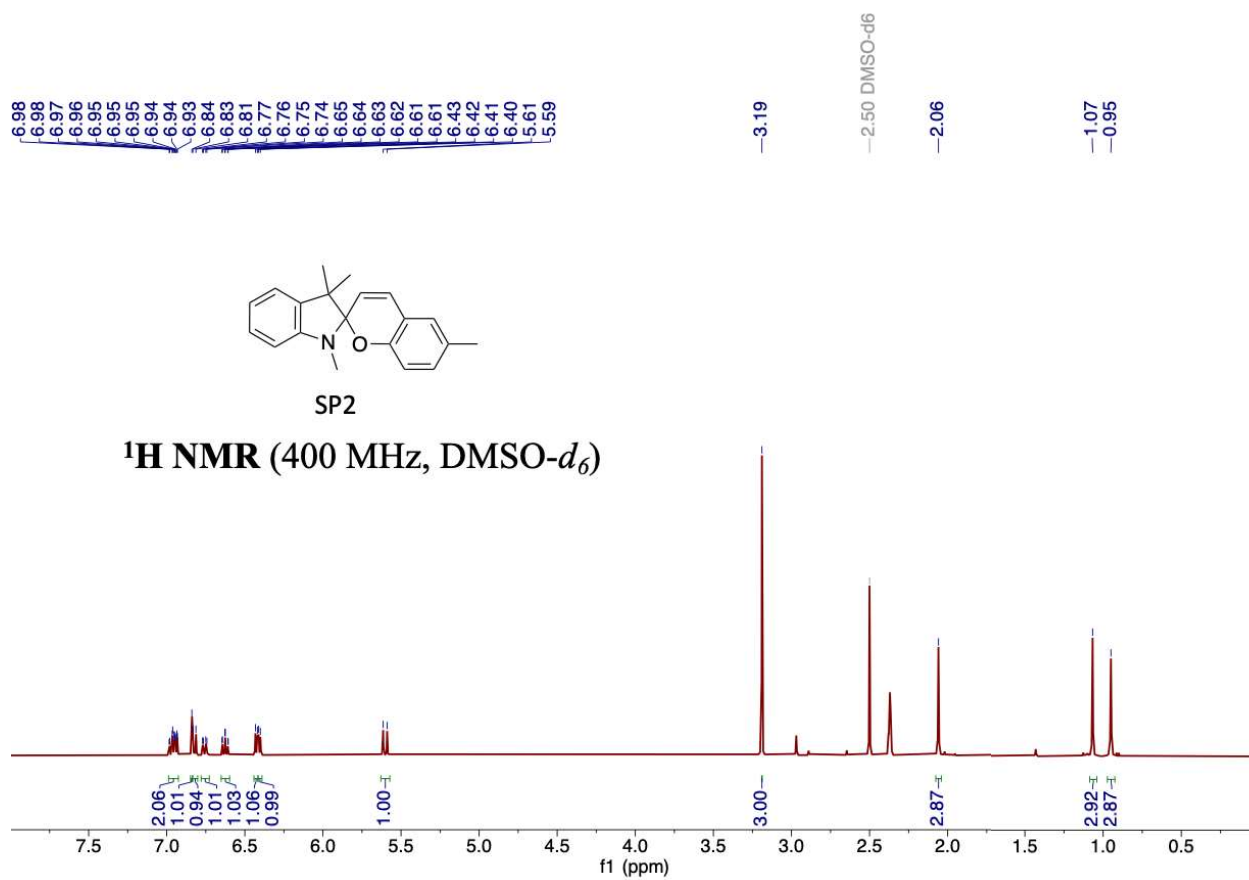
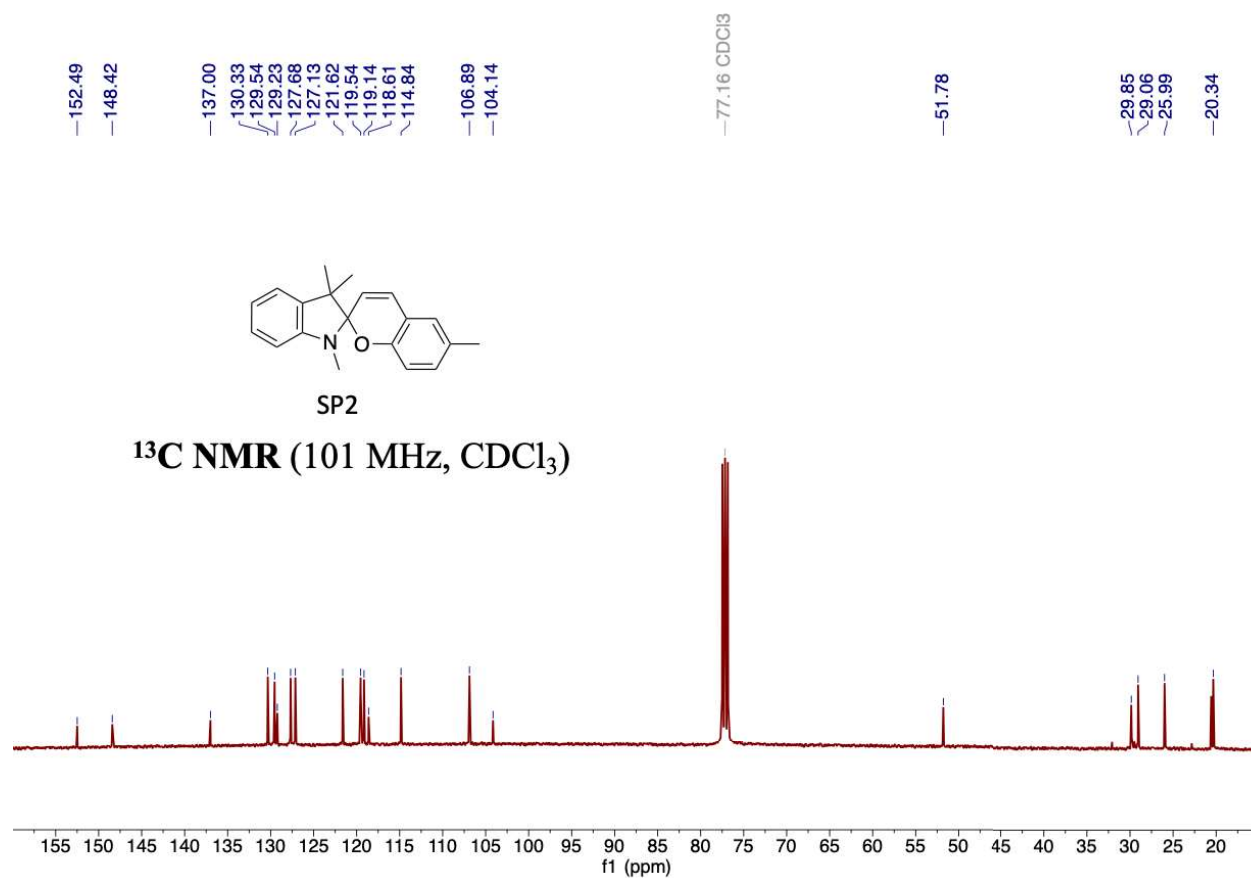


Figure S47. ^1H NMR spectrum of SP2.



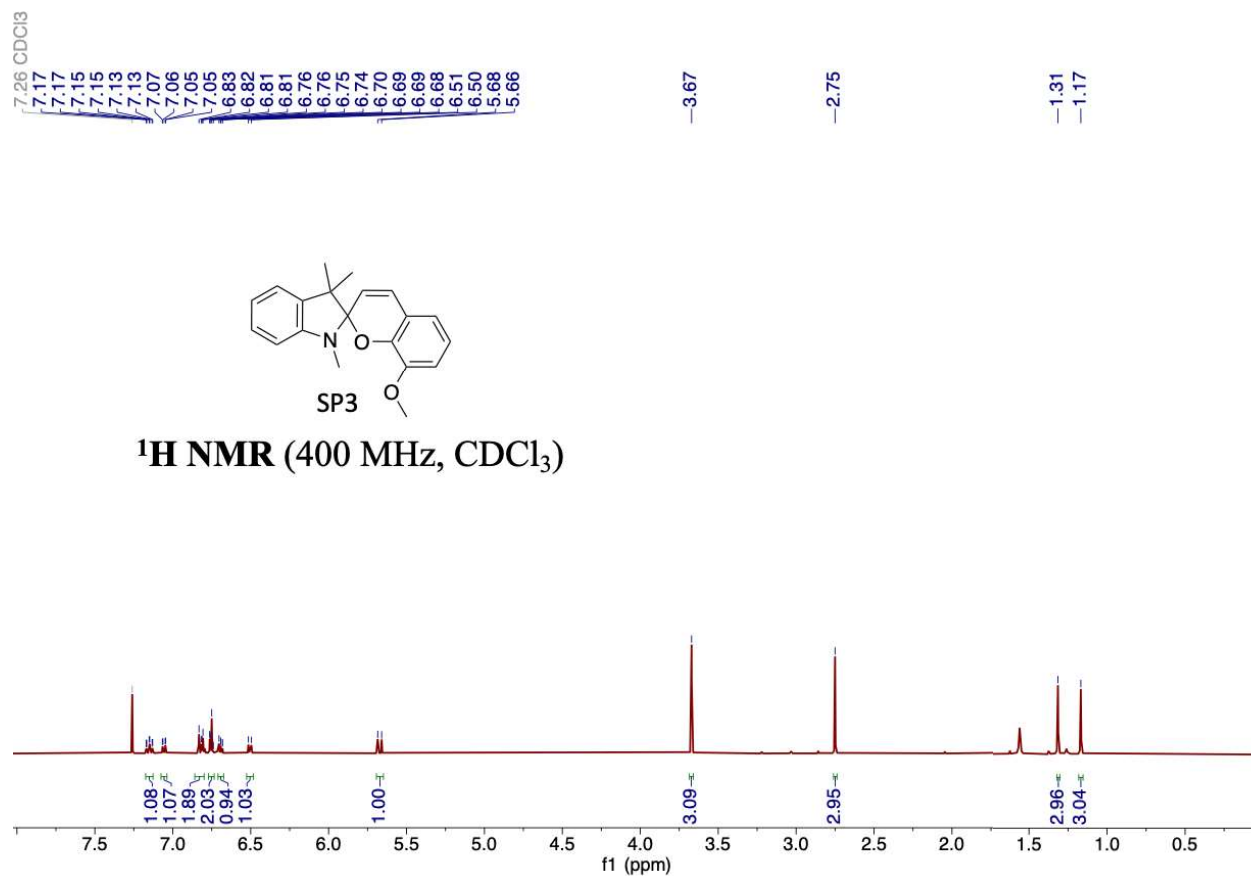


Figure S49. ¹H NMR spectrum of SP3.

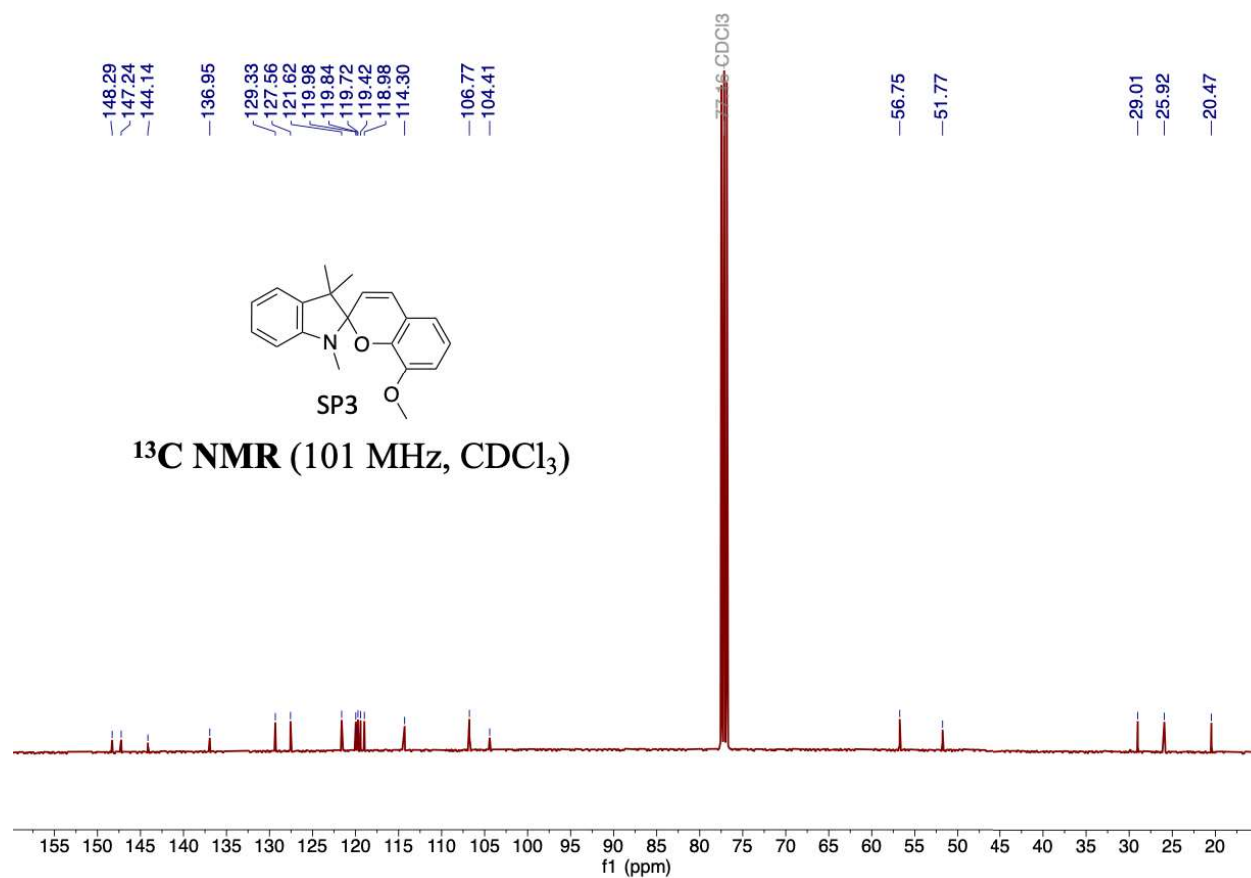


Figure S50. ¹³C NMR spectrum of SP3.

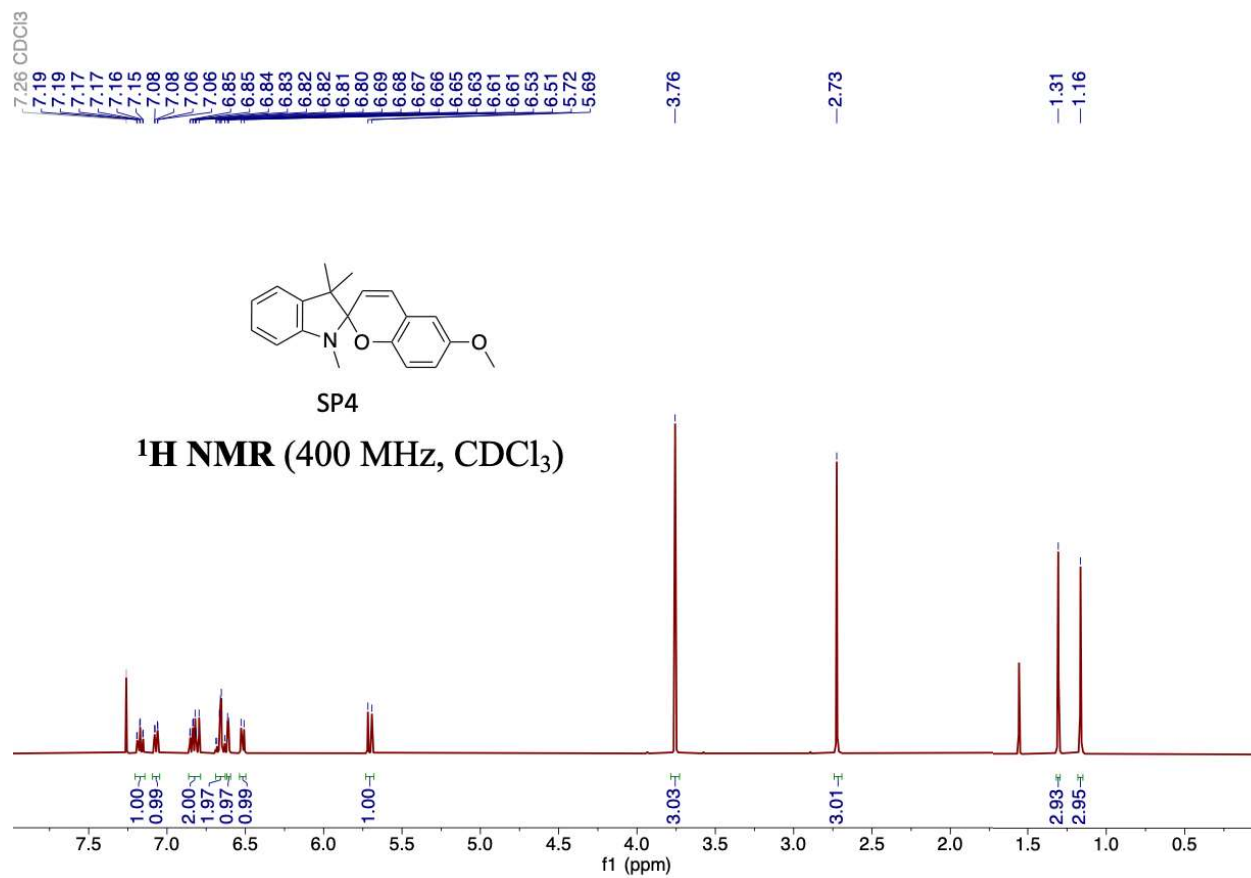


Figure S51. ^1H NMR spectrum of SP4.

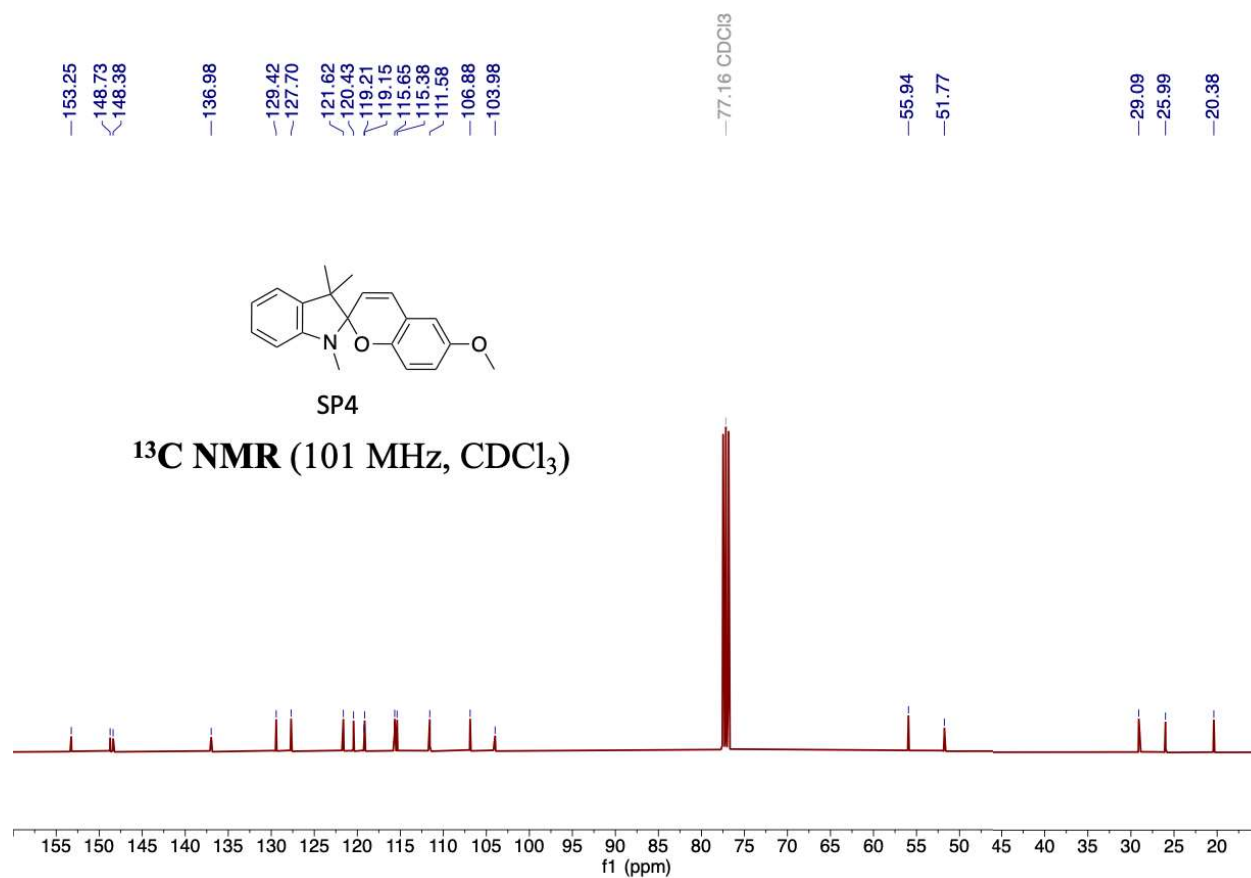


Figure S52. ^{13}C NMR spectrum of SP4.

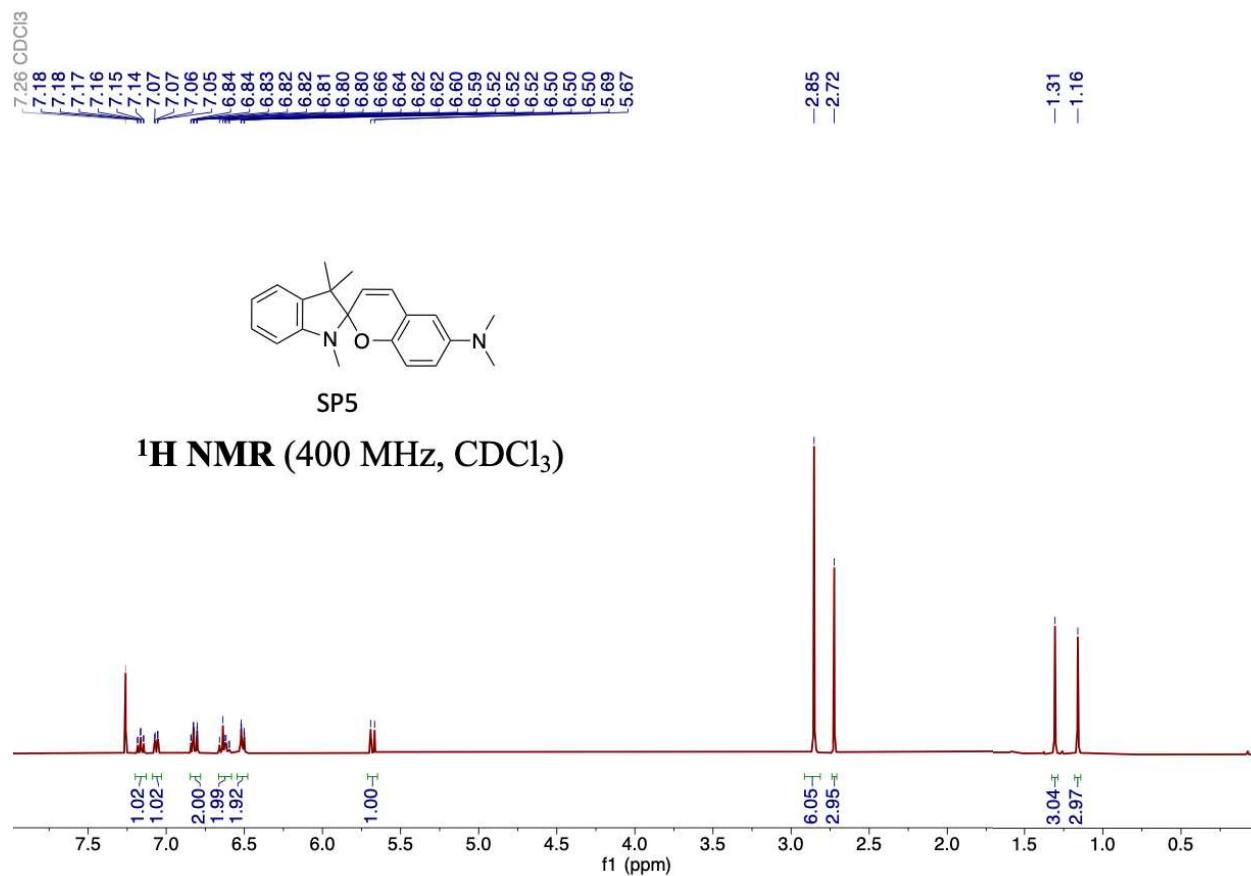


Figure S53. ^1H NMR spectrum of SP5.

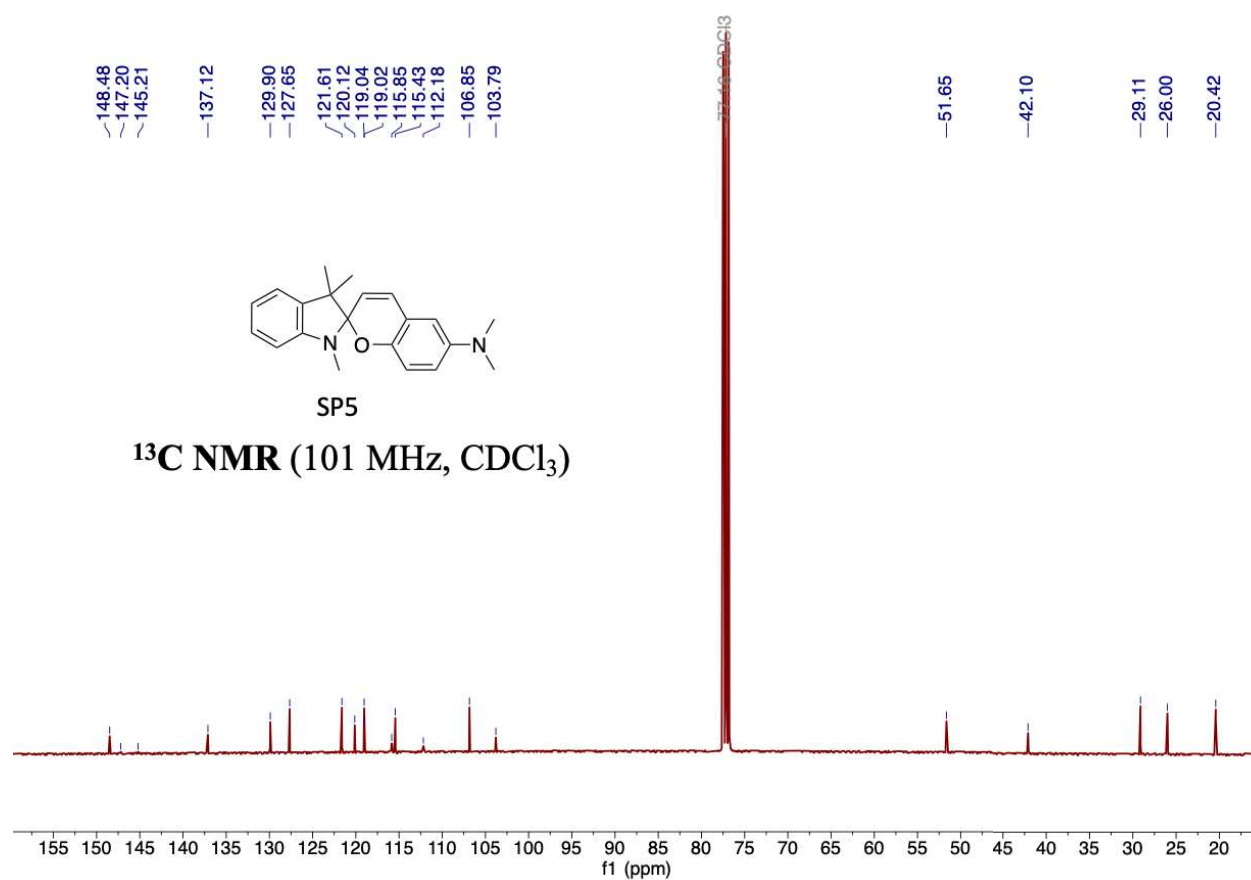


Figure S54. ^{13}C NMR spectrum of SP5.

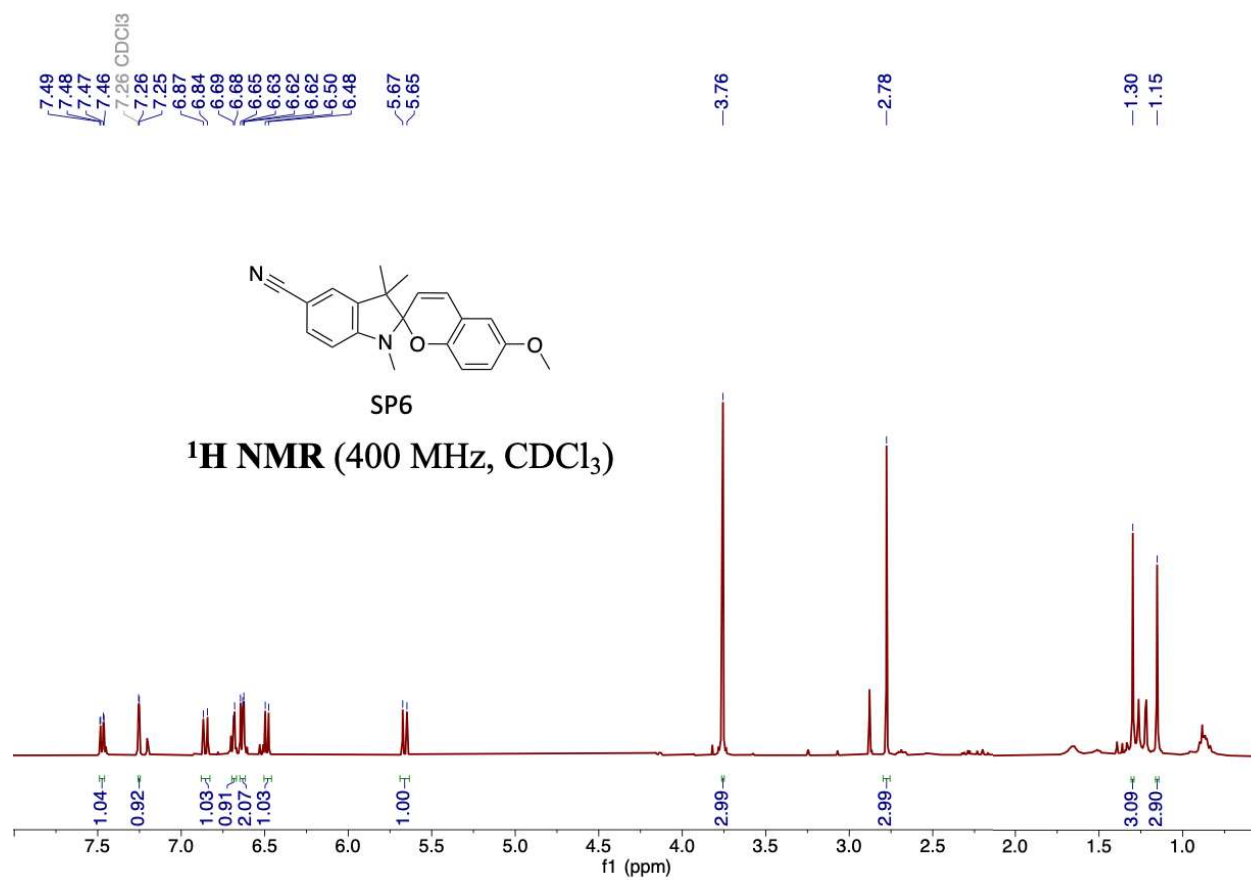


Figure S55. ¹H NMR spectrum of SP6.

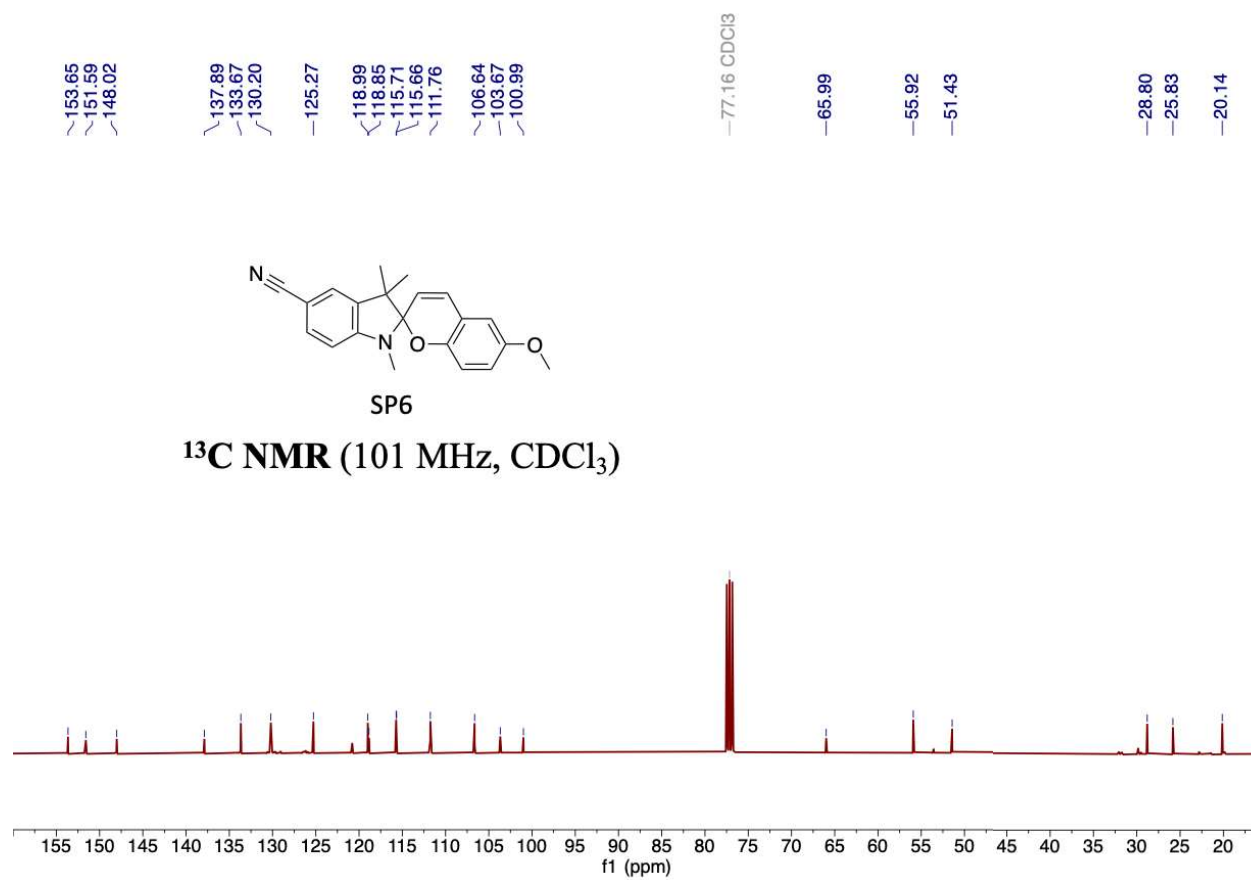


Figure S56. ^{13}C NMR spectrum of SP6.

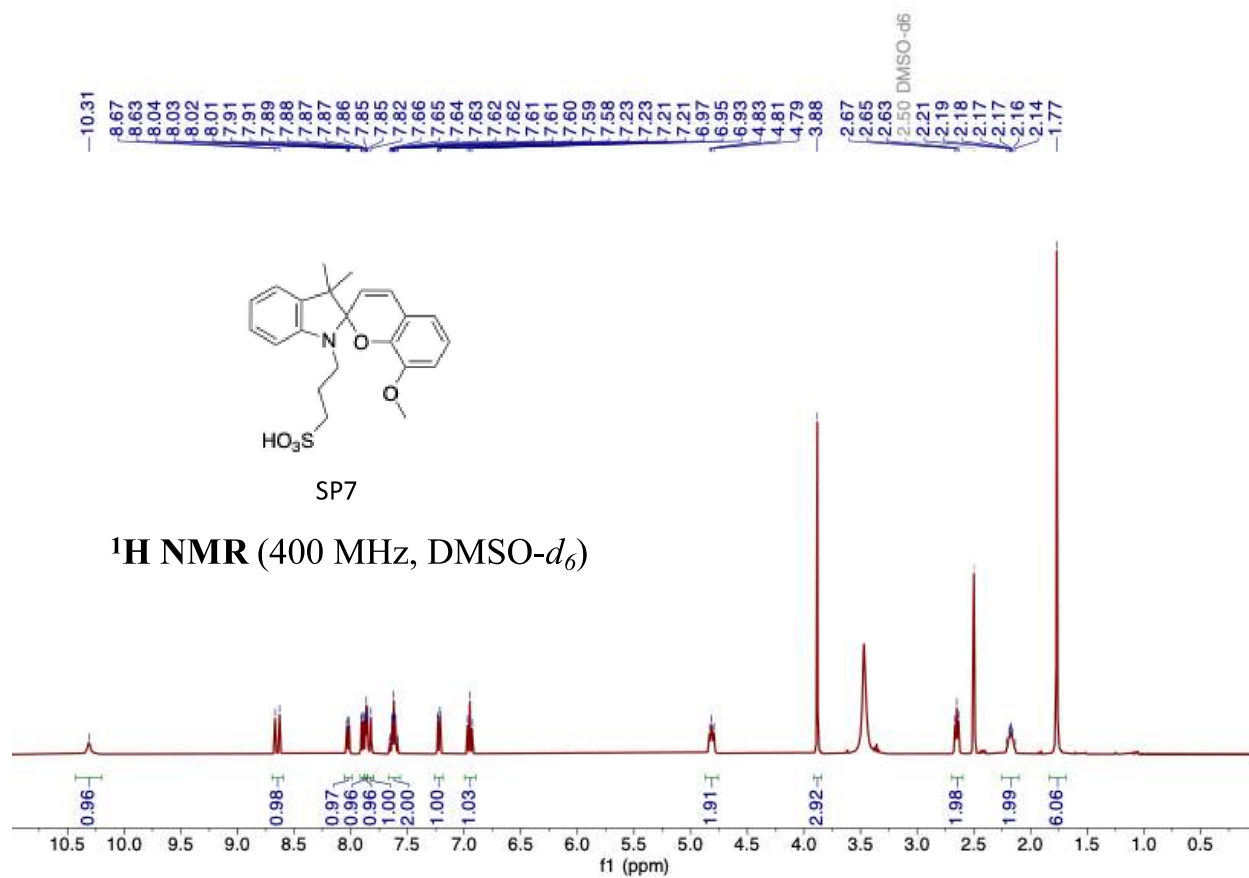


Figure S57. ¹H NMR spectrum of SP7.

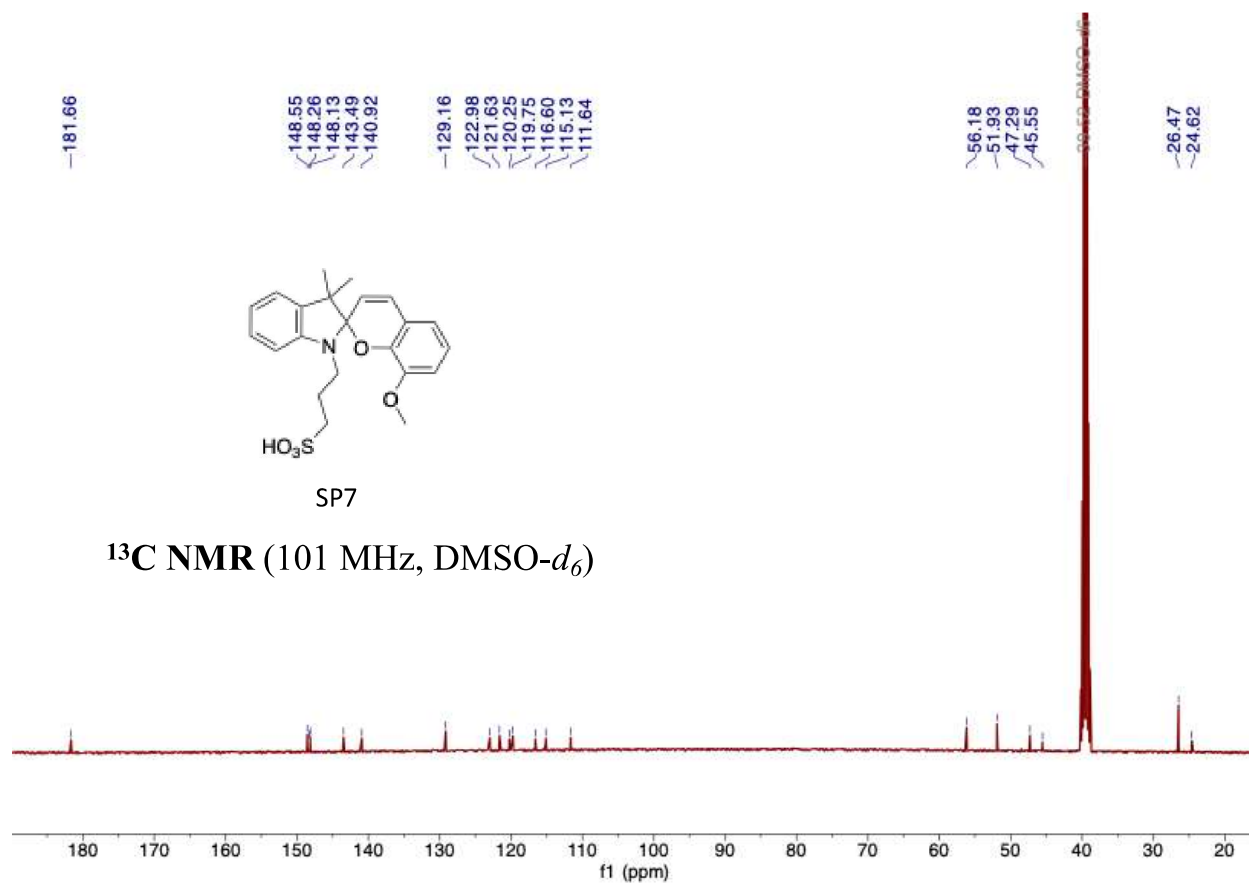


Figure S58. ^{13}C NMR spectrum of SP7.

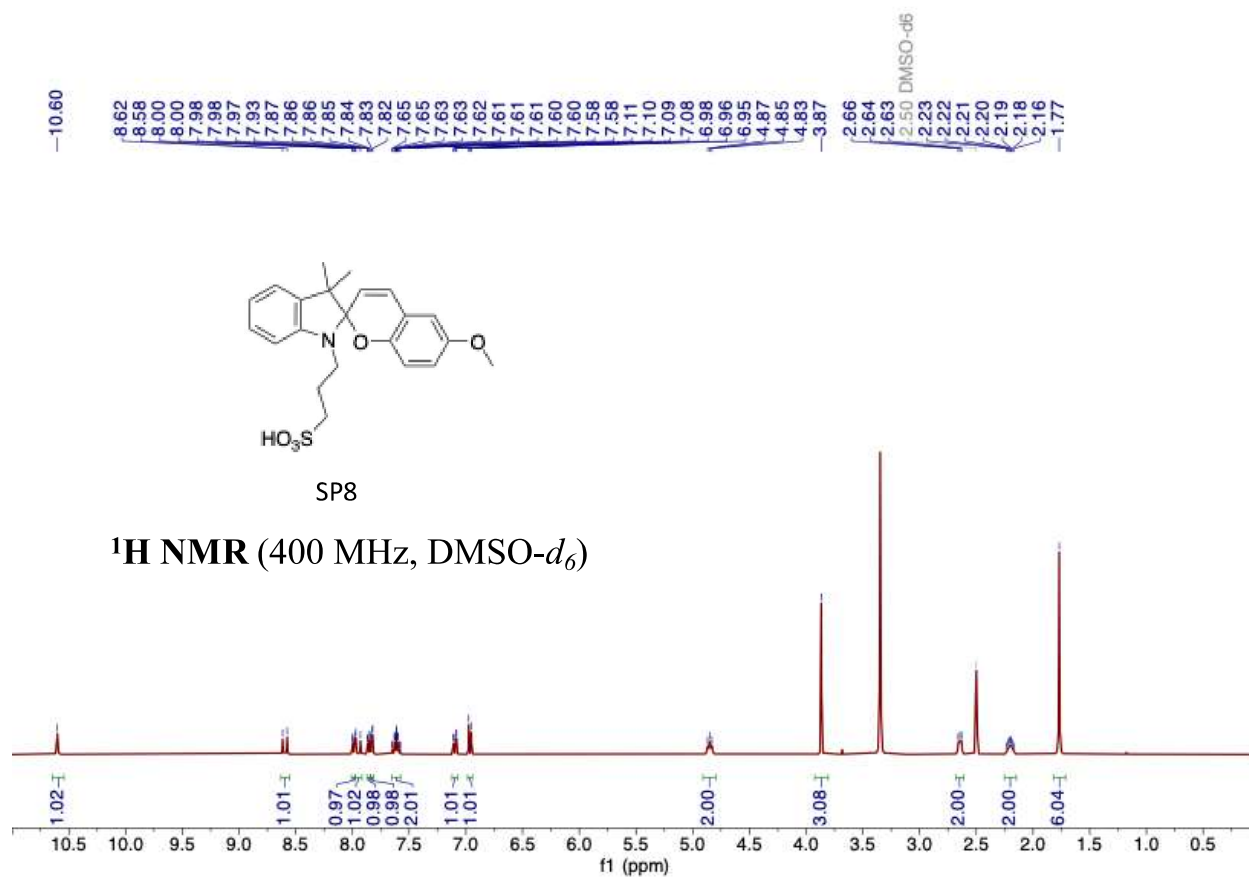


Figure S59. ¹H NMR spectrum of SP8.

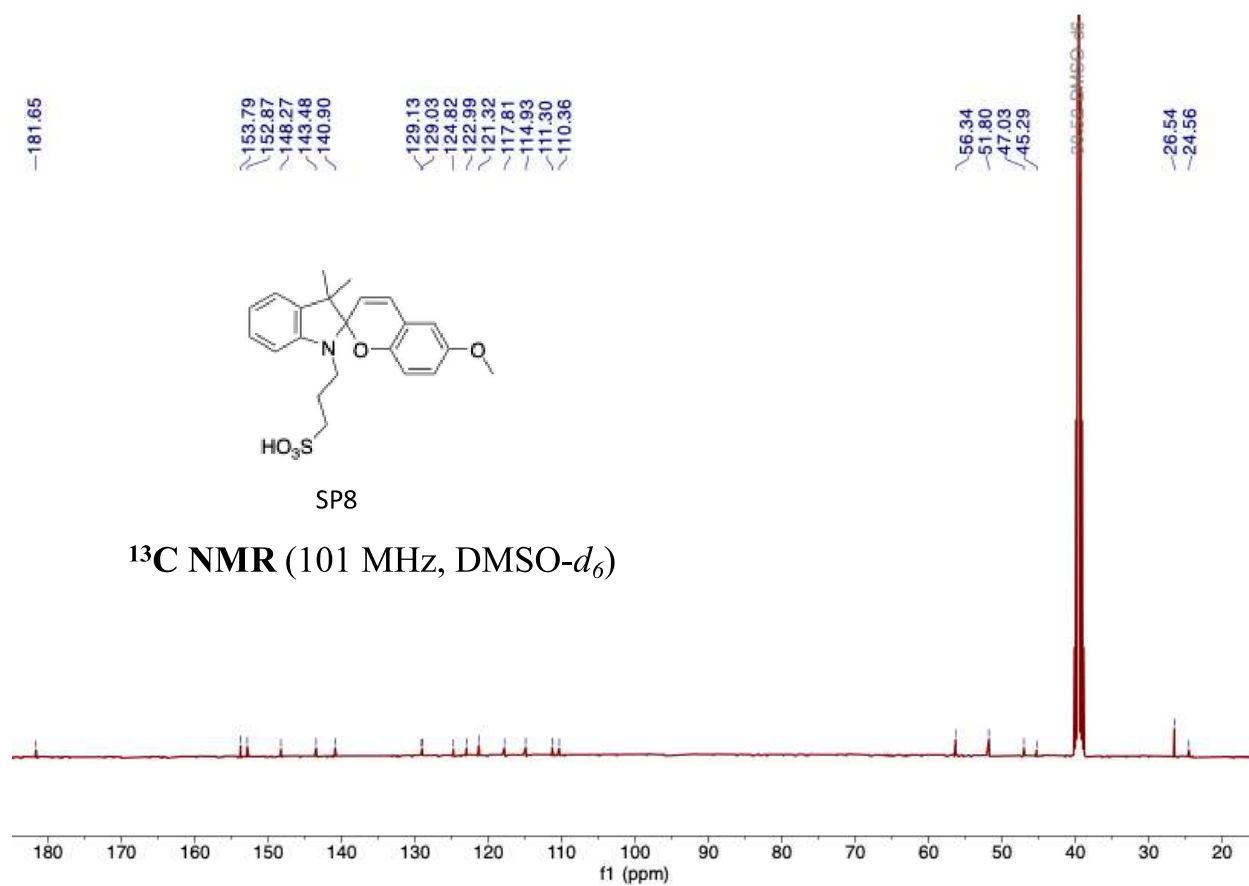


Figure S60. ¹³C NMR spectrum of **SP8**.

SI References

- (39) Darwish, N.; Aragonès, A. C.; Darwish, T.; Ciampi, S.; Díez-Pérez, I. Multi-Responsive Photo- and Chemo-Electrical Single-Molecule Switches. *Nano Lett.* **2014**, *14* (12), 7064–7070. DOI: 10.1021/nl5034599.
- (40) Gaur, P.; Kumar, A.; Dey, G.; Kumar, R.; Bhattacharyya, S.; Ghosh, S. Selenium Incorporated Cationic Organochalcogen: Live Cell Compatible and Highly Photostable Molecular Stain for Imaging and Localization of Intracellular DNA. *ACS Appl. Mater. Interfaces* **2016**, *8* (17), 10690–10699. DOI: 10.1021/acsami.6b00675.
- (41) Pargaonkar, J. G.; Patil, S. K.; Vajekar, S. N. Greener Route for the Synthesis of Photo- and Thermochromic Spiropyrans Using a Highly Efficient, Reusable, and Biocompatible Choline Hydroxide in an Aqueous Medium. *Synth. Commun.* **2018**, *48* (2), 208–215. DOI: 10.1080/00397911.2017.1395053.
- (42) Berton, C.; Busiello, D. M.; Zamuner, S.; Scopelliti, R.; Fadaei-Tirani, F.; Severin, K.; Pezzato, C. Light-Switchable Buffers. *Angew. Chem. Int. Ed.* **2021**, *60* (40), 21737–21740. DOI: 10.1002/anie.202109250.
- (43) Berton, C.; Busiello, D. M.; Zamuner, S.; Solari, E.; Scopelliti, R.; Fadaei-Tirani, F.; Severin, K.; Pezzato, C. Thermodynamics and Kinetics of Protonated Merocyanine Photoacids in Water. *Chem. Sci.* **2020**, *11* (32), 8457–8468. DOI: 10.1039/D0SC03152F.
- (44) de Vries, A.; Goloviznina, K.; Reiter, M.; Salanne, M.; Lukatskaya, M. R. Durable Light-Driven pH Switch Enabled by Solvation Environment Tuning of Metastable Photoacids. *ChemRxiv*. **2023**, Preprint chemrxiv-2023-s60n5-v2. DOI: 10.26434/chemrxiv-2023-s60n5-v2.
- (45) Rieth, A. J.; Gonzalez, M. I.; Kudisch, B.; Nava, M.; Nocera, D. G. How Radical Are “Radical” Photocatalysts? A Closed-Shell Meisenheimer Complex Is Identified as a Super-Reducing Photoreagent. *J. Am. Chem. Soc.* **2021**, *143* (35), 14352–14359. DOI: 10.1021/jacs.1c06844.
- (46) Holder, P. G.; Pizano, A. A.; Anderson, B. L.; Stubbe, J.; Nocera, D. G. Deciphering Radical Transport in the Large Subunit of Class I Ribonucleotide Reductase. *J. Am. Chem. Soc.* **2012**, *134* (2), 1172–1180. DOI: 10.1021/ja209016j.

- (47) Müller, P.; Brettel, K. $[\text{Ru}(\text{Bpy})_3]^{2+}$ as a Reference in Transient Absorption Spectroscopy: Differential Absorption Coefficients for Formation of the Long-Lived $^3\text{MLCT}$ Excited State. *Photochem. Photobiol. Sci.* **2012**, *11* (4), 632–636. DOI: 10.1039/C2PP05333K.
- (48) Gaussian 16, Revision A.03, Frisch, M. J.; Trucks, G. W.; Schlegel, H. B.; Scuseria, G. E.; Robb, M. A.; Cheeseman, J. R.; Scalmani, G.; Barone, V.; Petersson, G. A.; Nakatsuji, H.; Li, X.; Caricato, M.; Marenich, A. V.; Bloino, J.; Janesko, B. G.; Gomperts, R.; Mennucci, B.; Hratchian, H. P.; Ortiz, J. V.; Izmaylov, A. F.; Sonnenberg, J. L.; Williams-Young, D.; Ding, F.; Lipparini, F.; Egidi, F.; Goings, J.; Peng, B.; Petrone, A.; Henderson, T.; Ranasinghe, D.; Zakrzewski, V. G.; Gao, J.; Rega, N.; Zheng, G.; Liang, W.; Hada, M.; Ehara, M.; Toyota, K.; Fukuda, R.; Hasegawa, J.; Ishida, M.; Nakajima, T.; Honda, Y.; Kitao, O.; Nakai, H.; Vreven, T.; Throssell, K.; Montgomery, J. A., Jr.; Peralta, J. E.; Ogliaro, F.; Bearpark, M. J.; Heyd, J. J.; Brothers, E. N.; Kudin, K. N.; Staroverov, V. N.; Keith, T. A.; Kobayashi, R.; Normand, J.; Raghavachari, K.; Rendell, A. P.; Burant, J. C.; Iyengar, S. S.; Tomasi, J.; Cossi, M.; Millam, J. M.; Klene, M.; Adamo, C.; Cammi, R.; Ochterski, J. W.; Martin, R. L.; Morokuma, K.; Farkas, O.; Foresman, J. B.; Fox, D. J. Gaussian, Inc., Wallingford CT, 2016.
- (49) Becke, A. D. Density-functional Thermochemistry. III. The Role of Exact Exchange. *The J. of Chem. Phys.* **1993**, *98* (7), 5648–5652. DOI: 10.1063/1.464913.
- (50) Lee, C.; Yang, W.; Parr, R. G. Development of the Colle-Salvetti Correlation-Energy Formula into a Functional of the Electron Density. *Phys. Rev. B* **1988**, *37* (2), 785–789. DOI: 10.1103/PhysRevB.37.785.
- (51) Marenich, A. V.; Cramer, C. J.; Truhlar, D. G. Universal Solvation Model Based on Solute Electron Density and on a Continuum Model of the Solvent Defined by the Bulk Dielectric Constant and Atomic Surface Tensions. *J. Phys. Chem. B* **2009**, *113* (18), 6378–6396. DOI: 10.1021/jp810292n.
- (52) Alharbi, A. W. H. Metastable-State Photoacid: A Comprehensive Theoretical Study of the Photoreaction, Reverse Reaction, Thermal Isomerization, and TD-DFT Absorption in Solvent. Ph.D Dissertation, Florida Institute of Technology, Melbourne, FL, 2019. <http://hdl.handle.net/11141/2947>